Design, Modelling, and Development of Adaptive Robot Grippers and Hands for Robust Grasping and Dexterous Manipulation

Geng Gao

A thesis submitted in fulfilment of the requirements for the degree of
Doctor of Philosophy in Mechatronics Engineering,
The University of Auckland, 2022.

Abstract

Robots are increasingly becoming an integral part of our lives, participating and collaborating with humans in various roles, from automating tasks in industry, service, and home environments to assisting and augmenting humans to regain their original quality of living or further improve their capabilities. As such, the tasks executed by robotic systems are also constantly growing in sophistication. Grasping and dexterous manipulation are critical capabilities that allow humans to execute these complex everyday life tasks, enabling them to interact with their environment (e.g., grasping an object, pushing a button, opening a door, etc.). In robotics, for such complex tasks the devices that are typically employed are either fully actuated, multi-fingered, and rigid robot hands that are expensive and that require advanced sensing elements and complicated control laws or simple robotic grippers that offer limited dexterity and rely on robotic manipulators to accomplish the tasks. In this PhD thesis, we focus on the design, analysis, and development of adaptive, underactuated, and soft robot grippers and hands that can provide robust grasping and dexterous manipulation capabilities to robotic systems operating in dynamic and unstructured environments. To do so, we propose new designs and methods of introducing compliance to the end-effector structures, new selectively lockable differential mechanisms, new multi-modal gripping systems, reconfigurable bases that increase the dexterity of an end-effector without increasing complexity, and variable stiffness actuators that increase the system capabilities in both grasping and manipulation. All the designs and mechanisms proposed have been analyzed and integrated in a series of robotic grippers and hands that can be efficiently used in a wide range of applications, requiring minimal sensing and control in order to be operated. In order to evaluate the performance of the proposed robot grippers and hands, we conducted a plethora of experiments focusing on their grasping, manipulation, reconfiguration, stiffness modulation, and force exertion capabilities.

I dedicate this thesis to my family for instilling in me the belief that anything is possible in life.

Acknowledgements

I express my deepest gratitude to my supervisor, Dr. Minas Liarokapis, for his invaluable guidance, advice, and effort during my studies. His academic expertise and enthusiasm have helped to sharpen my thinking and expand my creativity, bringing the work I produce to a higher level. His support and mentorship have pushed me to achieve goals and seize opportunities I did not think were possible. I want to thank my co-supervisor, Assoc. Prof. Kean C Aw for his thoughts and feedback throughout my PhD.

I want to acknowledge the lab technicians and staff for their technical assistance and support with lab equipment and consumables in my research.

I want to thank all the students of the New Dexterity research team and the Mechatronics Lab students (Anany Dwivedi, Alex Hayashi, Bonnie Guan, Cheming Chang, Gal Gorjup, Jayden Chapman, Joao Buzzatto, Junbang Liang, Lucas Gerez, Mojitaba Shahmohamamadi, Nathan Elangovan, Tzu-Jui Lin, and Yongje Kwon) for their assistance, support, and friendship. I want to give a special thanks to Anany Dwivedi for helping me with experiments and always accompanying me during late-night grinds to make the work more enjoyable.

I am indebted to my friends for always keeping my life exciting and ensuring I have a life outside work.

Most of all, I thank my parents for always believing in me and motivating me. For ensuring that I have a stable place to return to and their understanding and patients with me as I became more absorbed with my work. Without their love and support, this work would not have been possible.

Contents

List of Figures

List of Tables

Abbreviations

ABS	Acrylonitrile Butadiene Styrene
ADL	Activities of Daily Living
CAD	Computer Aided Design
CAE	Computer Aided Engineering
DOF	Degrees of Freedom
DIP	Distal Interphalangeal
EMG	Electromyography
FEA	Finite Element Analysis
GUI	Graphical User Interface
HDM	Hybrid Deposition Manufacturing
IMU	Inertial Measurement Unit
IROS	Intelligent Robots and Systems
MCP	Metacarpal
NIST	National Institute on Standards and Technology
PCB	Printed Circuit Boards
PET	Poly-Ethylene Terephthalate
PID	Proportional Integral Derivative
PIP	Proximal Interphalangeal
PLA	Polylactic Acid
RGMC	Robotic Grasping and Manipulation Challenge
ROM	Range of Motion
ROS	Robot Operating System
SMA	Shape Memory Alloy
SMP	Shape Memory Polymer
STL	Stereolithography
UAHPEC	University of Auckland Human Participants Ethics Committee
UAV	Unmanned Aerial Vehicle
UHMWPE	Ultra-High Molecular Weight Polyethylene
YCB	Yale-CMU-Berkeley

Part I

Introduction

Chapter 1

Background

Humans are capable of executing a plethora of tasks and are able to interact and engage with their surrounding environment in a meaningful manner. A key component of these interactions is through their hands allowing them to wield tools, grasp/ manipulate objects, or to simply push objects aside. The human hand achieves this through a complex network of bones, ligaments, tendons, blood vessels, connective tissue, and nerves all working together to produce complex grasping and manipulation motions [1]. In order for robots to do the same, researchers have striven to emulate the human hand's dexterity by replicating the human hand's kinematics, and structures matching its 24 degrees of freedom (DOF) [2, 3, 4, 5]. However, challenges related to weight, size, cost, sensing, and control complexity arise from directly mimicking the human hand, making it difficult to utilize these devices. Instead, many industry solutions default to simple parallel jaw grippers with limited grasping capabilities. Although a simple pinch grasp can be used to execute a variety of tasks, when grasping humans do not just perform a single grasp alone, but re-orient, or re-position the grasped objects during post-grasp. In order to improve grasp quality, or to expose certain areas of the objects. However, most robot end-effectors are only designed to grasp once and rely on the redundancy of the robot arms they are attached to, to position and orient the objects correctly. Relying only on a singular grasp confines the configuration space of the objects to the configuration space of the arm. This may not be desirable as joint limits and singularities can limit the possible motions needed to manipulate an object. Similarly, the presence of obstacles in the nearby environment can further constrain the arms workspace. Added dexterity towards the end of the arm can be beneficial as precise and minute motions can be implemented through a gripper [6]. In order to adjust objects instead of a robot arm, which

can be more power intensive due to the inertia of the system. With a dexterous end-effector re-grasping procedures required for simplistic grippers can be avoided as this procedure may not always be possible or ideal to execute.

Traditionally robot grippers and hands have been designed to be fully actuated [7, 8] and have demonstrated the capabilities to not only do grasping, but are capable of executing complex manipulation motions. Although this is achievable, the requirement for highly structured environments, good calibration, expensive components, or significantly large amounts of training data for learning [9] make pursuing such a design difficult to replicate or reproduce outside of a research lab. As a result, there has been a shift in design paradigms of robot grippers and hands moving from conventional rigid and fully actuated systems to designs that incorporate underactuation and compliant materials to achieve adaptive and soft behaviors. These systems [10, 11, 12] in the form of adaptive and soft grippers have shown promise in being able to accomplish grasping and basic manipulation tasks in unstructured and dynamic environments with open loop control, and affordable components. The integration of soft and compliant materials not only improves adaptability and handling of delicate objects, it also enables such systems to be inherently safer around humans as they can passively comply during human-robot interactions [13]. By leveraging these properties not only robots, but amputees can benefit from this design methodology making way for highly affordable, lightweight, and functional prosthetic devices [14].

While showing favorable results in executing dexterous tasks, underactuated and soft grippers also have their own limitations. The multiple unconstrained degrees of freedom can lead to decreased controllability and force exertion at the fingertips of the robotic hand, which can result in undesired reconfigurations (e.g., ejection) during grasping as the underactuated mechanisms will continue to move until fully constrained (e.g., phalanges experience contact with object surface, reach physical limits, or reach and equilibrium state) [15]. Furthermore, as the number of available actuators is constrained in developing underactuated hands the accessible number of grasp types and control of over individual joint trajectories for in-hand manipulation will also be reduced. Hence, accessing only a portion of the dexterity that there fully actuated counter parts have. Soft robotic systems suffer additional disadvantages, although the soft and compliant nature of the design enables it to effortlessly adapt to the external environment around it, this same property results in low control accuracy, low force exertion, and low resistance to deformation. This constrains soft robotic designs to handling delicate and fragile tasks [13].

1.1 Objectives

The goal of this PhD thesis research is to create robotic grasping and manipulation systems, which can facilitate an efficient, dexterous, robust, and intuitive execution of complex tasks in dynamic and unstructured environments. To accomplish this, we focus on the design, analysis, and development of different mechanisms as well as transmission and actuation systems and structures for robotic end-effectors aimed at improving the grasping and manipulation capabilities of adaptive robotic end-effectors in a plethora of different applications. In particular, the main objectives of this PhD thesis are:

1. To investigate how structural compliance and extra, manipulation-oriented degrees of freedom can be integrated locally into the finger units of robotic end-effectors to facilitate the execution of complex, sophisticated tasks such as assembly tasks and implement robotic grippers demonstrating the concepts.

2. To investigate the role of reconfigurable finger base frames on increasing the robot gripper dexterity and manipulation capabilities without sacrificing grasping performance and how they can enable the efficient operation of the robot gripping and hand systems in human-centric environments.

3. To explore the implementation of new selectively lockable differential systems and locking mechanisms that can increase the capabilities of underactuated adaptive robot and prosthetic hands without increasing their cost, offering affordable dexterity.

4. Explore the use of soft robotic technologies such as highly reconfigurable, multi-stage, compliant, and inflatable systems for the development of ultra-affordable disposable grippers for handling hazardous materials.

5. Investigate and develop variable stiffness systems, that can be used to replace passive elastic elements commonly used in adaptive and soft underactuated robotic systems, allowing for improved control and increased force exertion capabilities without compromising the benefits of using structural compliance (e.g., ability to conform to the object shape, grasp robustness, ability to grasp under object pose uncertainties etc.).

1.2 Ethics Approval

Experiments involving human participants have received the approval from the University of Auckland Human Participants Ethics Committee (UAHPEC) with the reference number #019043. Prior to the study, all participating subjects provided written and informed consent to the experimental procedures.

1.3 Thesis Organization

The thesis is divided into three main parts: Adaptive Grippers and Hands for Robotic Systems (Part II), Adaptive Fingers and Hands for prosthetic Systems (Part III), and Soft and Variable Stiffness Systems (Part IV).

The chapters of Part II are organized as follows:

- Chapter 2 presents the equipment and apparatus utilized in this work, as well as apparatus developed for specifically conducting experiments for evaluating the developed robots hands [1].
- Chapter 3 presents a multi-modal gripper that combines different grasping modes that synergistically complement each other for executing flexible robotic assembly tasks. The gripper combines four grasping modes, Structural compliance, and a local DOF to perform grasping and manipulation [2].
- Chapter 4 presents two anthropomorphic robot hands constructed with monolithic finger structures capable of performing robust power grasps for executing a variety of different tasks. Both robot hand designs utilize different thumb designs for evaluating the benefits of incorporating an additional DOF at the base of the thumb. The additional DOF facilitates hand aperture adjustment and improved in-hand manipulation capabilities.
- Chapter 5 presents a reconfigurable adaptive robot hand that combines both anthropomorphic and interdigitated configurations. The hand is capable of

[1] Section 2.6 of the chapter is based on [16], © 2020, IEEE. Reprinted, with permission, from Geng Gao, Gal Gorjup, Ruobing Yu, Patrick jarvis, and Minas Liarokapis, Modular, accessible, sensorized objects for evaluating the grasping and manipulation capabilities of grippers and hands, IEEE Robotics and Automation Letters, 2020.

[2] Majority of the chapter is based on [17], © 2020, IEEE. Reprinted, with permission, from Gal Gorjup, Geng Gao, Anany Dwivedi, and Minas Liarokapis, A Flexible Robotic Assembly System Combining CAD Based Localization, Compliance Control, and a Multi-Modal Gripper, IEEE Robotics and Automation Letters, 2021.

switching between non-anthropomorphic and anthropomorphic configuration in order to achieve a wide range of grasps and manipulation modes, while taking advantage of the shape ergonomics of many objects that have been designed to be used in a human centered environment. [3].

The chapters of Part III are organized as follows:

- Chapter 6 presents an affordable, and light weight partial hand prosthesis with a high level of personalization that can accommodate different prosthetic fingers for a variety of partial hand amputees. Both body-powered and motorized solutions have been developed to accommodate different users [4].

- Chapter 7 presents a novel locking mechanism that can be used with differential mechanisms for providing full hand prosthetic systems with improved control over it fingers without compromising the weight, cost, and form-factor of the device [5] [6].

The chapters of Part IV are organized as follows:

- Chapter 8 presents a mechanically programmable jamming structure based on articulated mesh structures for the development of variable stiffness systems. The variable stiffness actuators can be used as a pin and flexure joint in the development of robotic grippers (e.g., adaptive and soft robot hands) and assistive devices (e.g., wearable exoskeleton).

[3] Majority of the chapter is based on [18], © 2021, IEEE. Reprinted, with permission, from Geng Gao, Jayden Chapman, Saori Matsunaga, Toshisada Mariyama, Bruce MacDonald, and Minas Liarokapis, A Dexterous, Reconfigurable, Adaptive Robot Hand Combining Anthropomorphic and Interdigitated Configurations, IEEE/RSJ International Conference on Intelligent Robots and Systems (IROS), 2021.

[4] Majority of the chapter is based on [19], © 2019, IEEE. Reprinted, with permission, from Geng Gao, Lucas Gerez, and Minas Liarokapis, Adaptive, tendon-driven, affordable prostheses for partial hand amputations: On body-powered and motor driven implementations, 41st Annual International Conference of the IEEE Engineering in Medicine and Biology Society (EMBC), 2019.

[5] Majority of the chapter is based on [20], © 2021, IEEE. Reprinted, with permission, from Geng Gao, Anany Dwivedi, and Minas Liarokapis, An Anthropomorphic Prosthetic Hand with an Active, Selectively Lockable Differential Mechanism: Towards Affordable Dexterity, IEEE/RSJ International Conference on Intelligent Robots and Systems (IROS), 2021.

[6] Majority of the chapter is based on [21], © 2021, IEEE. Reprinted, with permission, from Geng Gao, Mojtaba Shahmohammadi, Lucas Gerez, George Kontoudis, and Minas Liarokapis, On Differential Mechanisms for Underactuated, Lightweight, Adaptive Prosthetic Hands, Frontiers in Neurorobotics, 2021.

- Chapter 9 presents a soft telescopic, multi-stage actuator that can be perform extension and abduction motions in soft systems. We equip a soft gripper with these actuators for executing stable grasps in unstructured and dynamic environments. The low material cost of the actuators allows the developed gripper to be used in a disposable manner for handling hazardous waste [7].

[7] Majority of the chapter is based on [22], © 2020, IEEE. Reprinted, with permission, from Geng Gao, Che-ming Chang, Lucas Gerez, and Minas Liarokapis, A Pneumatically Driven, Disposable, Soft Robotic Gripper Equipped With Multi-Stage, Retractable, Telescopic Fingers, IEEE Transactions on Medical Robotics and Bionics, 2021.

Chapter 2

Apparatus

2.1 Motion Capture Systems

This section presents the motion capture systems used in this work for tracking object motions and robot finger trajectories.

2.1.1 Retro-Reflective Motion Tracking Systems

The retro-reflective motion tracking system employed the Vicon motion capture system composed of 8 MX-T series cameras (Fig. 2.1), which provides optical tracking of objects/ bodies through retro-reflective markers. The recordings are collected through a PC connected through a Giganet system providing xyz displacements and rotations in Euler angles or quaternions. The sampling rate of the device is 100 Hz. Other sensors and devices can also trigger the system to facilitate the synchronization of different data collection systems.

Figure 2.1: Vicon motion capture camera.

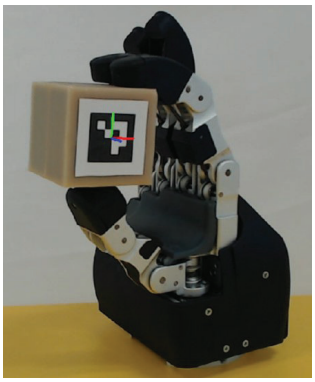

Figure 2.2: Example of motion capture using fiducial markers to capture object position and orientation during a manipulation task.

2.1.2 Fiducial Marker Base Motion Tracking

An alternative optical motion capture system is the utilization of fiducial markers. A webcam is used to track the fiducial markers, which contain particular patterns that allow them to be identified within the webcam's vision. The patterns followed the ArUco class [23] of fiducial markers. The OpenCV version [24] of the ArUco library was used to estimate the 6-DOF pose of the markers with respect to the camera frame. The webcam used was a Logitech C922 Pro Stream HD webcam recording video at 1080p resolution at a rate of 30 Hz.

2.1.3 Magnetic Motion Capture Systems

In scenarios where occlusion of the markers for tracking during grasping and manipulation tasks could be an issue, the Polhemus Liberty magnetic motion capture system (Fig. 2.3) was employed. The magnetic motion capture system uses a source that emits an electromagnetic field for sensors within its range to detect, to determine the position and pose. The liberty system is capable of equipping up to 16 sensors that can either be standard or micro in size. The system's sampling rate is 240 Hz with an accuracy of 0.76 mm in position and 0.15 deg in orientation. Interfacing with the device was done through the supplied proprietary software provided by Polhemus or through an open source Robot Operating System (ROS) [25] based driver.

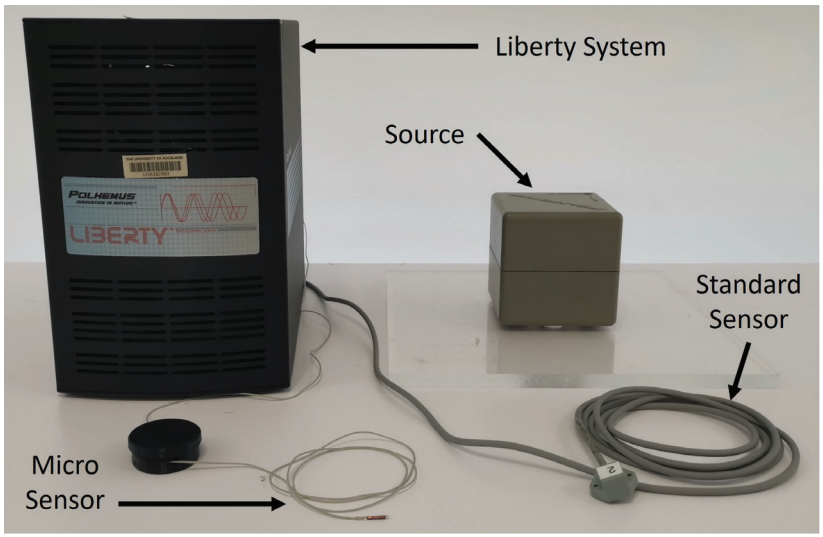

Figure 2.3: The magnetic motion capture system is composed of a Polhemus Liberty system, a source, and sensors. Two different sensor sizes (micro and standard) are supported.

2.2 Force Measurements

2.2.1 Pull Force Recordings

Pull force experiments were conducted to evaluate the stability of grasped objects in soft robotic grippers and hands, which can easily deform under load. The Robotiq FT300 force torque sensor (Fig. 2.4) was used to measure the minimum pull force required to remove a grasped object from a gripper for different shaped objects. The sensor has a sampling rate of 100 Hz and a force and moment range of $\pm$ 300 N and $\pm$ 30 Nm.

Figure 2.4: Robotiq FT300 force torque sensor.

Figure 2.5: Two different dynamometers were used to collect grasping forces. Subfigure a) presents the Biopac MP36 data acquisition unit (Biopac Systems, Inc., Goleta, California) with a SS25LA dynamometer. Subfigure b) shows another dynamometer, which uses straight bar load cells for reading the force values.

2.2.2 Grasp Force Measurements

Precision and Power grasp forces of the developed robot grippers and hands were collected through a Biopac MP36 data acquisition unit (Biopac Systems, Inc., Goleta, California) through the use of a SS25LA dynamometer (Fig. 2.5a). The device had a sampling rate of 100 kHz and was able to evaluate grasp forces between 0 to 490 N. Additionally, straight bar load cells capable of reading a max force of 981 N were used to develop dynamometers (Fig. 2.5b) that could be used to measure power grasp forces following the guidelines provided by the National Institute of Standards and Technology (NIST) [26].

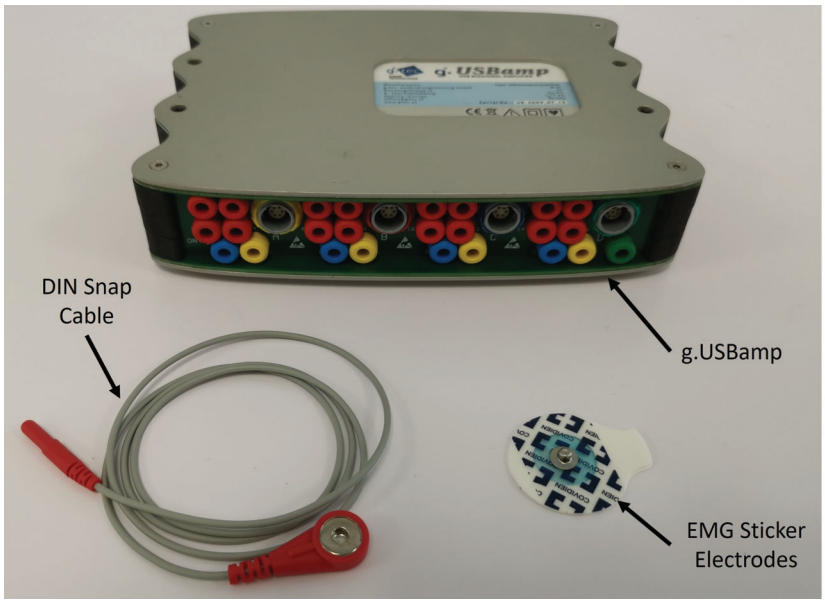

Figure 2.6: The g.USBamp consists of a 16 channel bioamplifier that uses DIN snap cables to connect the EMG sticker electrodes to the bioamplifier.

2.3 Bioamplifiers

2.3.1 g.USBamp

The Guger Technologies (g.tec) g.USBamp (Fig. 2.6) contains 16 monopolar EMG channels, which can be configured to acquire 8 bipolar channel sets. The bioamplifier supports onboard notch and bandpass filtering, resulting in a maximum sampling rate of 64 Hz. Collecting the bio-signals involves attaching disposable EMG sticker electrodes, which each contain conductive gel (Ag/AgCl) to ensure high quality signals are collected. C++ drivers with a ROS wrapper [27] was used to interface with the bioamplifier for controlling the developed robot hands.

2.3.2 Myon 320

The Myon 320 wireless surface EMG bioamplifer was used to acquire the muscle signals for tasks requiring an increased range of motion. The system supports up to 16 transmitters, each composed of a bipolar electrode pair. Similar to the g.USBamp and disposable EMG sticker electrodes were used. The system's sampling rate is 4000 Hz per channel with a 30 m wireless operating range.

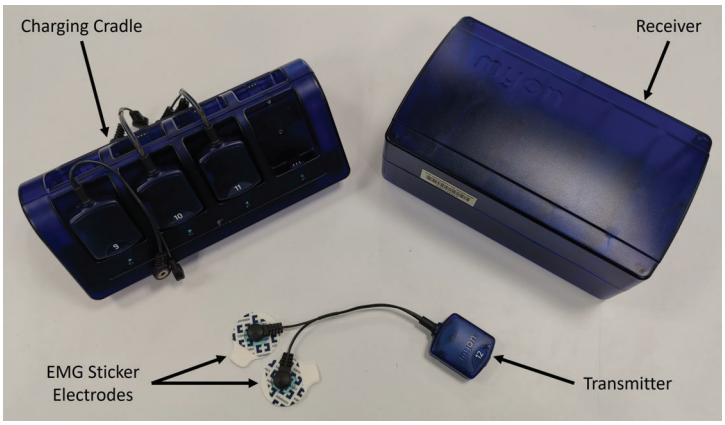

Figure 2.7: The Myon 320 is a wireless bioamplifier composed of a receiver and transmitter to acquire the signals. An accompanying charging cradle facilitates the charging of the transmitters. EMG sticker electrodes are used to attach the transmitter to the surface of the user's muscles.

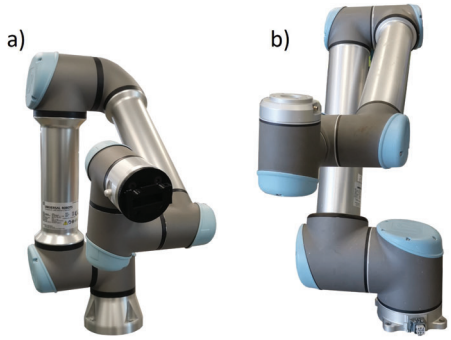

Figure 2.8: Collaborative robot arms by Universal robots: a) UR5e and b) UR10.

2.4 Robotic Arms

2.4.1 Universal Robot Arm

The developed grippers and hands were mounted on collaborative, 6 DOF robot arms by Universal Robots. The majority of the work is conducted with the UR5 and UR5e models (Fig. 2.8a) of the robot arms with payload capabilities of 5 kg, reach of 850 mm, and speed of 1 m/s. The UR10 robot arm (Fig. 2.8b) was utilized for experiments requiring a larger workspace and payload carrying capacities. The payload of the particular arm is 10 kg with a reach of 1300 mm and a speed of 1m/s. The arms were controlled via kinesthetic teach through the teach pendant of the arm, and for more complex tasks, ROS was employed.

Figure 2.9: Mitsubishi Melfa RV-4FRL industrial robot arm.

2.4.2 Mitsubishi Melfa RV-4FRL Robot Arm

An alternative arm used was the Mitsubishi Melfa RV-4FRL robot arm (Fig. 2.9), capable of holding a max payload of 4 kg and moving at a speed of 9048 mm/s. The arm was controlled via the teach pendant or ROS to execute tasks.

Figure 2.10: The YCB object set was used to assess the grasping capabilities of the grippers. Some of these objects can be seen on the left of the figure. Accompanying the YCB object set, other heavy, soft, fragile, and medical related objects were used (right side of the figure).

2.5 Object Set for Grasping

The grasping capabilities of the different robot grippers and hands developed in this work were assessed with the YCB object set [28]. The YCB object set is composed of 77 objects, which can be divided into objects related to Food,

kitchen, tool, shape, and task items encompassing a variety of everyday life tasks. Additionally, 15 objects not included in the YCB object set were also added to evaluate the gripper's performance in handling heavy, soft, and medical related objects. Table 2.1 presents the dimension and the weight of the objects. Some of the different objects selected for evaluating the gripper can be seen in Fig. 2.10.

Table 2.1: External object set properties

Objects	**Dimension (mm)**	**Weight (g)**
Egg	60 x 45 x 45	335
Cherry	30 x 27 x 24	66
Syringe	105 x 30 x 21	41
Petri Dish	84 x 84 x 16	40
Bandages	79 x 28 x 28	39
Used Glove	133 x 110 x 25	28
Used Tissue	80 x 85 x 67	22
Used Mask	175 x 95 x 1	13.7
Tweezers	143 x 12 x 13	147
scalpel	140 x 12 x 5	122
Chemical Jar	180 x 45 x 45	2930
1.5 L Water Bottle	305 x 88 x 88	1523
Wood Block	89 x 89 x 123	2332
Sponge	212 x 58 x 102	103
Socks	50 x 80 x 270	143

2.6 Modular, Accessible, Sensorized Objects

2.6.1 Background

With the ever-increasing presence of robotic agents in factory and home environments, significant industrial and research efforts have been put into the development of dexterous robot hands and grippers. Such end-effectors offer robust grasping and dexterous, in-hand manipulation capabilities that increase the system's efficiency, precision, and adaptability to different task requirements. Even though equivalent dexterity from an object-centric viewpoint could possibly be achieved by a dexterous robot arm paired with a simple gripper, a dexterous end-effector is often more appropriate [29]. Good examples are tasks that require in-hand tool re-orientation (without re-grasping) or tasks in cluttered environments where arm motion is heavily constrained.

Figure 2.11: The proposed sensorized object set consists of primitive shapes in three sizes that can be reassembled in various combinations. The surface friction and stiffness can be selected by employing different molding materials. Object halves contain cavities enabling the adjustment of weight and weight distribution in objects. The object set has been designed to be compatible with a variety of motion capture sensing options such as the magnetic motion capture micro-sensors of the Polhemus Liberty, retroreflective markers for tracking with an optical motion capture system (e.g., Vicon), ArUco markers that can be tracked with a camera, or an inertial measurement unit (IMU).

Currently, many dexterous end-effector variants are available to a robot system designer, ranging from anthropomorphic hands [2, 30, 31], to more task-oriented grippers [32, 33]. Even though each design is generally accompanied by a range of tests and experiments highlighting selected performance aspects, it remains challenging to assess which hand is most appropriate for a specific application. This is particularly relevant for tasks that require a certain degree of in-hand manipulation capability, where a unified performance evaluation standard is yet to be adopted. Defining meaningful benchmarking methods for in-hand manipulation is difficult because the protocols are closely linked to the objects used in the tests. Manipulation tasks generally involve complex physical phenomena that cannot be appropriately evaluated in a simulated environment. Hence, challenging and time-consuming real life experiments are required to obtain reliable results.

Thus, when defining a benchmark, it is important to choose an appropriate object set that has the following characteristics:

1. **Allow for Efficient Pose Tracking:** Unlike grasping, in-hand manipulation performance can rarely rely on discrete success metrics, so precise object motion tracking is of paramount importance for the creation of useful benchmarks. The object set should therefore be able to accommodate some form of motion capture technology, which is absent in most existing sets.

2. **Provide a Minimal, Sufficiently Diverse Solution:** The object set needs to be diverse enough to cover the broad range of applications and compact enough to permit fast and effortless testing and experimentation. A minimal set will also allow for easy storage.

3. **Provide Accessibility:** A condition for widespread adoption of unified benchmarking frameworks is that the object set used should be easily accessible to users and research groups anywhere in the world.

This section presents a modular, sensorized object set for assessing the grasping and dexterous, in-hand manipulation capabilities of grippers and hands. To facilitate object motion tracking, the set is equipped with modules that can accommodate various motion capture markers or sensors. These removable sensor mounts are designed to have a negligible effect on the objects' inertia and to minimally obstruct their motion. The size vs diversity trade-off is solved through a modular design, allowing the user to mix and match object parts and obtain a large selection of different shapes from a small number of initial components (minimal set). The objects contain cavities that can be utilized to adjust their weight and its distribution, if required. The objects come in rigid and soft surface variants, allowing the user to assess performance with different contact conditions. The set solves the accessibility issue by employing common rapid prototyping methods in its fabrication process and making use of easily accessible materials. The design and manufacturing instructions are made available in an open source manner.

Even though the main application of the proposed object set is gripper and hand performance assessment, it is also suitable for a wide range of alternative use cases. Beyond providing quantitative measures for hand capability and dexterity comparisons, the objects can be of great use in human arm or hand rehabilitation and clinical assessment. The patient's level of recovery can be effectively monitored and used as a basis for designing case-specific training sessions that focus on weakened muscle groups as the objects are compatible with several types of motion capture systems, they allow for efficient comparison of tracking performance[1].

[1]Majority of the section is based on [16], © 2020, IEEE. Reprinted, with permission, from Geng Gao, Gal Gorjup, Ruobing Yu, Patrick jarvis, and Minas Liarokapis, Modular, accessible, sensorized objects for evaluating the grasping and manipulation capabilities of grippers and hands, IEEE Robotics and Automation Letters, 2020.

2.6.2 Related work

For dexterous robotic hands, the majority of object set resources focuses on grasping and manipulation that largely depend on robot arm dexterity. Although some of the previously proposed objects are equipped with motion tracking capabilities and tactile sensors, there are no examples of easily accessible, modular, sensorized solutions. Moreover, most of the object sets proposed are mainly used to evaluate the grasping capabilities of both grippers and hands and not their efficiency in executing dexterous manipulation tasks.

Even though object sets are necessary for reliable evaluation of a robot's manipulation performance in the real world, only a few are clearly defined and available to the research community. The YCB object set [34] is a set of 75 objects and their corresponding 2D image and 3D model data. The set is aimed at benchmarking the capabilities of robot end-effectors for a wide range of tasks and consists of everyday life objects, objects used in assembly tasks during medical rehabilitation, and objects for industrial robotic applications. It is currently the most well-known and complete object set available that focuses mainly on quantifying a robot arm-hand system's ability to grasp and manipulate objects. The set can also be augmented with visual markers for in-hand manipulation [35], although this is not the collection's primary purpose. The YCB object set is readily available upon request. Another list of physical objects was presented within the frame of the Amazon Picking Challenge [36], where the picking task was perception oriented and object models were not provided. Building on the former, the ACRV Picking Benchmark [37] defines a set of 42 common objects and their labeled images for an extended shelf picking benchmark.

Although they are not part of a standard set, some instances of individual sensorized objects for assessing grasping and manipulation capabilities of human and robot hands have been developed. In [38], two instrumented objects for investigating human grasp properties were presented. The objects were designed to assess only three-finger grasp configurations, focusing on contact force measurements. In [39], the authors presented an object equipped with tactile and motion tracking sensors, which was in [40] utilized to evaluate human grasp quality. These are not readily available to the research community and their manufacturing procedures are not trivial, making widespread adoption difficult.

An object collection that was not explicitly defined, but is perhaps the closest to this proposal, was employed within a standard defined by NIST [26], which was further explored in [41]. The standard presents the foundations for robot hand

performance benchmarking and among others includes protocols for quantifying in-hand manipulation and object pose estimation. Although the benchmark recognises the importance of object shapes and properties on dexterous manipulation performance, it does not define a standard set to be used in the experiments. It does, however, advise that the tests should be conducted across a range of diverse objects. Their examples include a cube, sphere, and cylinder that have been retrofitted with reflective markers for tracking with a visual motion capture system. The external marker mount is quite large compared to the objects, affecting their inertial properties and possibly hindering the execution of certain in-hand manipulation motions. To address those issues, the objects proposed in this work are equipped with motion capture sensors in a way that preserves the object shape and inertia characteristics.

A number of data sets that consist of object scans, images, and models have also been proposed. These are appropriate for experiments and planning in simulation, or as training sets for various machine learning algorithms. BigBIRD [42], for instance, features a data set providing high quality image and 3D point cloud data for each of its 125 objects. Another example is the KIT object models database [43], which is targeted at applications in service robotics. It consists of 3D point cloud data, aligned with 2D images for over a hundred typical household items. A large-scale endeavor aimed mainly at grasp planning is the Columbia Grasp Database [44], which provides 3D models of roughly 8000 objects, along with successful grasp labels for many robot hands.

2.6.3 Modular, Sensorized Objects

In this work, a range of modular, sensorized objects is created by combining a set of primitive object shapes. The structures of the sensorized objects consist of five to thirteen modular, 3D printed parts. In particular, the list is as follows: a plastic screw (which holds the object parts together), two object halves, two removable urethane marker mounts, and eight removable object weights (these are optional components). Such a structure is depicted in Fig. 2.12, subfigure a). The proposed objects can be created with a variety of materials that facilitate the selection of the desired object stiffness and friction, and they can be equipped with different motion tracking markers and sensors.

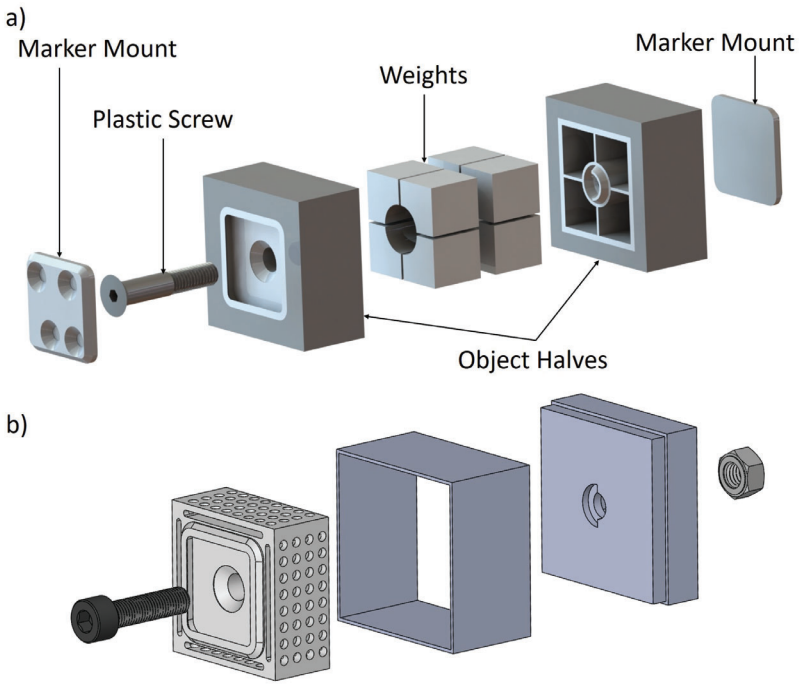

Figure 2.12: The proposed construction of the modular, sensorized soft cube is depicted in subfigure a). Starting from the left of the figure, the sensorized object consists of a urethane based retroreflective marker mount, a plastic screw, one object half, the object weights, the other object half, and another urethane based retroreflective marker mount. The urethane mount houses four retroreflective marker sockets that are configured asymmetrically, to allow reliable 6 DOF (degrees of freedom) pose tracking with an optical motion capture system (e.g., Vicon). To minimize occlusion issues, the mounts are placed on opposing object faces. Subfigure b) shows the exploded view of a mold for a soft cube.

2.6.3.1 Object Geometries

The object set consists of sphere, cube, and cylinder object halves (the cylinder is split both axially and radially), which can be joined together to form a combination of diverse objects for grasping and manipulation experiments (see Fig. 2.13). The different shape combinations are based on a minimal number of parts that achieves a diverse set of simple and complex geometries. Geometries with sharp bends or corners (the objects of Fig. 2.13d) force end-effectors to perform more complex manipulation motions like finger gaiting [45] or to maneuver around the object geometry in order to reach certain object surfaces. Such complex motions give to the researchers' insight into how certain hands or grippers will behave when

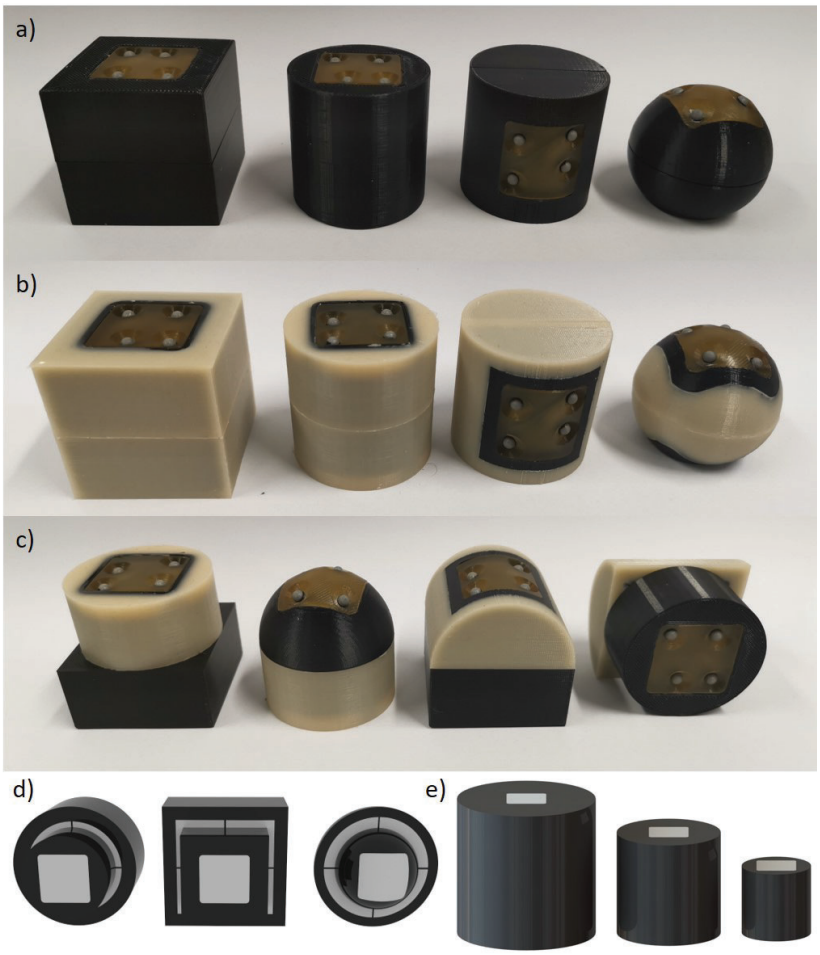

Figure 2.13: Subfigures a) and b) present the primitive shapes of proposed rigid and soft sensorized object variants, respectively. Subfigure c) demonstrates examples of irregularly shaped configurations obtained by combining the modules. Subfigure d) shows a set of objects with varying sizes that can be used with hands of different sizes.

handling geometrically complex objects. Additionally, three object sizes have been developed to be used with a wide range of hand and gripper sizes. The three sizes for cylindrical objects can be seen in Fig. 2.13e and all object dimensions can be found in Table 2.2.

2.6.3.2 Material Selection

Each object half contains four compartments, which can be filled or left empty to generate various controllable weights and variations of the center of mass in

Table 2.2: The dimensions of the proposed sensorized objects for different object sizes and geometries.

Object Geometry		**Dimensions [mm]**
Small	Cube	50 x 50 x 50
	Cylinder (Radially Split)	50 x 50
	Cylinder (Axially Split)	50 x 50
	Sphere	50
Medium	Cube	75 x 75 x 75
	Cylinder (Radially Split)	75 x 75
	Cylinder (Axially Split)	75 x 75
	Sphere	75
Large	Cube	100 x 100 x 100
	Cylinder (Radially Split)	100 x 100
	Cylinder (Axially Split)	100 x 100
	Sphere	100

an object. The introduction of an easily tunable center of mass in the proposed objects allows for rapid adjustment of the experimental conditions while assessing the robustness and dexterity of a hand, by altering a single object characteristic.

The achievable mass variations depend on the density of the selected material. The maximum achievable weight deviations of the proposed sensorized objects for different materials can be found in Table 2.3. It must be noted that when using a magnetic motion capture system, metallic weights must be avoided. Surface friction and hardness can be varied in different object halves by combining different elastomer materials molded onto the rigid part. Elastomer materials with Shore hardness of 30A (Youngs Modulus of 1.07 MPa) and above (like urethane rubbers, e.g. Smooth-On Vytaflex 30) are all compatible materials for producing various surface frictions and stiffnesses.

Table 2.3: Maximum achievable weight deviations of the proposed sensorized objects. All objects are considered to be solid (non-hollow). Different materials can be chosen for the fabrication of the object set.

Object Geometry		**Max Internal Weight Deviation [g]**				
		PLA	ABS	PETG	Resins	Aluminium
Small	Cube	42.56	35.70	47.36	39.47 - 42.90	92.66
	Cylinder (Radially Split)	27.97	23.46	31.13	25.94 - 28.20	60.91
	Cylinder (Axially Split)	29.07	24.38	32.35	26.96 - 29.30	63.29
	Sphere	17.26	14.48	19.21	16.01 - 17.4	37.58
Medium	Cube	248.20	208.17	276.22	230.18 - 250.20	540.43
	Cylinder (Radially Split)	167.65	140.61	186.58	155.48 - 169.00	365.04
	Cylinder (Axially Split)	183.12	153.59	203.80	169.83 - 184.60	398.74
	Sphere	148.40	124.47	165.16	137.63 - 149.60	323.14
Large	Cube	731.40	613.43	813.98	678.32 - 737.3	1592.57
	Cylinder (Radially Split)	517.72	434.22	576.18	480.15 - 521.90	1127.30
	Cylinder (Axially Split)	544.21	456.44	605.65	504.71 - 548.60	1184.98
	Sphere	422.79	354.60	470.52	392.10 - 426.20	920.59

2.6.3.3 Fabrication / Assembly Process

To increase accessibility, rapid prototyping methods like hybrid deposition manufacturing (HDM) [46] and 3D printing were utilized. These techniques employ a simple fabrication process and allow for efficient integration of various materials (e.g., polylactic acid (PLA), Acrylonitrile butadiene styrene (ABS), resin, etc.). The object set can thus be made in a short time frame while remaining affordable.

3D Printing Components The rigid bodies and molding components of the proposed sensorized objects are produced through 3D printing. Object halves with rigid outer surfaces (PLA or ABS material) are printed directly and do not require additional molding steps. Object halves with compliant, elastomer surfaces and alternative friction properties require 3D printing of various molds and inner object cores that facilitate molding. The inner object cores are designed as object halves with a porous outer wall that anchors the elastomer material in place.

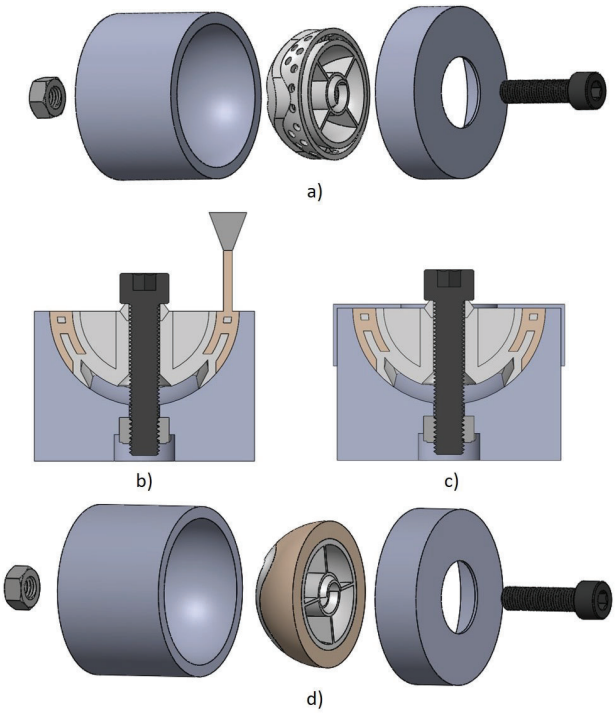

Figure 2.14: Molding process for creating a soft-surface sphere half. Subfigure a) displays the assembly of molding components for a soft sphere half. Subfigures b) and c) present the deposition process, where elastomer material is injected into the cavity of the mold and then sealed to achieve the required outer surface. Subfigure d) shows the disassembly after the elastomer material has been cured.

Mold Assembly Depending on the module being fabricated, the mold assembly steps can vary from preparation of a single mold part, to the assembly of several mold components around a soft object core (as it can be seen in Fig. 2.14a) for the material deposition step.

Deposition Once a mold is assembled, the elastomer material is deposited into the mold cavity, as depicted in Fig. 2.14b. The elastomer can be used to produce appropriate mounts for attaching retroreflective markers or ArUco markers, or to cover the object halves, providing varying object surface properties.

Mold Disassembly After the curing process is completed, the molded components can be removed from the molds and assembled together with the other 3D printed parts to produce a complete object, as shown in Fig. 2.14d.

Table 2.4: Comparison of different motion capture systems.

Motion Capture System	**Accuracy**		**Noise**		**Sampling Rate** [Hz]
	Translation [mm]	**Rotation** [deg]	**Translation** [mm]	**Rotation** [deg]	
Optical Motion Capture	0.076 - 0.129	0.48 - 0.82	0.015	0.095	100
Magnetic Motion Capture	0.76	0.15	0.017	0.05	240
ArUco Markers	1.90 - 2.17	0.59 - 1.12	0.77 - 5.57	0.076 - 0.26	30
IMU	N/A	1.25	N/A	0.055	104

The CAD and STL files of the sensorized objects, as well as detailed fabrication and assembly instructions, can be found at the following URL:

https://github.com/newdexterity/Sensorized-Objects

2.6.3.4 Sensing

The object set was made compatible with four motion capture system types that allow accurate trajectory tracking. The first is an optical motion capture system (e.g., Vicon), which utilizes retroreflective markers for tracking the object pose, as seen in Fig. 2.15a. The second is a magnetic motion capture system (e.g., Polhemus Liberty), the micro sensor of which can be mounted inside a properly designed plastic screw (Fig. 2.15b), reaching the center of the object. The third is based on an inertial measurement unit (IMU), along with a microcontroller and bluetooth module (Ardunio NANO 33 IoT), powered by a 180 mAh lithium polymer battery. These components are fixed within the object half with dedicated cavities, as depicted in Fig. 2.15d. The IMU system is accompanied by sample Arduino code that performs orientation tracking using the Madgwick filter [47] and publishes the angles through Bluetooth. Position tracking with the IMU system was not implemented due to the high sensitivity to acceleration error in the double integration process. In case none of the first three systems is available to the users, a set of marker mounts compatible with Augmented Reality (AR) tags or ArUco markers is provided (Fig. 2.15c).

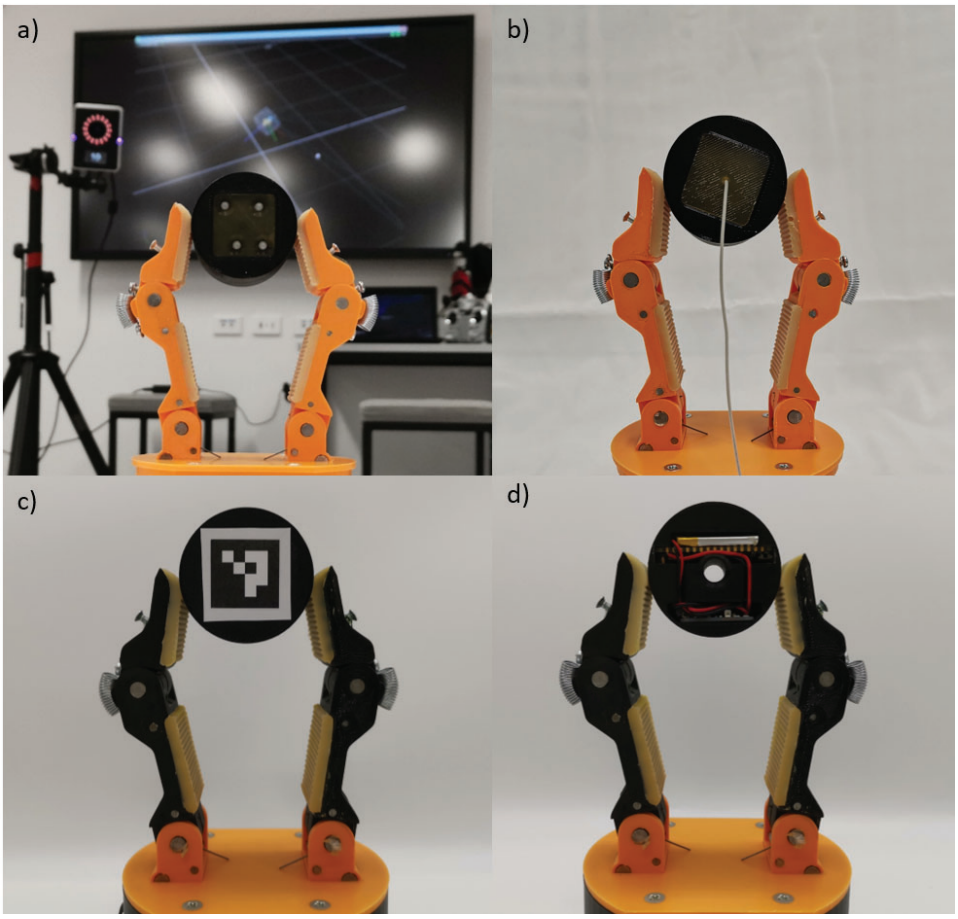

Figure 2.15: Instances of an experiment conducted with a sensorized object and a simple, two fingered gripper executing an equilibrium point manipulation task. The object motion tracking is accomplished with: a) the Vicon optical motion tracking system that utilizes reflective markers, b) the Polhemus Liberty magnetic motion capture system that employs a micro sensor inserted in the object core through the urethane pad, c) the ArUco marker attached to a urethane pad tracked through a standard web camera, and d) the IMU attached inside an object half.

A comparison of the supported motion capture systems characteristics is presented in Table 2.4. The translation accuracy and noise (precision) for the optical motion capture system (Vicon) were obtained from [48]. The rotation accuracy and noise values for the Vicon system were estimated with respect to the retroreflective marker separation on the sensor pad. The accuracy values for the magnetic motion capture systems were obtained from the Polhemus Liberty user manual [49]. The noise values for the magnetic motion capture system were obtained from static sensor measurements. The accuracy and noise characteristics for AR tag-based

motion tracking were obtained experimentally, using the ArUco class of fiducial markers [23] and a Logitech C922 Pro Stream HD webcam with 1080p resolution at 30 frames per second. A marker of size 25 mm was attached to a sensorized cube and tracked with the webcam. The cube was simultaneously tracked with the Vicon system, which was chosen as the ground truth. For this purpose, larger Vicon markers were placed with higher separation along the object to ensure higher tracking accuracy. The translational accuracy was estimated by linearly offsetting the cube and comparing the distances measured by the two systems. The rotational accuracy was estimated by rotating the cube by 90 degrees along a fixed axis and comparing the measured angles. The translational and rotational noise was computed as the standard deviation of the position and angle offsets from the mean estimated pose in a static configuration. The accuracy and noise experiments for the ArUco markers were performed at 20 cm and 100 cm from the camera. The rotation accuracy and noise for the IMU system were obtained in a similar fashion, using the Vicon system as reference.

Depending on the manipulation task, the best suited motion capture system could change. For instance, the optical motion capture system (Vicon) offers data with the highest accuracy and a low amount of noise. However, when conducting more complex manipulation motions such as caging manipulation, the markers may be covered by the hand, causing occlusions and affecting the data collection process. This effect can also be observed in the AR tags and ArUco markers, where the tags and markers must be visible to the camera. The magnetic motion capture system (Polhemus Liberty) mitigates the occlusion issue of the previous two systems, but is sensitive to the presence of large metallic objects. The thin micro-sensor cable of the magnetic motion capture system may impact the object dynamics if there is tension on the cable, and may obstruct the hand's motion when performing certain manipulation tasks. The IMU system does not suffer from occlusion issues and can operate untethered, but it cannot be accommodated by all object sizes (e.g., the small rigid sphere, and the small soft objects range) due to size limitations of the employed electronics (i.e., microcontroller board, battery, and step-up regulator). Another disadvantage of the IMU system is the significant drift that affects position tracking. The distinct disadvantages of the four examined motion capture systems can be mitigated by taking advantage of the multi-modal sensing capabilities of the proposed sensorized object set. By combining different classes of motion capture approaches, the quality and accuracy of the captured data can be significantly improved. For instance, a low-cost solution for full object pose tracking can rely on AR tags and the IMU, fusing the two

data streams to compensate for occlusion and drift issues of the separate systems. The proposed object set does not incorporate force sensing modules to preserve fabrication simplicity, object size, and overall accessibility. Furthermore, the lack of such additional sensors allows the set to be highly reconfigurable and maintain a low cost. Even though measuring force values and profiles is essential for many manipulation tasks, there are several aspects of dexterous, in-hand manipulation that can be effectively assessed purely through object pose tracking and object kinematics. For such applications, the proposed object set is very well suited.

2.6.3.5 Object Models

The objects were designed in the SolidWorks CAD software, and the resulting source models were made available through the accompanying sensorized objects website and repository. Disseminating source designs allows for fast parameter modification and extraction, facilitating community involvement in improving and evolving the object set. The repository also contains STL models of all objects, which can be readily used with various rapid prototyping methods. In addition, the models can be used as collision objects in various planning frameworks, as well as for point cloud registration in perception systems. Combined with the provided mass and surface material data, the object models can also be effectively utilised in simulated environments. They are very well suited for simulation-to-reality applications, as their integrated tracking capability enables straightforward comparison between simulated and real trajectories.

2.6.4 Functional Demonstration

The pose tracking capability of the sensorized objects can be used to give insight into the ranges of motion, repeatability, and drift of the system. It can be employed to assess and compare the performance of robot grippers, as well as human hands, as depicted in Fig. 2.16. The objects can also provide pose feedback to the hand to quickly test closed-loop control algorithms. Through the highly accessible and customizable shapes and weights of objects that the proposed set offers, the time needed to prepare experimental examples can be significantly reduced.

For demonstration purposes, a performance assessment of the NDX-A* hand [50] was conducted, as presented in Fig. 2.17. The demonstration examines the robot hand's robustness in executing a combined rolling and translation manipulation motion over 10 cycles with a chosen sensorized object. The hand's performance was assessed in terms of drift and repeatability for the executed ma-

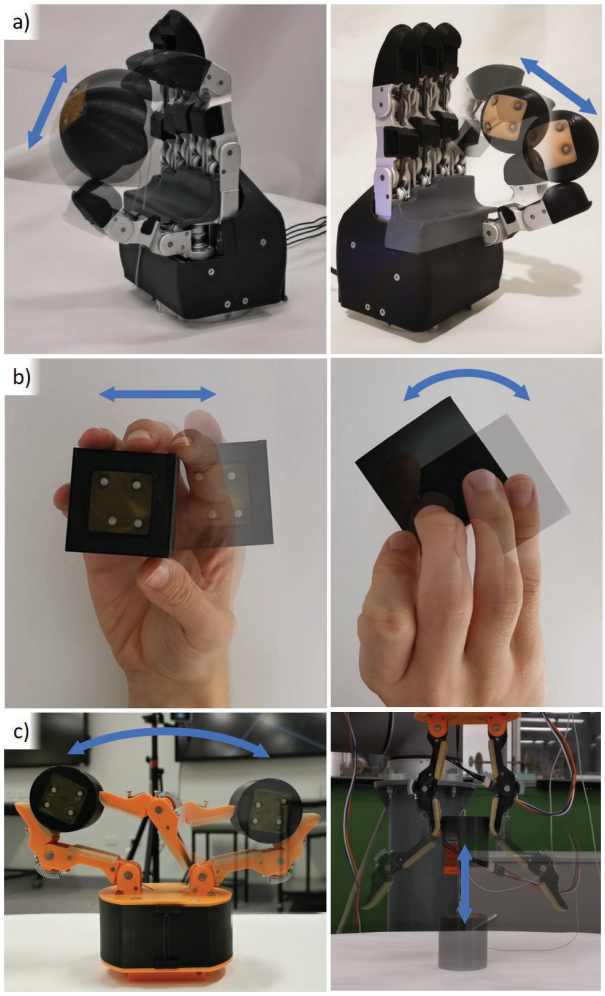

Figure 2.16: The functional demonstration shows various objects from the sensorized object set being manipulated with different in-hand manipulation strategies by different hands and grippers. Subfigure a) displays an NDX-A* robot hand [50] performing fixed point and rolling manipulation motions. Similarly, subfigure b) shows in-hand translation and rotation tasks executed by the human hand. The T42 gripper [51] is used to perform manipulation, as well as grasping and releasing experiments in subfigure c).

nipulation motion, computed from the cycle endpoints. Drift was computed by averaging the positional and rotational differences between subsequent endpoints. Repeatability was calculated as the average positional and rotational difference between the initial endpoint and the drift-corrected cycle endpoints. The experiments were performed with a small rigid-surface sphere and a soft-surface sphere without additional weights, tracked with the Polhemus Liberty motion capture

system. Although the robot hand is composed of metallic components, the noise can be significantly minimized by ensuring the magnetic sensor is close to the Polhemus source and by avoiding grasps that enclose the sensor in metal, such as caging grasps. The results (Table 2.5 and Fig. 2.17) can give insight into whether a certain end-effector is suitable for a chosen task based on the maximum acceptable error for that task. Furthermore, they can be used for diagnosing slip in the system through controlled variation of individual object and motion characteristics, in this case the surface compliance. For instance, the obtained drift results indicate a need for increased finger pad friction or increased contact forces that should be exerted on the object.

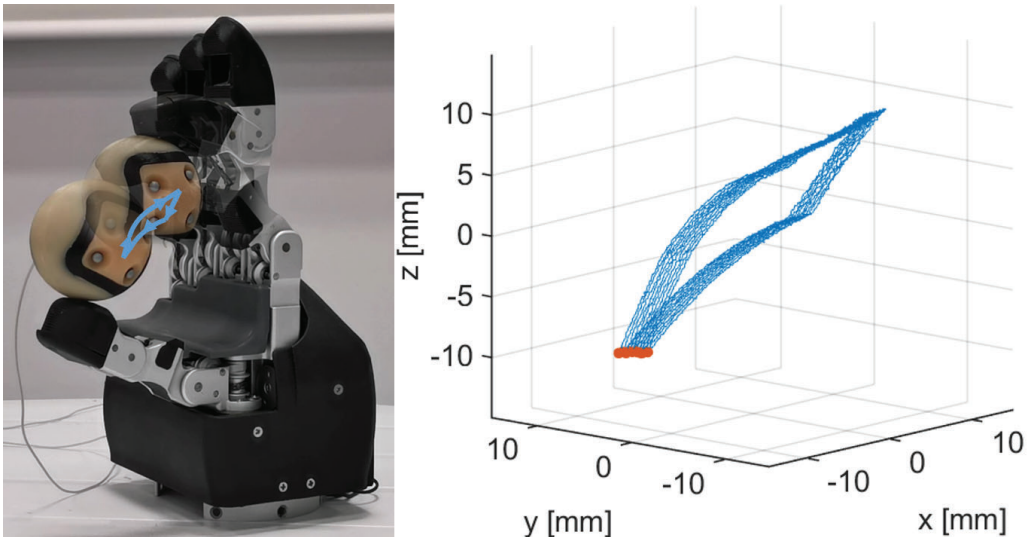

Figure 2.17: Experimental data of a manipulation task executed with a soft sphere and the NDX-A* robot hand. Ten trials of the manipulation task have been executed. Cycle endpoints (highlighted in red) enable a holistic assessment of the repeatability and drift. Such data also allows the user to assess the performance and dexterity of the employed gripper or hand.

A webpage presenting the object set and a video with experiments can be found at the following URL:

http://newdexterity.org/sensorizedobjects

2.6.5 Conclusions and Future Directions

This work focused on a modular and accessible sensorized object set for benchmarking the grasping and dexterous, in-hand manipulation capabilities of human

Table 2.5: Manipulation repeatability and drift for two different object surfaces for a spherical object.

Manipulation Results		**Rigid Surface**		**Soft Surface**	
		Mean	**Standard Deviation**	**Mean**	**Standard Deviation**
Repeatability	Translation [mm]	0.26	0.18	0.21	0.12
	Rotation [deg]	1.27	0.59	0.4	0.14
Drift	Translation [mm]	0.33	0.14	0.22	0.11
	Rotation [deg]	2.35	0.01	0.87	0.002

and robot hands. The object models, fabrication processes, and assembly information have been discussed and have been made publicly available. A series of experiments involving the proposed sensorized objects have been conducted and paradigmatic experimental data has been presented. Regarding future directions, the object set can be extended to include additional shapes and softer surface materials. As the set is modular, this would exponentially increase the number of possible configurations and testing conditions. The object collection can also be adapted to allow assessing tasks closer to real-life applications, such as screwing, pouring, and insertion. Implementation of a set of accompanying benchmarks and protocols can enhance the utilization of the object set and give researchers additional ways in which the objects can be used. Another possible direction would be to add force sensing capabilities to the proposed objects.

Part II

Adaptive Grippers and Hands for Robotic Systems

Chapter 3

A Multi-Modal Gripper for a Flexible Robotic Assembly System

3.1 Background

Recent advancements in robotics and industrial automation have laid the groundwork for manufacturing processes that are faster, safer, and more cost-effective. Low production costs, increased efficiency, and a reduction in faulty products are the results of high speed and reliability associated with utilizing robotic systems. Worker health and safety are also protected by automated production, which reduces the danger of work-related musculoskeletal illnesses [52, 53]. Although robotic systems have a high customization potential, robotic systems still require a significant amount of time and effort to deploy and reconfigure [54]. As a result, small and medium-sized businesses, which generally have low production volumes and rapidly changing job requirements, find it difficult to access such systems. Furthermore, such businesses generally have limited robotics expertise, meaning systems that are not only adaptable but also simple to configure are required.

Assembly of product components is critical in modern manufacturing, and it is one of the most difficult applications that necessitates a wide range of robotic technologies. Even a simple assembly activity can include a variety of sub-tasks, ranging from component insertions and fastening to cable routing and connections. Different execution strategies are required for these sub-tasks, requiring accurate component localization, sophisticated manipulation, and controlled force exertion.

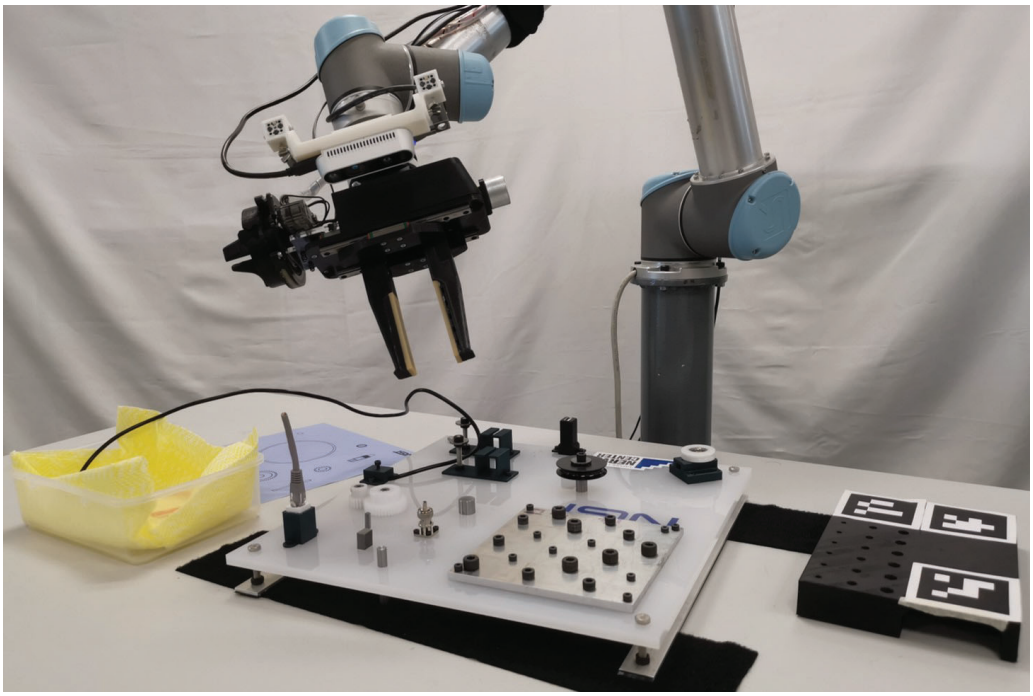

Figure 3.1: The proposed multi-modal gripper and robotic assembly system used for the IEEE/RSJ IROS 2020 Robotic Grasping and Manipulation Competition in the Manufacturing Track category.

Furthermore, completing a task is frequently a requirement for moving on to the next assembly stage. Customized fixtures and jigs are generally the default solution for these problems in order to maintain consistent repeatability during task execution under position and calibration uncertainties. As a result, many industrial solutions utilize task specific end-effectors dedicated for the different components and tasks, which can escalate to numerous end-effector tools and require time consuming tool changing routines. Because such methods are specialized to specific components and assembly layouts, change in the task requirements causes additional development delays and make the overall manufacturing system inflexible.

Smaller batch productions are starting to become the new trend to keep up with the rapid pace of innovation, hence, the flexibility and reconfigurability of robotic assembly systems' is increasingly becoming a crucial feature [55]. This chapter presents a multi-modal gripper for a flexible robotic assembly system that utilizes compliance and CAD localization to perform complex assembly tasks quickly and reliably. A Graphical User Interface (GUI) accompanying the system can be used to quickly identify the component types and categories in new

assemblies, making task sequencing easier. The CAD based localization [56] extracted component poses and assembly information to inform the robot of the necessary assembly tasks and routines with minimal human intervention. The proposed multi-modal gripper design includes a parallel-jaw element, a three-fingered rotating module, and an electromagnet module to reduce retooling time, while providing the robotic assembly system with different grasping and manipulation modalities. Lastly, the gripper's passive compliance and the arm's active compliance guarantee that force profiles are adequate and that minor positioning errors are compensated for [1].

The Robotic Grasping and Manipulation Competition (RGMC), manufacturing track of the 2019 IEEE/RSJ International Conference on Intelligent Robots and Systems (IROS) was used to experimentally evaluate the initial version of the proposed system. Furthermore, magnet-based disassembly processes were tested to assess the improvement on the efficiency of such operations.

3.2 Related Work

There has been a surge in interest in adopting robotic assembly systems to automate industrial operations, resulting in enhanced production speed and efficiency, as well as higher product quality and lower labor costs [57]. Various contests have been created to encourage researchers to produce unique and robust solutions that solve a variety of difficulties in the field of industrial automation and robotic production [58, 59]. These task boards involve handling different tools, visual/ physical obstructions, and various component of differing size and shape.

Teaching and playback has been the default and most prominent method for controlling robots to execute autonomous tasks in industry. When performing teaching, users can kinesthetically displace the robot along desired paths and record its joint values through gravity compensation mode, or simply move the robot via the control of a joystick or teach pendant. Once, recorded these trajectories can be replayed through the controller [60, 61]. Although this solution is simple and quick to program, it lacks flexibility and reusability. This inflexibility of such systems comes from the need to retrain and reprogram whole tasks, when small changes are made on the automated assembly process, which is time consuming

[1] Majority of the chapter is based on [17], © 2021, IEEE. Reprinted, with permission, from Gal Gorjup, Geng Gao, Anany Dwivedi, and Minas Liarokapis, A Flexible Robotic Assembly System Combining CAD Based Localization, Compliance Control, and a Multi-Modal Gripper, IEEE Robotics and Automation Letters, 2021.

and tedious in rapidly changing production processes. Furthermore, depending on the factory tasks to be programmed the user maybe exposed to dangerous environments. Lastly, downtime and production losses will occur during retaining and reprogramming of the robot.

The use of vision-based technologies for detecting and localizing components can increase the flexibility of production tasks. To facilitate object detection and tracking, vision-based approaches can be created utilizing either an image database of the objects or a well-defined geometric model [62, 63]. Additionally, visual servoing can be employed for developing self-aligning end-effectors [64]. An advantage of this methodology over the teach and playback methods is that it can remove the robot programmer from the system configuration phase on the factory floor. However, the need for a large image database in order to train the system to recognize components, limits this teaching strategy and leads to longer setup times. Visual occlusions and environmental lighting are also factors that affect the performance of vision-based systems.

Over the years, Computer Aided Design (CAD) has become a critical component of most product development processes for visualization and simulation. CAD models are utilized to describe exact component geometry as well as positioning information in assembly tasks. Despite their prevalence, many robotic systems that perform manufacturing and assembly tasks do not utilize this information. The collected information from these CAD files can be used in applications ranging from simple component localization to automated planning of entire assembly processes, dramatically increasing the rate of system adaption to innovative products [65]. The training speed and performance of various reinforcement learning algorithms can be improved by using motion plans acquired through CAD-based techniques. The utilization of CAD models can be used to generate stable pose simulations for perception-based systems [66].

Part misalignment induced by positioning or pose estimation uncertainties is one of the most common sources of error in assembly activities. Not compensating for these errors can result in contact forces, that can harm or damage the robot or components of the assembly. Active compliance and force control-based techniques have been proposed by researchers to help address these challenges. Another method for lowering positioning uncertainty is to use dedicated grippers, customized fixtures, and jigs, however, this comes at the cost of longer reconfiguration times. Additionally, the need for frequent retooling when conducting assembly tasks that require a variety of assembly routines can introduce additional delays. Versatile systems can be used to circumvent this problem. In [62],

a general-purpose design with two robot arms, one with a pinching gripper and the other with a rotating gripper was developed. In [67], a gripper combining two different modalities (a parallel-jaw element and a suction module) was used to compete in the Amazon Picking Challenge.

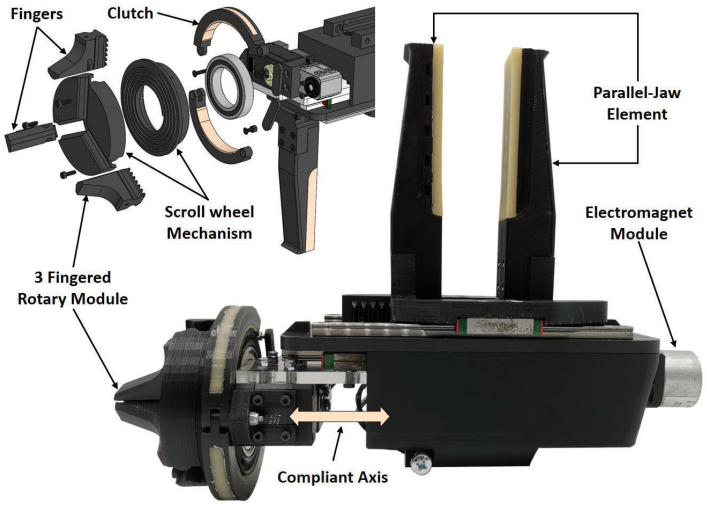

Figure 3.2: An electromagnetic module, a parallel-jaw element, and a three-fingered rotary module are the three elements that make up the gripper. The parallel-jaw component of the gripper has modular fingers with conformable finger pads. Through the use of a rack and pinon gear system, pinching and extension primitives can be achieved with a single motor. When performing insertion activities, the electromagnetic module was designed with a mechanically compliant axis to passively compensate for positioning and localization errors. The three-fingered rotary module was also installed on the compliant translational axis. The rotary module is capable of both rotary motions and grasping tasks enabled by the use of a scroll wheel mechanism and clutch system. The combination of a scroll wheel and a clutch mechanism was used to create a rotary module capable of grasping and rotary motions.

3.3 Gripper Design

Various procedures (e.g., insertion, routing, or threading) are required in manufacturing and robotic assembly activities, with some needing a combination of these skills. Hence, we proposed a novel gripper design that is composed of a parallel-jaw element with an axially compliant, electromagnetic module, and an axially compliant, non-backdrivable three-fingered rotating module. The gripper uses an

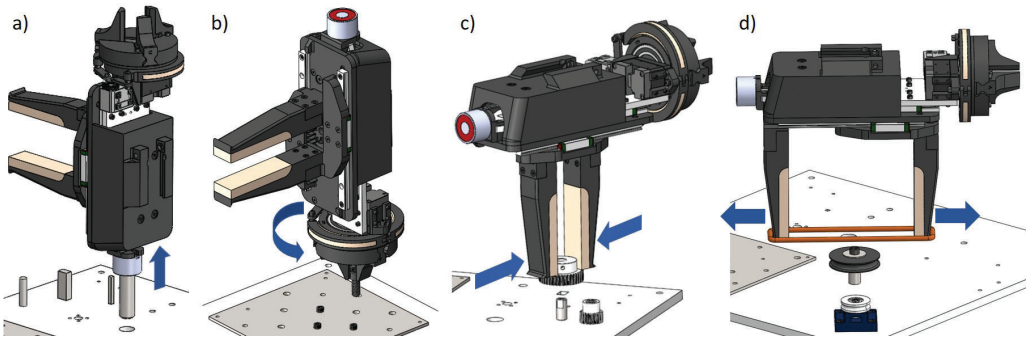

Figure 3.3: The multi-modal gripper is capable of different grasping primitives to facilitate the execution of the different competition tasks. Subfigure a) presents the electromagnet being used to pick up the pegs. Subfigure b) shows the rotary module being used to perform a fastening tasks. Subfigure c) depicts the parallel-jaw module of the gripper being used to grasp and assemble a gear for the insertion task. Subfigure d) presents the parallel-jaw element using the external surfaces of the gripper to perform the extension primitive.

electromagnet and three smart motors for actuation: two Dynamixel XM-430-W350-R, and one Dynamixel XL-320. The gripper's first module is a parallel-jaw element made up of two highly compliant finger pads on modular fingers that allow it to conform to a variety of object geometries. To enable linear opening and closing motions of the fingers a rack and pinion mechanism was employed. An electromagnet is employed to supplement the parallel-jaw element and broaden the existing object manipulation options. To offer both rotation and grasping of objects, the rotation module uses a scroll wheel mechanism to achieve the non-backdrivable characteristic for both grasping and rotation (e.g., for fastening, screwing etc.). The rotary module has a built in clutch mechanism to allow for switching between the grasping and rotary states through a single low torque motor (Dynamixel XL-320). An exploded view of the gripper is shown in Fig. 3.2. To reduce control complexity and correct for positioning errors during assembly, mechanical compliance has been incorporated into the translation axis of the electromagnet and rotating modules. The proposed gripper is capable of executing four complementary grasp primitives. These primitives can be seen in Fig. 3.3 as pinching, extension, rotation, and electromagnetic interaction.

3.3.0.1 Pinch

The pinch grasp primitive accommodates the execution of insertion and wire routing tasks through the two modular fingers of the parallel jaw gripper.

3.3.0.2 Extension

The extension primitive uses the back sides of the fingers (Fig. 3.3d) to apply force to the internal surfaces of objects for grasping (e.g. belt assembly).

3.3.0.3 Rotation

A variety of manufacturing tasks require rotary motion from drilling holes and milling workpieces to screwing and unscrewing bolts. To supplement the parallel-jaw element, a non-backdrivable, three-fingered rotary module is used to accomplish rotary motions. Drill bits, screws, and other rotary tool bits can be securely grasped by the rotary module, which can also rotate continuously in any direction. In the transitional axis of the rotary module structural compliance was incorporated in order to adjust for inaccuracies in the robots trajectories when completing tasks. The max clamping force of the 3D printed rotary module was 23.97 N, which is sufficient to assemble and dismantle the fasteners of the RGMC task boards. By utilizing alternative material (e.g., aluminum) to fabricate the mechanism a higher clamping force can be achieved.

3.3.0.4 Electromagnetic Interaction

Using an electromagnet (Fig. 3.3a), ferromagnetic objects such as metallic pegs can be handled in an efficient manner. The electromagnetic module, like the rotation primitive, is linked to a mechanically compliant translational axis. The electromagnetic module has a greater grasping efficiency for ferromagnetic components (as demonstrated in Section 3.6.2.2) than the parallel and three-fingered modules. Additionally, it can function in situations where the accessible space is limited and could constrain the fingers and other modalities. The max lateral holding force of the different competition pegs once grasped by the electromagnet is presented in Table 3.1. The maximum holding force is 37.5 N when the electromagnet's entire surface area is used (for example, when picking up a metal sheet).

Table 3.1: Maximum lateral holding force of pegs with the electromagnets

Pegs	**4 mm Square Peg**	**12 mm x 8 mm Rectangle Peg**	**8 mm Round Peg**	**16 mm Round Peg**
Max Lateral Force (N)	0.81	0.84	0.71	3.1

3.4 Assembly Framework

The Assembly framework was developed by Gal Gorjup in the New Dexterity research group [17]. The assembly framework architecture is shown in Fig. 3.4. The system is composed of multiple components: the CAD interface, the GUI, the perception, the arm control interface, the gripper interface, and the assembly master. Many product development workflows utilize CAD as a core component for design, visualization, and simulations. Hence, many products are accompanied by CAD data, which is readily available and can provide information on the goal poses of each component. The CAD interface serves as a method of using this CAD data by taking the models as input and collecting the component poses and collision models. The GUI allows the user to interface with the assembly process to assign component type, assembly sequences, and disable/ enable different components within the assembly to execute and alter the assembly process. The perception module is used to locate and extract ArUco pose data. The arm control interface connects to the robot arm and force-torque sensor, and uses Moveit motion planning to create the desired motion trajectories of the arm with respect to the collision space provided by the extracted CAD model. The incorporation of a compliance controller is used to adjust the trajectory of the robot when external forces are applied. This is important during task segments that experience contact (e.g. insertion tasks or screwing), by adjusting the stiffness and damping coefficients the adaptability of the robot can be tuned. This ability to actively comply during contact also aids in overcoming calibration and positioning errors of the component poses. A custom gripper interface was developed with inputs to change grasp type and effort related to the gripper. Finally, the assembly master handles the process state control and synchronization of the subsystems based on the component specific subroutines. The subroutines contain the strategy for executing the different tasks within the task board based on the part type, grasp selection, alignment, assembly, and release. The calibration of the robot, task board, kit layout, kit tray, fastener rack, and components were completed with either vision or kinesthetic teaching. Vision based calibration was executed with fiducial markers to estimate the pose within the global workspace. Although vision calibration has low accuracy during estimations, perception-based calibration could still be used for the kit tray and fastener rack where accuracy was not critical. For higher accuracy pose estimation kinesthetic teaching was used where the robots end-effector was physically displaced and used to point to locations of interest on the task board

and kit layout. The pose of the robot was extracted with forward kinematics of the robot. With this method the locations can be accurately located.

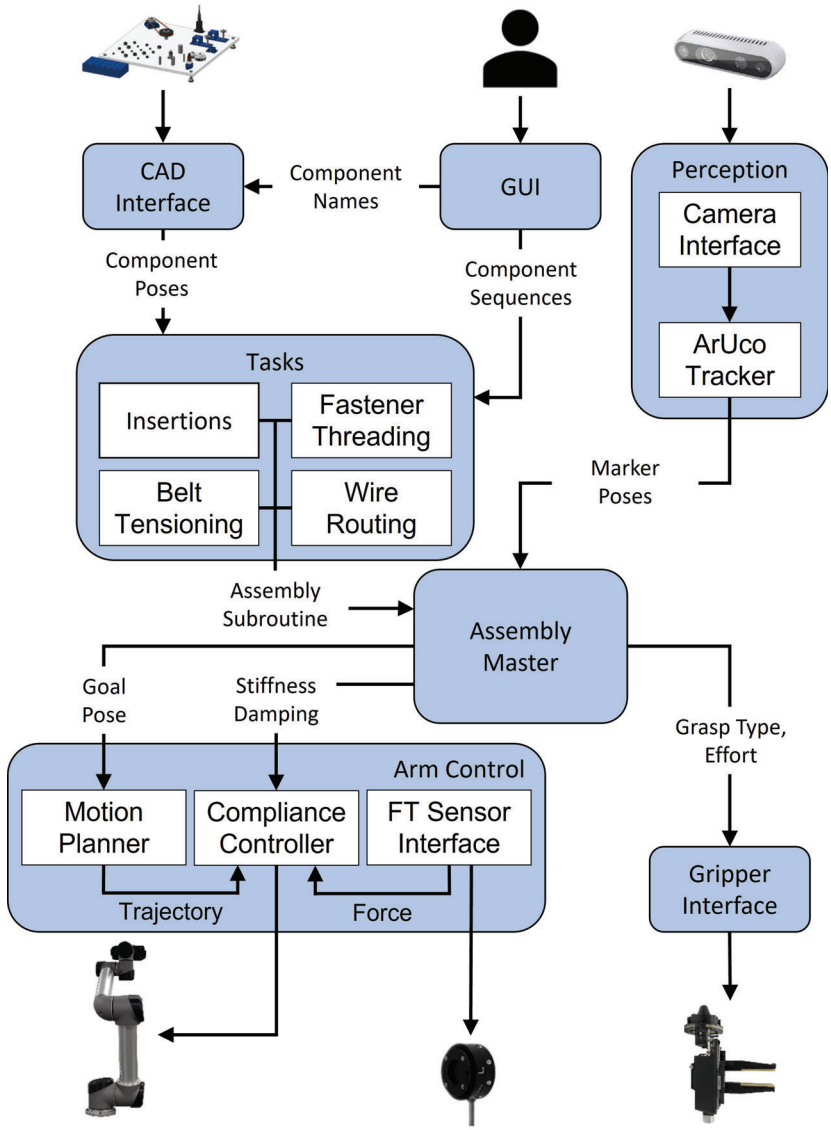

Figure 3.4: The flow diagram describing the control structure of the developed flexible robotic assembly systems.

3.5 Manufacturing Track of RGMC

The National Institute of Standards and Technology (NIST) created the competition standards for the Manufacturing Track of the RGMC. On a dedicated

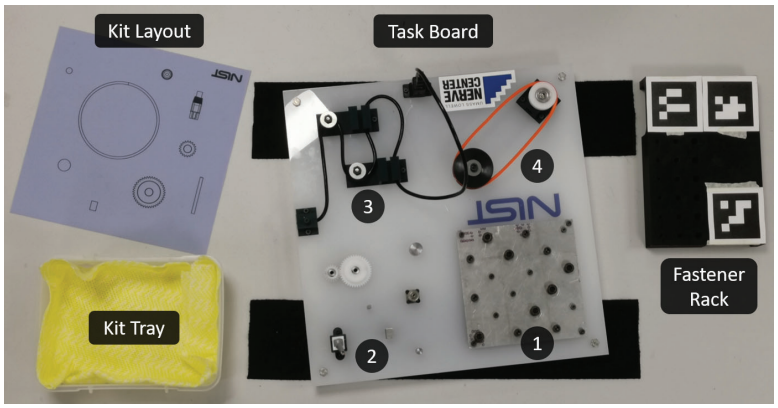

Figure 3.5: The task board contains four different tasks: 1) Fastener Threading, 2) Insertions, 3) Wire Routing, and 4) Belt Threading and Tensioning. The kit tray is used for collecting disassembled parts during disassembly tasks. The fastener rack was only used during assembly tasks where at the beginning of assembly the fasteners would be located in the rack. Before task execution, the kit layout and fastener rack were utilized to arrange the components for assembly jobs.

competition task board composed with four representative assembly work classes (Fig. 3.5), the competition required disassembly and assembly activities to be performed. These classes encompass *Fastener Threading*, *Insertions*, *Wire Routing*, and *Belt Threading and Tensioning* based tasks. In the *Fastener Threading* class, six of each M8, M6, and M4 socket cap bolts were available to be used for threading the 18 different bolts into threaded holes on an aluminum plate. The *Insertions* class uses a USB connector, RJ45 connector, a BNC connector, two meshing gears, and different sized pegs to evaluate different industrial insertion tasks. Routing of a USB cable around and through two vertical pins and two brackets, before being plugged in was the task criteria of the *Wire Routing* class. An elastic belt tensioned on one static and one moveable pulley was used in the *Belt Threading and Tensioning* class. To ensure the developed robotic systems could not be preprogrammed the component and class quadrant position and orientation was randomized. Before the start of the competition participants were given practice boards and their accompanying CAD files, and only at the start of the competition were the competition task board, CAD files, and kit layout revealed to the teams.

A points based system was used in the competition with assembly tasks worth twice as many points as disassembly tasks. During disassembly routines, each component that was successfully removed from the board and placed into the kit tray were worth the same number of points. However, for the USB cable additional

Table 3.2: Competition scores. N/A stands for "Not Attempted".

Class	Assembly		Disassembly	
	Placement	Assembled	Removed	Placed in Tray
Fastener	16 / 18	13 / 18	N / A	N / A
Insertion	6 / 9	4 / 9	8 / 9	8 / 9
Wire	N / A	N / A	4 / 4	1 / 1*
Belt	1 / 1*	0 / 1	1 / 1	1 / 1

points were given for each time it was unhooked from the brackets. At the start of the assembly phase the fasteners were placed in a fastener rack, the USB cable was put into the starting bracket (unrouted), and the remaining assembly components were arranged on the kit layout. When a component made contact with the task board, participants received partial points. The contestants were given the new, unseen kit layout, and task board, as well as their CAD files of the task board and kit layout at the start of the competition. Participants had 80 minutes to attempt assembly tasks and 40 minutes to complete disassembly tasks, with extra points awarded for accomplishing all sub-tasks early. This time constraint accounted for adjusting the system to the new task board, assembly time, and disassembly time. After the autonomous operation began, no manual intervention or tool alterations were permitted. Participants were allowed to continue assembly or disassembly whenever they wanted, but would need to give up any previously earned points related to the task.

3.6 Results

3.6.1 IROS RGMC Competitions

3.6.1.1 2019 Competition

The component start and end poses were automatically retrieved from CAD files for both the task board and kit layout that were provided. The global origin of the kit layout and task board were found using kinesthetic pose calibration. The kit tray's pose was determined using ArUco marker-based calibration. Once correctly setup, the system was able to execute the tasks quite well, placing first in the competition. The highlights of the competition are depicted in Fig. 3.6.

Table 3.2 compares the total number of pieces in a task class to the results of successfully assembled and disassembled components. The number of components successfully grasped and placed on the task board is presented in the first column

Placement. The second column *Assembled* shows the number of parts correctly assembled. The first task attempted was the Belt fastening task. The belt assembly was not successful, despite the fact that it was effectively gripped and positioned in the correct position. Because the trial was cancelled and re-attempted, the points of the partially completed belt were not included in the final score[2].

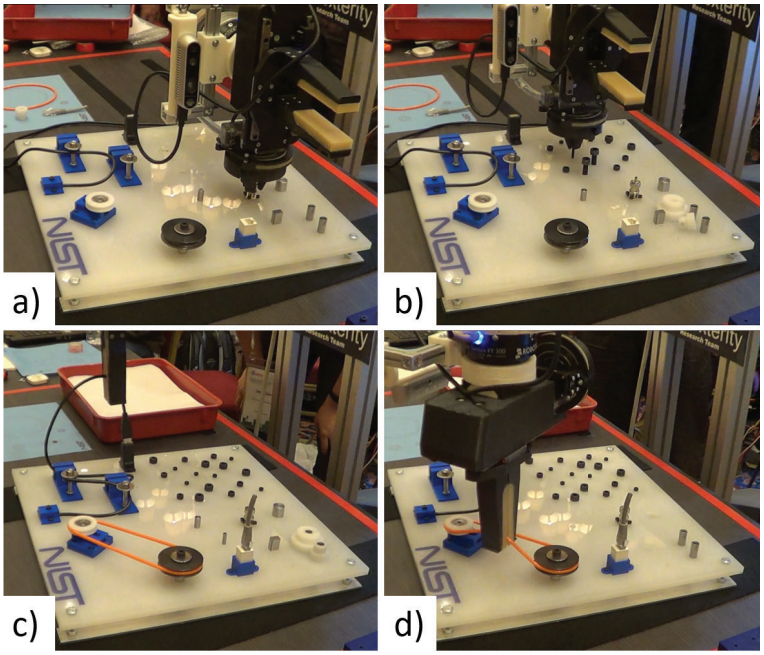

Figure 3.6: The developed flexible robotic assembly system competing in the IEEE/RSJ IROS 2019 Robotic Grasping and Manipulation Competition. The Subfigure illustrate the system executing: a) BNC connector assembly, b) fastener threading, c) cable disassembly, and d) belt disassembly.

The insertion class was attempted first for the final assembly trial with successful insertion of the three large pegs and the BNC connector. For the gears they were successfully grasped and moved to the board, but were not successfully assembled. Once, the insertion task was complete, the fastener routine was executed, nearly all the fasteners were successfully placed, with 10 being fully threaded and 13 being partially threaded. The fastener threading process took more than 30 minutes, even though the rotary module was running at maximum speed (46 rev/min). Due to the restriction on time the wire routing task was not attempted.

[2]Results with asterisk are not counted in the final score in Table 3.2

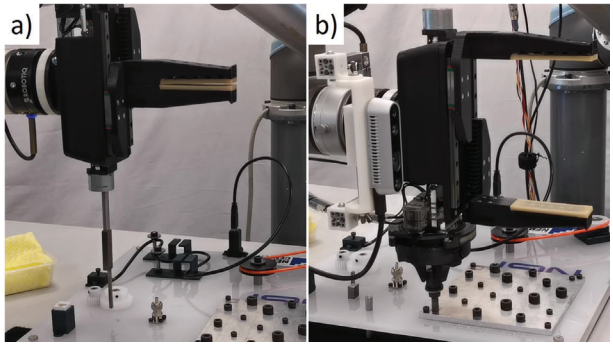

Figure 3.7: The different disassembly methods developed using magnetic interactions. The electromagnetic module can be seen grasping multiple pegs in subfigure a). Subfigure b) presents the rotary module using a magnetic tool to perform unscrewing.

The performance of the disassembly task is shown in Table 3.2 presented in the *Removed* column. The column *Placed in Tray* presents the results of successfully disassembled components. The USB cable was successfully unplugged and removed from all four brackets first, during wire routing task. Even though placing the USB cable in the kit tray did not contribute to the competition score, this was still done during USB cable disassembly to ensure the cable would not interfere with other disassembly tasks. Following this, the belt was disassembled and placed into the kit tray. Only the RJ45 connector was not successfully removed and placed into the kit tray during the insertion class disassembly. During the fastener disassembly tasks, the robot control hardware totally shutdown and became unresponsive for the remaining time of the competition, possibly owing to a grid overload or power surge at the location. The fastener disassembly tasks were not tried at the competition as a result of the outage. However, all disassembly tasks were done without problems during the test runs.

3.6.1.2 IROS 2020 Competition

The initial version of the GUI was used in the 2020 competition. Although there were some initial difficulties with the task board's global pose calibration, the system performed better in the disassembly stage than in 2019. The system was able to successfully remove all the insertion and belt components. Due to time constraints the fastener disassembly was ended early with only 4/18 parts being removed and the wire disassembly was only partially disassembled (1/4). The

assembly phase yielded no points due to a robot hardware failure, and the system finished third in the competition.

3.6.2 Efficiency Evaluation

3.6.2.1 GUI Efficiency

A user study was conducted to assess the efficiency of the generated GUI by evaluating the time needed to configure the system. The average time to perform the experiments took 5 minutes and 3 seconds to fully configure the system across all 12 participants. When comparing this approach with manually editing the text configuration files (12 min and 25 sec), the GUI offered a 59% increase in speed.

3.6.2.2 Magnet-Based Disassembly

After the 2019 tournament, the electromagnetic module was introduced to improve the speed and robustness of peg disassembly. When disassembling the four pegs with the parallel-jaw gripper with active compliance to aid with alignment, an average time of 94 seconds was required. Because the electromagnet does not need to align itself precisely to pick up the pegs a faster finishing time was achieved of 78 seconds. The magnetic module could also be used to grasp multiple pegs, as seen in Fig. 3.7a where the pegs are stacked on top of each other. This significantly reduced the time by 44.6% giving a time of 52 seconds. A magnetic tool was also designed for the rotary module allowing the gripper to unscrew fasteners which are organized in a cluttered manner. This is shown in Fig. 3.7b. The magnetic tool is composed of a permanent magnet with a urethane cover to provide the appropriate friction for loosening fasteners. The tool was picked up by the rotary module, pressed on the fastener, and rotated to raise the fastener head above the adjacent components, ensuring sufficient clearance for the rotary fingers to pick it up. The rotary module grasped the magnetic tool, pressed it against the fastener, and spun it to unscrew the fastener head above neighboring components, allowing the rotary fingers to grasp it without collisions.

3.6.2.3 Video

A video presenting the framework and robots performance can be found at:

www.newdexterity.org/irosrgmc

3.7 Discussion and Conclusion

Both hardware and software components of the system were developed to work synergistically together to adapt and complete changing task requirements. Despite potential errors being introduced to the robots motion for fastening tasks, the rotary module's passively compliant translational axis, ensured that the fasteners can be threaded with minimal friction. In conjunction with the active compliance of the arm, the three-fingered rotary module was designed to facilitate automatic alignment for grasping components. Additionally, the magnetic module facilitates increased efficiency and speed in handling ferrous and magnetic components.

The system has a lot of opportunity for growth, and the problems it has faced so far have taught us several lessons. Although using CAD data can provide estimation of component poses without suffering from vision-related errors, a calibration step is still required potentially adding inaccuracies to the estimation. Resulting in parts missing their appropriate slots or becoming jammed due to misalignment's, which were the main cause of assembly and disassembly failures. Continuous calibration, in which the system starts with an initial localization estimate of the task board that is gradually refined during task execution, could be a potential solution to imperfect initial calibrations. For example, these calibration estimates can be readjusted by the camera whenever the markers are in view or the gripper passively aligns to a fixed component. The system's inability to detect operational breakdowns is a related issue. A partially threaded fastener next to another hole, for example, can collide with the gripper, torque-stop the robot, and demand a complete restart of the task. By utilizing vision to evaluate the current state of the board for comparison with the CAD model the robot could then plan accordingly to avoid such issues. Another issue is the unpredictability of the CAD assembly formats. Due to the files not following a standardized format, assembly origins can be oriented and positioned differently between files, which can cause a significant delay. This was the case in the 2019 competition where the test and competition files used different component origins. Hence, the calibration had to be properly aligned before beginning task execution. This could be remedied by including a simple alignment tool in the graphical user interface that allows the user to check and change the calibrated assembly position.

This chapter presents a multi-modal gripper for flexible robotic assembly system, which uses a CAD based localization, and compliance control. By collecting component poses and geometry from accompanying CAD files, the created system can quickly adapt to various job configurations with minimal human interaction.

An accompanying Graphical User Interface (GUI) is used to define the component assembly sequence and category type, as well as providing visualization of the task board. The developed system utilizes a gripper equipped with four different grasping primitives through the synergistic combination of parallel-jaw, rotary, and electromagnetic elements. An arm and gripper compliance, both active and passive, were incorporated to compensate for calibration and positioning errors during task execution. A magnet-based disassembly method was investigated to improve the speed and reliability of the system. While participating in and winning a worldwide grasping and manipulating competition (IEEE/RSJ IROS 2019 and 2020 RGMC) proved the efficacy of the proposed system.

3.8 Future Directions

Regarding future directions, we plan to improve the grasping efficiency and time execution of tasks by adding an additional pair of active local DOF's to the fingertips of the pinching modality. Improvements to the speed of the rotary module will be made by employing brushless DC motors to execute the main rotary motion. An accompanying perception system for detecting assembly failures will be explored to further improve to robustness of the CAD based assembly framework.

Chapter 4

Adaptive Humanlike Robot Hand for Power Grasping

4.1 Background

As robotics and automation technology advance so do the roles they play in our lives moving from highly structured industrial production lines to unstructured and dynamic environments around humans. For robots to efficiently operate in human-centric environments incorporating anthropomorphic attributes can be advantageous in assisting with interacting with such a complex environment. A key attribute that enables humans to carry out numerous complex tasks is the use of the human hand enabling humans to interact through grasping and manipulation of objects and tools. Researchers have aimed to replicate such dexterity within robots through directly modelling the human hands properties. Although possible, this results in fully-actuated, rigid designs, which require expensive components, complex control algorithms, and sophisticated sensing to create multi-fingered, anthropomorphic, dexterous robot hands [68, 69, 4, 5]. This design approach also makes it difficult to achieve a dexterous, anthropomorphic robot hand without compromising the weight and form factor of the device because of the many actuators and sensors needed for this approach [70]. To empower robots with higher levels of dexterity in order to conduct tasks of higher complexity researchers have explored alternative methods to control such devices such as machine learning methods capable of enabling a robot hand to solve a Rubik's cube one handed [9]. Although machine learning methods provide increased generalizability and reduced complexity of control for highly actuated anthropomorphic robot hands, they require significantly large amounts of data and computational resources in

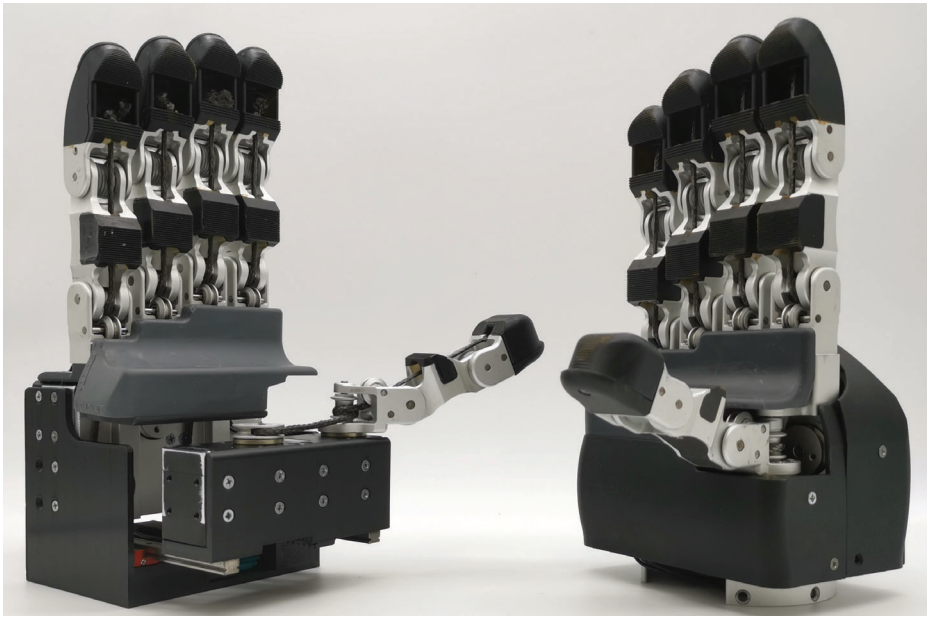

Figure 4.1: The human like adaptive underactuated tendon driven robot hands with and without an additional DOF for facilitating thumb base translation for adjusting the aperture of the hand.

order to learn how to carry out a single task. As a result, many robots in industry are equipped with simple parallel jaw grippers with limited dexterity.

During the last decade, the utilization of compliant elements and underactuation has provided an alternative means of designing lightweight and simple to control robot hands capable of executing robust grasping in unstructured environments with high object pose uncertainty [10, 11, 12]. By incorporating intrinsic and extrinsic compliance through the use of intelligent material selection and mechanism design, robotic end-effector can be designed to be mechanically intelligent. This allows such robot grippers and hands to be capable of passively adapting to its environment with intuitive and simple control strategies [71, 72]. The integration of structural compliance has not only allowed for increased adaptability and improved handling of fragile objects, but also facilitates safer interaction between humans and robotic devices [73, 74]. As a result, underactuated and compliant mechanisms have been utilized to develop a wide variety of adaptive grippers capable of grasping and manipulation. With the applications ranging from prosthetic hands [19] giving amputees an improved quality of life to adaptive grippers on underwater robots [75] for improved interactions between the robot and its surrounding environment.

In this chapter, we present two adaptive, human-like robot hands. An underactuated, tendon-driven, compliant, anthropomorphic robot hand that is capable of executing robust caging grasps under a wide range of environmental uncertainties (e.g., object pose uncertainties). The second robot hand design uses a similar structure to the first robot hand, but with an additional DOF at the thumb base facilitating translational motion for repositioning the thumb to improve its in-hand manipulation capabilities.

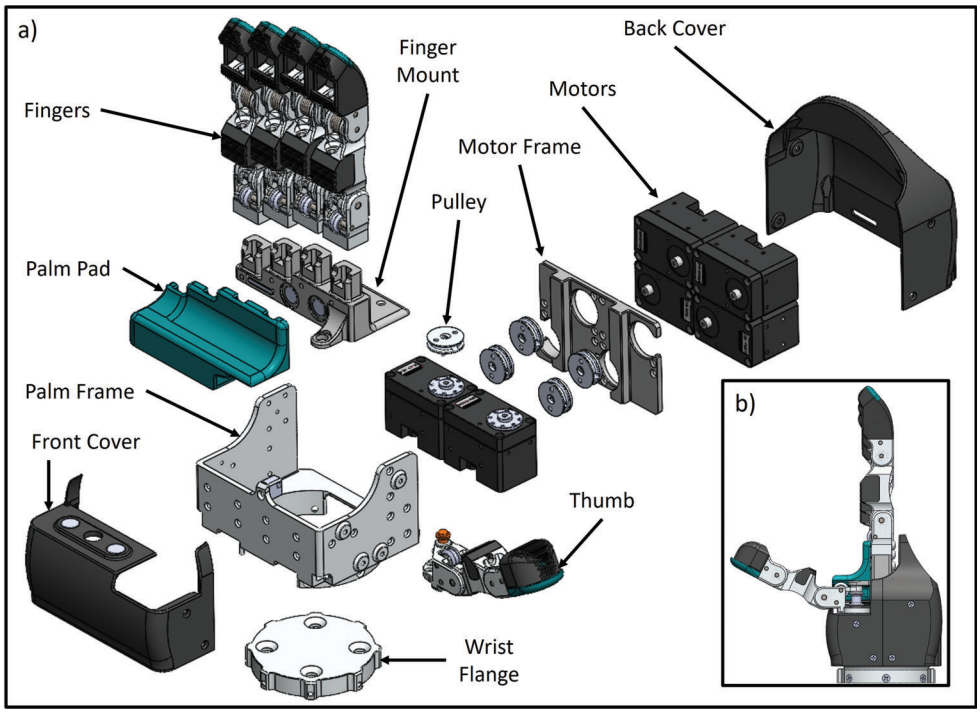

Figure 4.2: An exploded view (subfigure a)) of the robot hand with a rotating base frame, illustrating the construction and different components in the hand. Subfigure b) presents the maximum aperture of the hand.

4.2 Design

In this section, we described the design of two different robot hands. The structure of the hand can be seen in Fig. 4.2 and Fig. 4.3. The robot hands are composed of modular fingers, a thumb and a magnetic palm, which are attached to two different palm designs that differentiate the two hand designs apart.

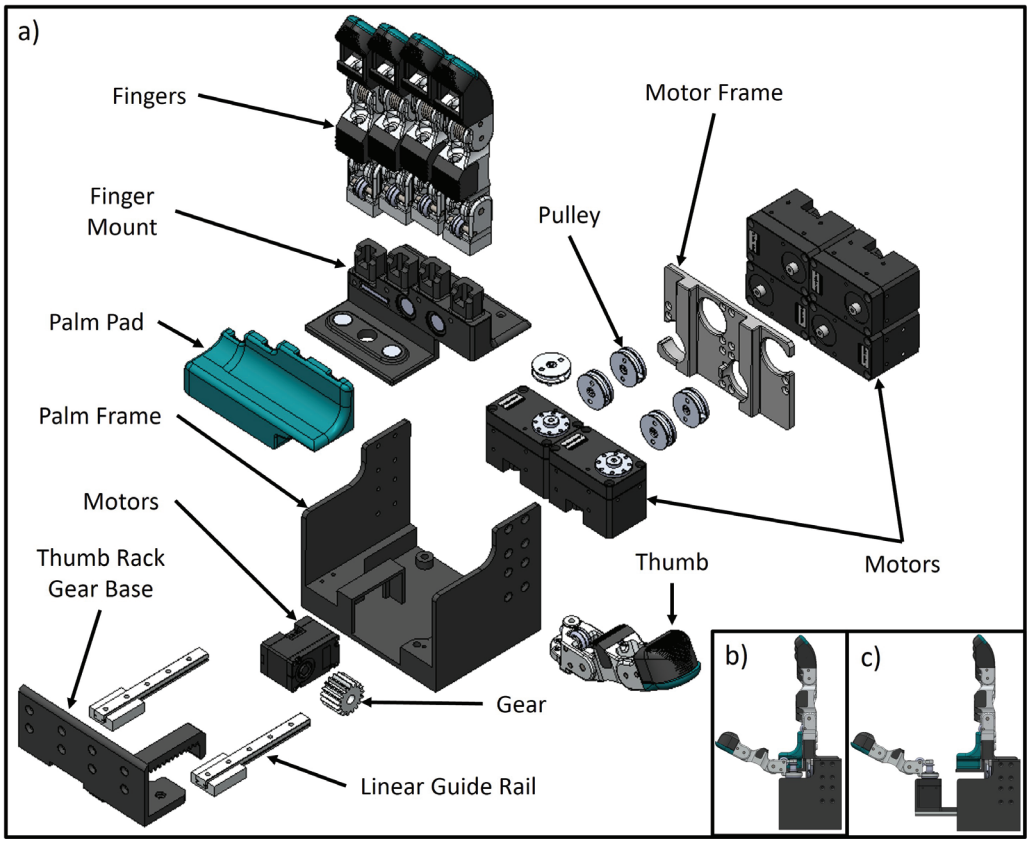

Figure 4.3: An exploded view of the robot hand with a base frame capable of both translation and rotation. The exploded view illustrated in subfigure a) presents the construction and different components and mechanisms utilized in the hand. Subfigure b) presents the side view of the hand when collapsed, and subfigure c) shows the thumb is fully extended.

4.3 Palm Design

Many anthropomorphic and robotic hand designs [76, 77, 78, 79, 80] utilized palms that provide fixed finger base frames to the five fingers of the hand. As a result of using this design paradigm, optimizations are done to find the optimal fixed palm design for all objects. However, for underactuated robot hands to achieve the maximum in-hand manipulation workspace over a range of different objects different palm sizes, which separate the finger base frames should be used [81]. More specifically, having a finger base frame separation distance, which is the same as the object width can provide the maximum object manipulation workspace [81, 82]. This indicates that there is no one solution that will provide the best manipulation workspace for all object sizes, instead a hand with a changing palm

size that can facilitate different finger base frame distances is a more generalizable solution for achieving a highly dexterous end-effector.

Inspired by our previous work focusing on the use of reconfigurable base frames in two-fingered grippers [83], we have designed two different palm designs to compare the improvement in manipulation capabilities. The first design (Fig. 4.2) utilizes a palm that uses a fixed finger base frame design for all the fingers, while the thumb has a rotating thumb base frame to achieve opposition. The second design (Fig. 4.3) is similar to the first design, but consist of an additional DOF in the base of the palm allowing the thumb base frame to reconfigure/ translate outwards to increase the aperture of the hand. Contained within the two different palm designs, 6 Dynamixel XM430-W350 motors are stored for actuating each finger and the thumb in order to execute flexion motions. The thumb also uses an additional actuator to perform opposition. The reconfigurable design uses an additional actuator (XC330-T228-T) with a set of linear guide rails and a rack and pinion mechanism to accomplish the translating motion of the thumb.

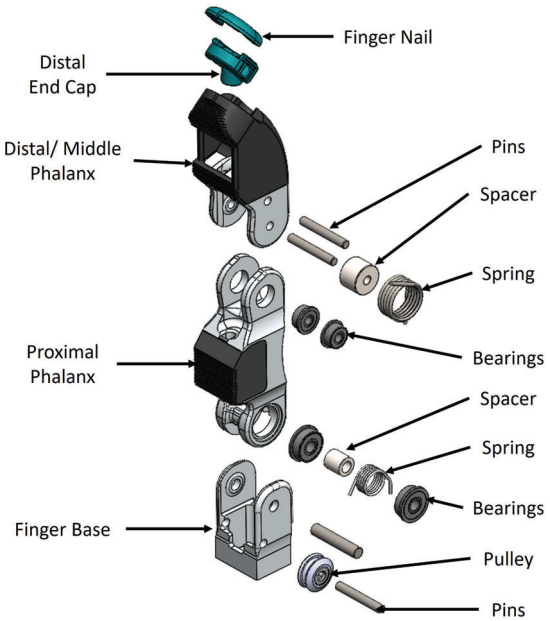

Figure 4.4: An exploded view of the robot finger used in the New Dexterity robot hand. The finger is composed of a finger base, proximal phalanx, distal/middle phalanx, distal end cap, and a detachable fingernail. Springs within the finger provide passive extension and bearing provide reduced friction within the joints.

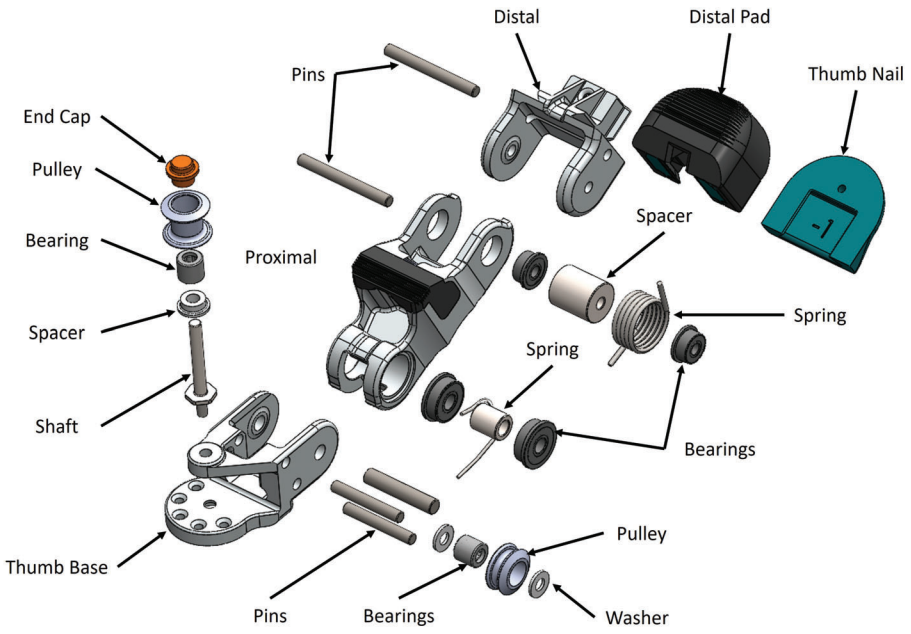

Figure 4.5: An exploded view construction of the thumb. Modular distal pad and thumb nail allows the tip of the finger to be easily altered. Bearings are used to reduce friction in the joint and torsional springs provide passive extension. Pulleys within the thumb reduce friction and enable rerouting of the thumb tendon.

4.3.1 Finger design

The design of the robotic fingers are composed of pin joints at the metacarpal phalangeal (MCP) and proximal interphalangeal (PIP) joints with the distal interphalangeal (DIP) joint being a flexural joint design. The flexure joint construction not only allows the fingertips to exhibit improved flexibility but also allows the distal and middle phalanges to be constructed as a monolithic structure increasing the urethane finger pads area for improved grasp contact. The monolithic structure is fabricated with urethane rubber (Smooth On PMC-780) using hybrid deposition manufacturing (HDM) [46] techniques, which allows the combination of rigid and soft materials to be molded together. This manufacturing technique is also used to construct the proximal phalanx. The finger is composed of a modular fingernail, distal/middle phalanx, proximal phalanx, and a set of bearings and torsional springs at each pin joint. A depiction of the finger is shown in Fig. 4.4. The torsional spring stiffness was selected such that the flexion profile of the fingers prioritizes the bending of the MCP joint before the PIP joint. Flexion of the PIP joint only occurs when the proximal phalanx makes contact or the MCP joint

reaches full flexion. The fingers are actuated through low friction polymer tendons, which were terminated at the fingertips and pulleys of each motor associated with the fingers. The tendon routing of the fingers are designed with the tendons to be set as far away from the joint as possible to maximize the applied torque on the joints by the tendon facilitating strong power grasp forces. Additionally, each finger is mounted on an interchangeable base that allows the fingers to be changed in a modular manner.

4.3.2 Thumb Design

The thumb follows a similar design approach as the fingers of the robot hand, but without the inclusion of the flexural joint at the DIP joint. Bearing at the pin joints facilitate low friction bending at the joints and torsional springs at the MCP and DIP joints of the thumb are selected such that the MCP joint flexes before the DIP joint like the fingers of the robot hand allowing the hand to perform both precision and power grasps. A pulley at the opposition joint of the thumb enables the actuating tendon to be rerouted, housing the actuators in a compact manner. The construction of the robot finger is illustrated in Fig. 4.5.

4.4 Experiments and Results

4.4.1 Force Exertion Experiment

Table 4.1: Maximum grasp forces exerted on the dynamometer.

Grasp Type	Force (N)
Pinch Grasp	1.4
Tripod Grasp	1.9
Power Grasp	81.2

The first experiment focused on the grasping forces, the robot hand was capable of exerting. Three different grasp types were selected and assessed: a pinch grasp, a tripod grasp, and a power grasp. The force measurements were collected with a dynamometer that was composed of 2 straight bar load cells. The data collected followed the national institute of standards and technology (NIST) grasp strength performance metric, where the dynamometer would be grasped in two different orientations: a 0 degree orientation when the load cell axis is parallel with the palm surface, and a 90 degree orientation when the load cell axis is perpendicular with

the palm surface. Once the two readings are collected, the Euclidean norm is used to calculate the maximum force exertion for a given grasp type. The maximum force exertion of the hand is shown in Table. 4.1. Because the tendon routing of the hand was designed around performing power grasps, precision grasps, which only require the fingertips as contact exhibited low forces due to reconfiguration. Although the precision grasp forces were low, for human-centric environments like household environments, power grasps are used 73.6 % of the time with the remaining time separated between precision grasps, and intermediate grasps [84] to execute different household task.

4.4.2 Object Grasping Experiment

This experiment evaluated the grasping performance of the robot hand. The YCB object set is composed of various everyday life objects and is designed to facilitate the benchmarking of grasping and manipulation used to assess the robot hand. Twelve objects from the object set ranging in weight, size, and shape were selected: small block, marble, credit card, tuna fish can, potted meat can, pear, apple, metal mug, mustard container, chips can, bleach cleanser, and hammer. The grasping capabilities of the hand can be seen in Fig. 4.6.

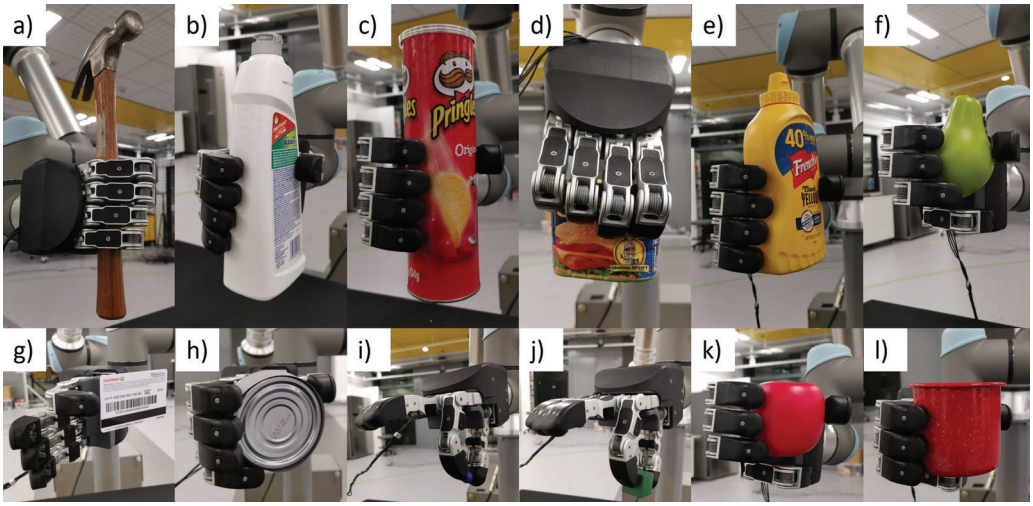

Figure 4.6: Grasping experiments were conducted with the YCB object set [34]. Twelve objects from this set were selected to assess the hand: a hammer, a bleach cleanser, a chips can, a potted meat can, a mustard container, a pear, a card, a tuna can, a marble, a small block, an apple, and a metal mug.

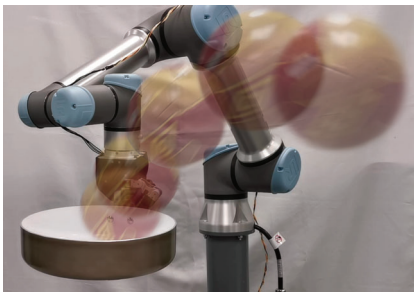

Figure 4.7: A grasp robustness test evaluating the hand's ability to hold the pan when a ball is thrown at it.

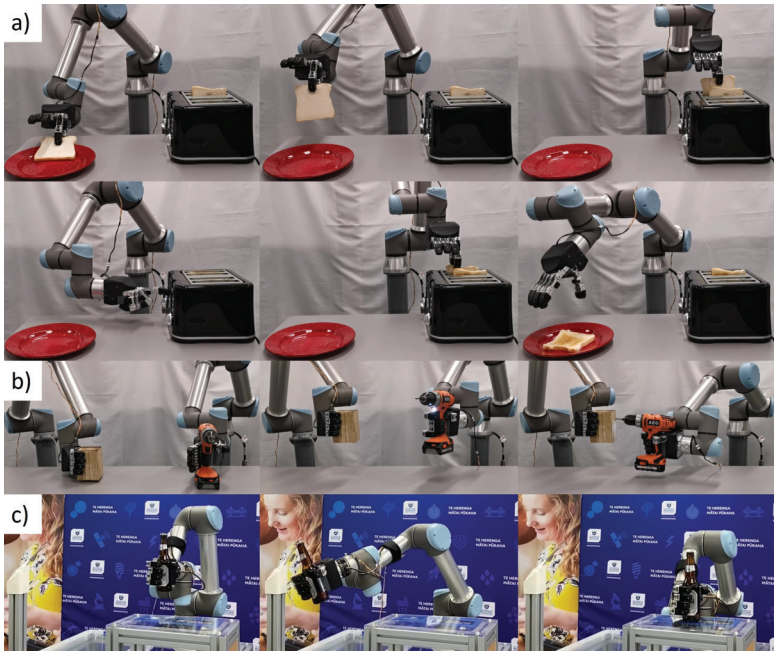

Figure 4.8: The hand performing different tasks with the task motions being executed from left to right in sequence. Subfigure a) shows the robot hand executing a cooking task of making toast. Subfigure b) present the hand performing a bimanual task of drilling a wood block. Lastly, subfigure c) shows the robot hand executing a service task of opening and serving beer.

4.4.3 Application and In-hand Manipulation Demonstrations

To demonstrate the robot hands grasping capabilities and grasp robustness a variety of different tasks were created to test the hand. The tasks included opening a beer bottle, cooking toast, drilling, and lastly holding a pan while it experiences object disturbances (Fig. 4.7). The different applications can be seen in Fig. 4.8.

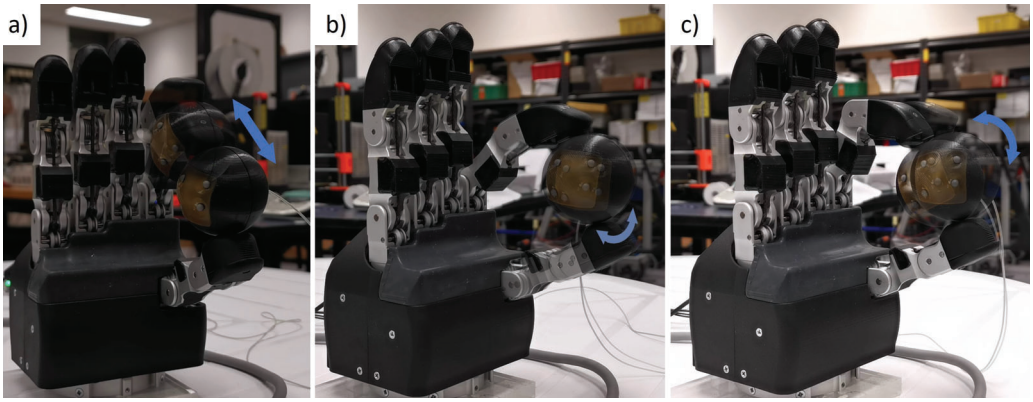

Figure 4.9: The manipulation demonstration of the hand manipulating a sphere [16] in different axis. Subfigure a) present the hand translating the sphere vertically up and down. Subfigure b) and c) shows the hand performing rolling manipulation motions with the sphere.

To further present the hands utility, different manipulation tasks were performed. In these demonstrations the hand executed pre-programmed manipulation motions with a sphere from the sensorized object set [16] to showcase the possible different manipulation motions it can achieve. The object was manipulated in different ways to demonstrate the hand's ability. The in-hand manipulation motions are presented in Fig. 4.9 and Fig. 4.10.

A comparison of the two different robot hand designs were conducted with cylindrical objects of differing diameters [16]. These manipulation motions are depicted in Fig. 4.10 with the object trajectories presented in Fig. 4.11. The object trajectories were collected with the Polhemus Liberty system equipped with micro magnetic sensors. When manipulating small objects like the small cylinder (as seen in Fig. 4.11) the manipulation trajectory achieved by the hands are similar. However for larger objects (Fig. 4.10c and Fig. 4.10f), the addition of the translating DOF at the thumb base allowed for aperture adjustment of the hand facilitating an improved in-hand manipulation workspace of more than 2 times the trajectory length with the large cylinder. By adjusting the hand aperture, the manipulation capabilities of the device can be improved allowing it to be generalized to a wider range of objects.

A video demonstrating the new dexterity adaptive robot hand executing in-hand manipulation and the different tasks can be found in the following URL:

www.newdexterity.org/NDXA

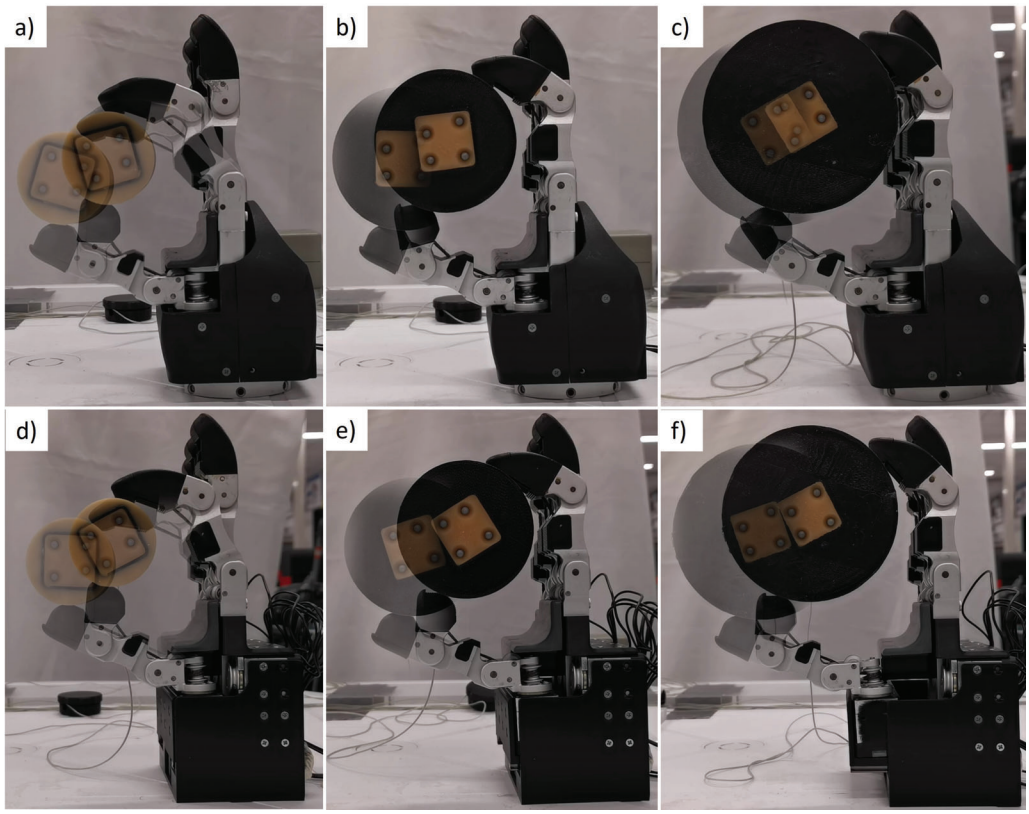

Figure 4.10: A comparison of the two different hands manipulation capabilities with and without a translational DOF at the thumb MCP joint. When manipulating smaller objects (subfigure a) and d)) both hands have a similar manipulation workspace as the second hand design uses the translational DOF in its compressed form. However when manipulating larger object (as seen in subfigure c) and f)), the translational DOF can be used to extend the thumb base position increasing the manipulation workspace of the object in comparison to the first design.

4.5 Conclusions

In this chapter, we presented two adaptive human-like robot hands, which are underactuated, tendon driven anthropomorphic robot hands. The hand is capable of performing robust grasps for a variety of everyday life objects, utilizing this grasping capability and it anthropomorphic form it is able to perform human-centric tasks. The second design utilizes a similar hand structure to the first design but incorporates an additional DOF at the thumb base for adjusting the hand aperture and improving the in-hand manipulation capability of the hand. The performance of the hand was evaluated through: i) force exertion tests of different grasp types,

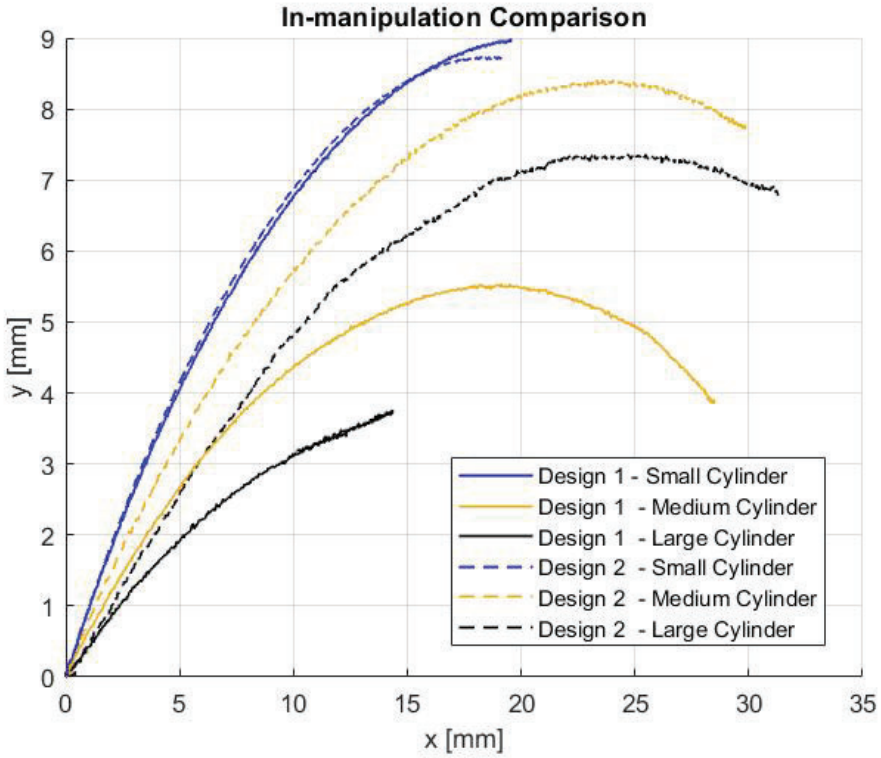

Figure 4.11: A comparison of the two different hands designs developed in performing in-hand manipulation of different sized cylinders. The plot presents the different trajectories of the objects when manipulated by the two different designs. Design 1 represents the hand design with a thumb base capable of only opposition, and design 2 represents the hand design with a thumb base that can execute opposition and translation.

ii) grasping experiments involving a diverse set of everyday life objects, iii) in-hand manipulation experiments, and iv) execution of different application tasks with the robot hand.

4.6 Future Directions

Regarding future directions, we plan to improve the pinch force capabilities of the hand through variable stiffness joints, which can be used in place of the current passive elastic elements (torsion springs) in the hand. This will allow the hand to execute improved pinch grasp forces in the stiffened state without compromising the power grasp efficiency of the hand as the joint stiffness can be reduced.

Chapter 5

A Dexterous, Reconfigurable, Adaptive Robot Hand Combining Anthropomorphic and Interdigitated Configurations

5.1 Background

The human hand is capable of interacting and executing a diverse set of tasks within many different environments from grasping small delicate objects to manipulating tools for construction. A key aspect of the human hand is the metacarpophalangeal (MCP) joint, as it facilitates both flexion/ extension and abduction/ adduction of the fingers [85]. This is an imperative feature in how dexterous manipulation tasks are executed by the human hand. Many attempts have been made by roboticists to replicate human hand dexterity in order to interact with the physical world. Roboticists have approached the problem through biomimicry, bioinspiration, or a combination of both [86, 87, 88, 89]. This produces solutions that range from highly complex designs with numerous sensors and actuators requiring complex control algorithms, expensive components, and sophisticated sensing [90, 91, 92] to highly simplified grippers [93] with limited capabilities.

In structured environments like traditional industrial assembly lines where access to parameters such as object geometries or obstacles can be easily acquired, the required end-effector can be highly customized to perform a desired task. However, in unstructured environments where the task execution parameters (e.g., ob-

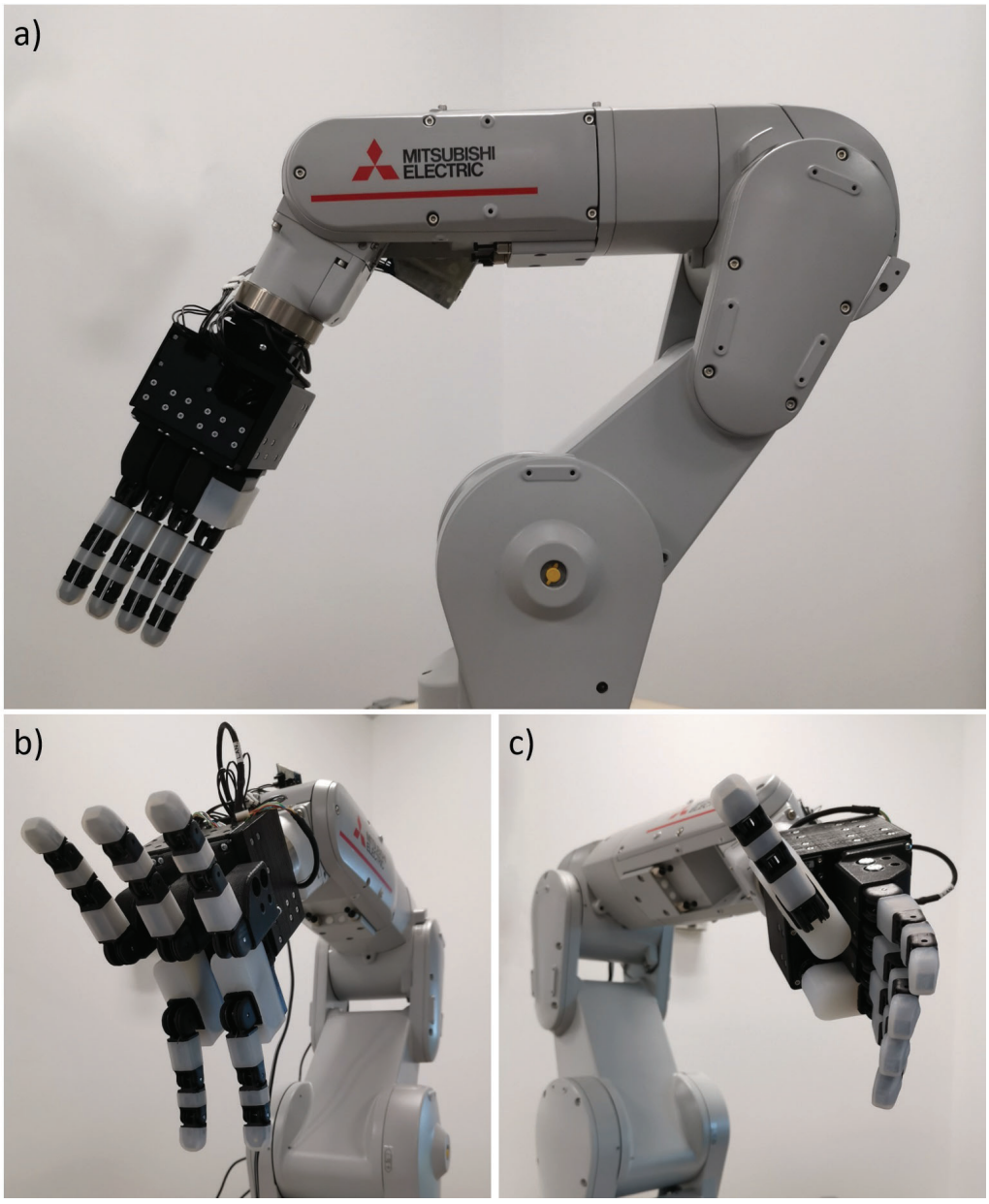

Figure 5.1: The multi-modal, reconfigurable, dexterous robot hand connected to the Mitsubishi Electric industrial robot MELFA RV-4FRL in an interdigitated (subfigure b) and an anthropomorphic (subfigure c) configuration.

ject and obstacle properties) are not easily obtainable, hands capable of executing a plethora of complex grasping and manipulation tasks with objects of various sizes, weights, and stiffness, are needed.

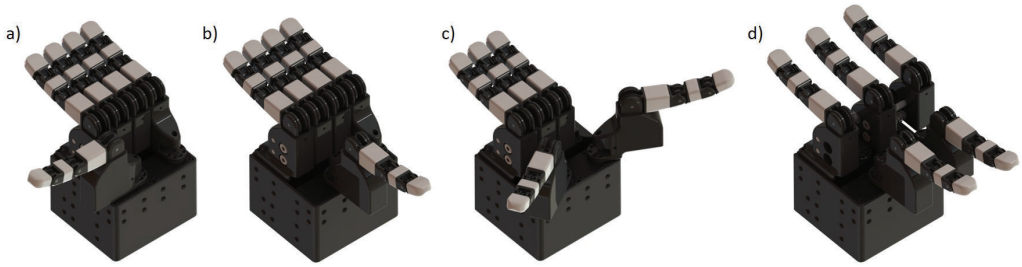

Figure 5.2: The multi-modal hand is capable of accomplishing a diverse set of grasping postures. The anthropomorphic hand configuration with an abducted and an opposed thumb configuration can be seen in subfigures a) and b) respectively. Subfigure c) shows the tripod configuration of the hand. Subfigure d) presents the interdigitated grasping posture.

Alternatively, underactuated designs [94, 95, 96, 74, 97, 98] require much simpler control schemes due to their inherent compliant nature allowing them to effortlessly conform to various object geometries. In comparison to fully actuated designs, this class of end-effectors simplifies the extraction of robust grasps under object pose uncertainties. This is generally implemented through flexure joints, spring loaded pin joints, and differential mechanisms, which connect the multiple degrees of freedom of the hand to a limited set of actuators.

Although underactuated hands have many benefits, many underactuated designs use fix base frames limiting the variety of grasp types that they can execute. Reconfigurable finger base frames have been employed to increase the number of grasping options a particular robot hand has available through changing the optimal position of fingers to better utilize the limited number of actuators for a given task. In [99, 100], the authors utilize this idea to perform a range of grasp types ranging from pinch and tripod grasps to interdigitated power grasps with only three fingers. However, many objects within the daily life of humans are designed with ergonomics to facilitate optimal use with the human hand. For robots to operate within a human-centered environment (e.g. service tasks) they should also include anthropomorphic features, which allow them to optimally interact with human ergonomic objects, and not rely on robot specific objects and tools [101].

In this chapter, we focus on the development of a multi-grasp, adaptive, reconfigurable, dexterous robot hand (as seen in Fig. 5.1) that can allow for simplified execution of dexterous manipulation tasks, increasing significantly the dexterity of existing industrial manipulators. Thus, the main goal is to design and develop a general purpose end-effector that will facilitate the execution of complex, dexterous

service robotics and industrial automation operations by appropriately employing underactuation and design simplicity without compromising dexterity. Increasing the dexterous capabilities of an end-effector without sacrificing control intuitiveness is not easy, but it can be accomplished by capturing the essential ideas behind the human hand anatomy without trying to replicate them. Due to the anthropomorphic design, the device has the advantage of being able to replace the human hand in interfacing with devices targeted at the consumer market (e.g., testing of industrial electronics). Also, the multi-modal nature of the hand allows it to be configured as a five-fingered gripper that can facilitate the execution of heavy-duty industrial automation tasks [1].

The rest of the chapter is organized as follows. Section 5.2 presents the design of the multi-grasp robot hand and its respective modules, Section 5.3 focuses on experimental validation of the concept through a wide range of experiments assessing the grasping and dexterous manipulation capabilities, as well as the force exertion capabilities of the device and compares it with other robot hands. Lastly, Section 5.4 concludes the chapter, discussing the contributions.

5.2 Designs and Methods

In this section, we describe the designs of the robot hand and finger structures developed. As seen in Fig. 5.1, the developed robot hand is capable of achieving multiple grasp configurations. An interdigitated finger configuration (shown in Fig. 5.1d) exists where a pair of fingers oppose three other fingers, with spaces between fingers allowing for uninhibited closure of each of the digits. Fig. 5.1a presents a conventional anthropomorphic configuration with the thumb abducted. A single thumb opposes four parallel fingers in a human-like configuration to better adapt to objects ergonomically designed for the human hand. A compliant telescopic mechanism exists on which the index, middle, and ring fingers are mounted, further extending the possible grasp types achievable by the robotic hand. Additional configurations can be achieved, such as a tripod grasp, as well as many intermediary grasps that occur between the transition from anthropomorphic to interdigitated and vice versa. Four of the possible configurations of the hand can be seen in Fig. 5.2.

[1] Majority of the chapter is based on [18], © 2021, IEEE. Reprinted, with permission, from Geng Gao, Jayden Chapman, Saori Matsunaga, Toshisada Mariyama, Bruce MacDonald, and Minas Liarokapis, A Dexterous, Reconfigurable, Adaptive Robot Hand Combining Anthropomorphic and Interdigitated Configurations, IEEE/RSJ International Conference on Intelligent Robots and Systems (IROS), 2021.

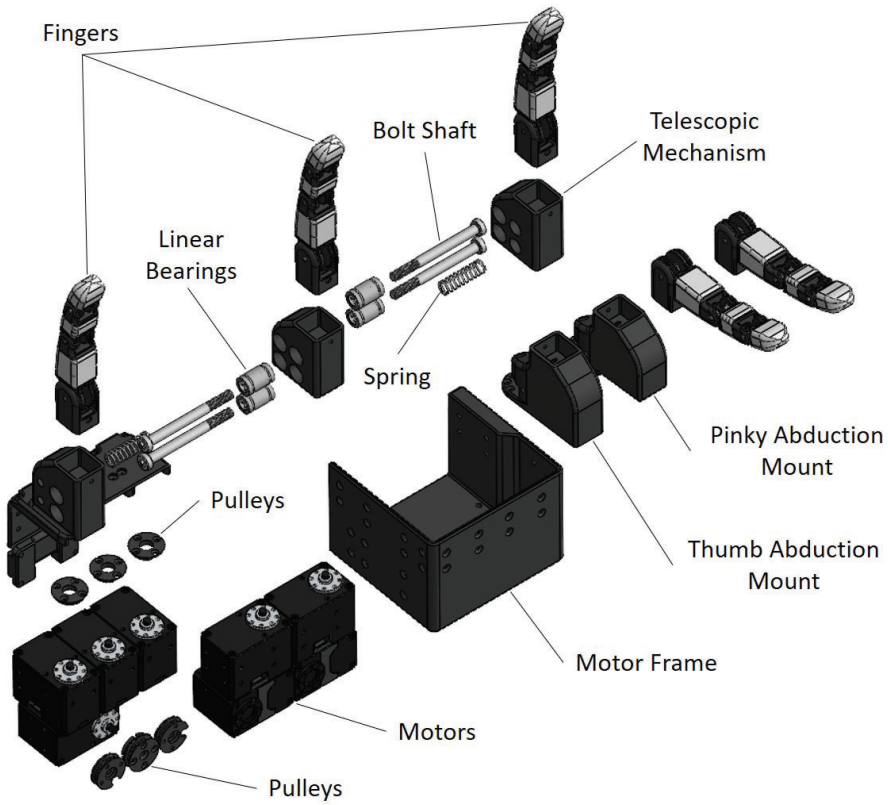

Figure 5.3: An exploded view of the multi-grasp anthropomorphic hand detailing the mechanism that allows for transitions between the anthropomorphic and inter-digitated configurations, as well as the layout of the 8 actuators.

The gripper uses a total of eight Dynamixel XM430-W350-R motors, each consisting of the motor unit along with integrated control and current sensing circuitry. Each finger is driven by a single Dynamixel motor, with the remaining three motors used to 1) control extension/ contraction of the telescopic mechanism and 2) and 3) to provide control for opposition for the thumb and pinky (the second thumb).

5.2.1 Telescopic Mechanism

As seen in Fig. 5.3, a telescopic mechanism has been utilized in order to increase the workspace and grasping capabilities of the gripper. The mechanism enables prismatic motion of the index, middle, and ring finger base frames to extend and contract to different positions. Compression springs allow for passive extension of the finger base frames, while an actuator is used to accomplish active contraction.

In the completely contracted state, the index, middle, ring, and pinky fingers are positioned as close together as possible so as to achieve an anthropomorphic configuration.

At the other extreme, when the passively extending mechanism achieves its maximum extension, the middle and ring fingers will extend away from the stationary index finger. Once the fingers are spaced out, an interdigitated grasp posture can be achieved allowing for full grasps where the fingers do not obstruct each other. In order for the mechanism to be robust to high loads when extended, two pairs of linear bearings were used. This allowed for the smooth extension/contraction of the fingers in addition to creating a sturdy frame for the fingers to rest on.

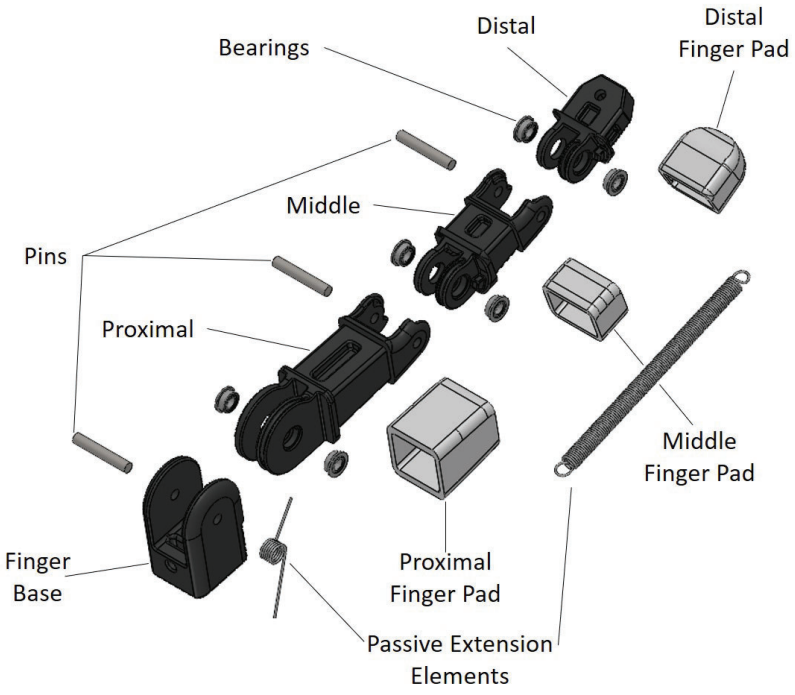

Figure 5.4: An exploded view of one instance of the tendon driven, passive extension, modular finger unit. The design consists of a proximal, middle, and distal phalanx. Integrated miniature bearings and replaceable silicone finger pads are used to reduce friction and provide increased grip.

5.2.2 Finger Design

Fig. 5.4 shows an exploded view of the finger module of the design. Each finger consists of a proximal, middle, and distal phalanx, along with an appropriate base for connecting the fingers to the chassis of the gripper. Each of the five pin-joint, passively extended, underactuated fingers are identical, therefore keeping the design intuitive and easy to manufacture. Each finger is actively closed by a single tendon terminated at both the distal and the pulley of the actuator used to drive the finger. Tendon routing follows a highly structured trajectory where the separation between the tendon and the center of rotation of each joint remains constant as the relative angles between adjacent phalanges are changed. This ensures that any reconfiguration of the robotic finger will occur in a similar fashion irrespectively of the current degree of closure (except when the maximum limit positions of the fingers joints have been reached).

In underactuated designs, where many components can move relative to each other when exposed to external loads, friction contributes greatly to the interaction of the components. Two MF63-ZZ miniature bearings were installed in each joint of the finger to reduce friction, thus enabling a much smoother trajectory during the opening/ closing of each finger. These bearings were incorporated through a press fit on the inner link of each phalanx, to ensure that when assembled, there was no possible way the bearing could come loose. Each phalanx of the fingers also incorporates a silicone molded finger pad to provide adequate friction and compliance between the hand and an object in order to establish contact points and forces required for the successful grasping of said object. These finger pads are easily replaceable when worn and can be manufactured through standard molding practices. A single extension spring is utilized between proximal and distal phalanges in each finger to ensure it returns to the fully opened state when the tension in the tendon is relaxed. Each end of the spring is secured by a screw at a set point to ensure robust attachment, and to minimize the difference in behavior between any two manufactured fingers. Additionally, a torsion spring is utilized between the proximal phalanx and the finger base to allow for a greater range of motion of each finger, allowing the gripper to achieve a larger aperture as a whole.

5.2.3 Reconfigurable Finger Base Frame

Many objects of daily living, such as tools or handles, have been designed with special consideration of the functionality of the human hand, with the goal of improving our interactions with such objects during grasping and manipulation. The

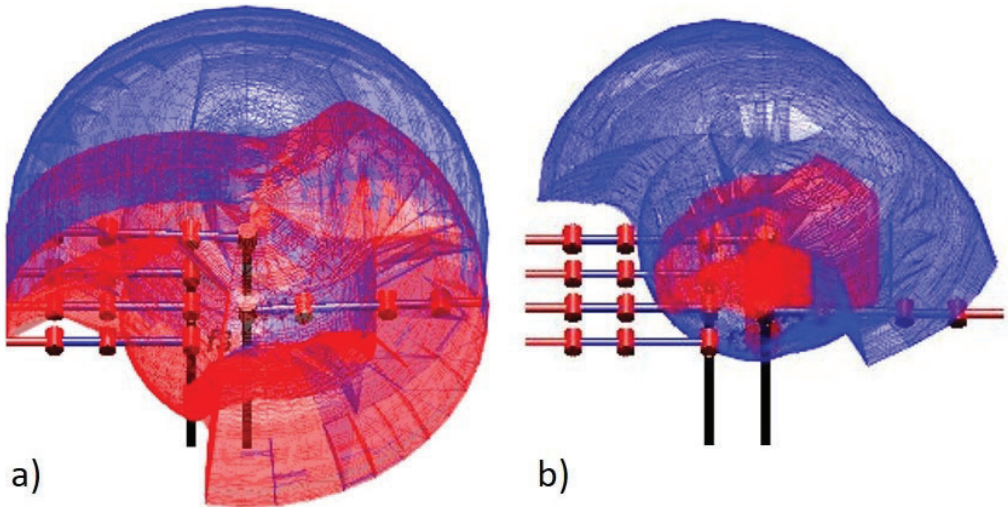

Figure 5.5: The workspace of the anthropomorphic configuration is represented by the red shaded region. The shaded blue region represents the increased workspace when the gripper is utilized in the interdigitated state. Subfigure a) shows the 3D representation of the full workspace of the hand when in an anthropomorphic only configuration and a changing interdigitated configuration. Subfigure b) presents the fingertip contact workspace where at least two fingertips are able to make contact with one another.

complex surfacing of products such as the use of grooves and swells are adopted in order to increase the contact area between hand and object, allowing the user to carry out successful grasping and manipulation of objects in a comfortable manner with minimal effort, and maximum effectiveness. These techniques are based on the anthropometry of the human hand, and as such, designing a robot hand to have similar characteristics is an important factor in achieving an optimal grasp. However, fully anthropomorphic hands are either highly actuated, becoming heavy, large, and requiring sophisticated control laws [68, 69], or are lightweight with limited dexterity [102, 103].

By arranging the actuators such that the hand is capable of transforming between an anthropomorphic and non-anthropomorphic structure, an increased dexterity in a compact form factor can be established with fewer actuators. The use of an opposable pinky and a coupled telescoping index, middle, and ring finger facilitates the reconfigurability of the finger base frames of the hand, allowing for anthropomorphic and non-anthropomorphic grasping states. A fingertip workspace representing the full range in which the fingertips of the hand can reach is depicted in Fig. 5.5a, with the red shaded region representing the anthro-

pomorphic workspace, and the blue space representing the reconfigurable finger base workspace. This involved taking the union of individual fingertip workspaces (W_H), creating the hand workspace as

$$\mathrm{W}_H = \mathrm{W}_I \cup \mathrm{W}_M \cup \mathrm{W}_R \cup \mathrm{W}_P \cup \mathrm{W}_T \tag{5.1}$$

where W_H is the workspace of the hand and W_I, W_M, W_R, and W_P denote the fingertip workspaces of the index, middle, ring, and pinky fingers of the hand. The individual fingertip workspaces were created by actuating the finger through the full range of motion (ROM) of all of its degrees of freedom (DOF) to generate a collection of points in space using the forward kinematics of the finger. This point cloud is then used to construct an *alphashape* that represents the fingertip workspace of one finger [83]. To ensure that the calculated workspace doesn't increase simply because the finger base frames are spread apart (reducing the finger to finger overlap), a fingertip to fingertip manipulation workspace of the hand is also generated (to analyze the effect of the reconfigurable finger base frame mechanism). For the anthropomorphic configuration the thumb is the only finger that is able to oppose the other fingers to establish fingertip to fingertip contact, while for the interdigitated configuration both the thumb and the pinky can achieve this. Thus, we get

$$\mathrm{W}_{HA} = \mathrm{W}_T^M \tag{5.2}$$

$$\mathrm{W}_{HI} = \mathrm{W}_T^M \cup \mathrm{W}_P^M \tag{5.3}$$

$$\mathrm{W}_T^M = \mathrm{W}_{TI}^{IM} \cup \mathrm{W}_{TM}^{IM} \cup \mathrm{W}_{TR}^{IM} \cup \mathrm{W}_{TP}^{IM} \tag{5.4}$$

$$\mathrm{W}_P^M = \mathrm{W}_{PI}^{IM} \cup \mathrm{W}_{PM}^{IM} \cup \mathrm{W}_{PR}^{IM} \cup \mathrm{W}_{PT}^{IM} \tag{5.5}$$

where W_{HA} and W_{HI} are the total fingertip to fingertip manipulation workspaces of the hand when using an anthropomorphic configuration (Hand Anthropomorphic, HA) and an interdigitated configuration (Hand Interdigitated, HI), respectively. Hence, only the thumb's fingertip to fingertip manipulation workspace (W_T^M) with the other fingers is needed when the configuration is anthropomorphic, while the union of W_T^M and W_P^M (the pinky's fingertip to fingertip manipulation workspace with all other fingers), is needed when the configuration is interdigitated. The W_T^M workspace is found by taking the union of the intersections of all possible fingertip to fingertip manipulation workspaces (Intersection of Manipulation workspaces, IM) between the thumb finger and each of the other four fingers. Similarly, the W_P^M workspace is found by taking the union of the intersections

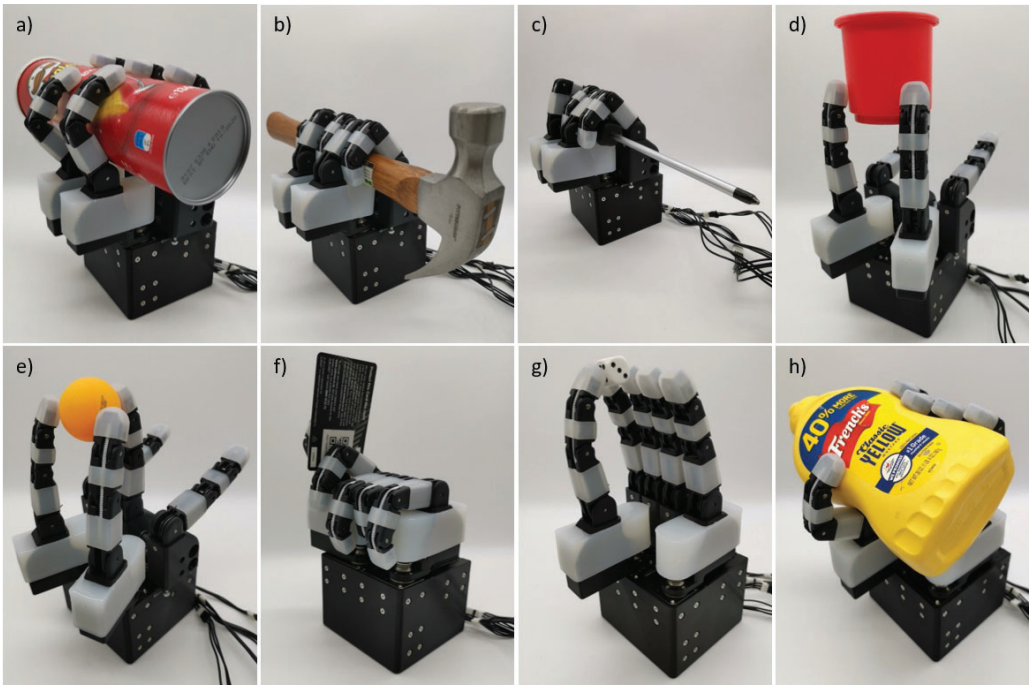

Figure 5.6: Grasping experiments were executed with the multi-grasp anthropomorphic robot hand with the YCB object set [104]. Eight objects from the set were used to evaluate the hand: a chip can, a hammer, a screwdriver, a red stacking block, a ball, a credit card, a dice and a mustard container.

of all possible fingertip to fingertip manipulation workspaces between the pinky finger and each of the other four fingers.

The total workspace is shown in Fig. 5.5b. The anthropomorphic configuration of the hand was able to achieve a full workspace volume of 2575.4 cm^3. However, by utilizing the reconfigurable finger base frames of the hand the workspace can be increased to 4034.9 cm^3, more than one and a half times the original workspace. In addition to using the reconfigurable base frames, the hand's fingertip to fingertip workspace can be increased from 313.3 cm^3 to 20598.8 cm^3.

5.3 Experimental Validation

The effect of changing finger base frames can greatly alter the force exertion capabilities. This can be observed by comparing the differing grasping strategies of the hand. For instance, between the interdigitated power grasp and the anthropomorphic power grasp, a force exertion difference of more than 24 N can be

observed. This highlights the importance of a reconfigurable base to improve the force applied on a given object to optimize the grasp quality. To successfully grasp a majority of everyday-life objects that humans encounter approximate contact forces between 10 N to 15 N [105] are required. As a result, the developed gripper is capable of grasping many daily life objects.

5.3.1 Grasping Experiments

This experiment focused on evaluating the grasping capabilities of the hand. As depicted in Fig. 5.6, eight different everyday-life objects from the YCB object set [104] have been successfully grasped by the hand in different configurations. This object set facilitates grasping and manipulation benchmarking with everyday-life objects. The objects selected were a chip can, a hammer, a screwdriver, a red stacking block, a ball, a credit card, a dice, and a mustard container. A current feedback control measuring the tendon tension experienced by the fingers was used to grasp the objects during the experiments. It can be seen that regularly shaped objects such as the chip can, the shaft of the hammer and the screwdriver have been grasped using the interdigitated finger configuration. This ensures that the maximum contact area of the hand is utilized, generating a highly stable grasp. This is especially important for objects that require non-optimal grasps and contact points that do not encompass the center of mass, in order to be successfully used. An example is a hammer that requires to be grasped from the handle to be successfully used as a tool. The proposed hand is also capable of reconfiguring the finger base frames to achieve a tripod configuration, which enables the underactuated fingers of the hand to apply contact forces more effectively towards the centroid of the objects. The anthropomorphic configuration of the hand was used to execute a variety of alternative grasps that the hand is capable of, for example, key grasps, pinch grasps, and power grasps. Also, the hand utilizes the anthropomorphic configuration to better conform to irregular object geometries like the mustard bottle (see Fig. 5.6h).

5.3.2 In-Hand Manipulation Demonstrations

Many tasks require dexterous, in-hand manipulation of an object to reposition and/or reorient it to a new configuration that is useful for the chosen task. Preprogrammed demonstrations of the in-hand manipulation motion capabilities of the hand were performed with objects using a modular, sensorized object set [106]

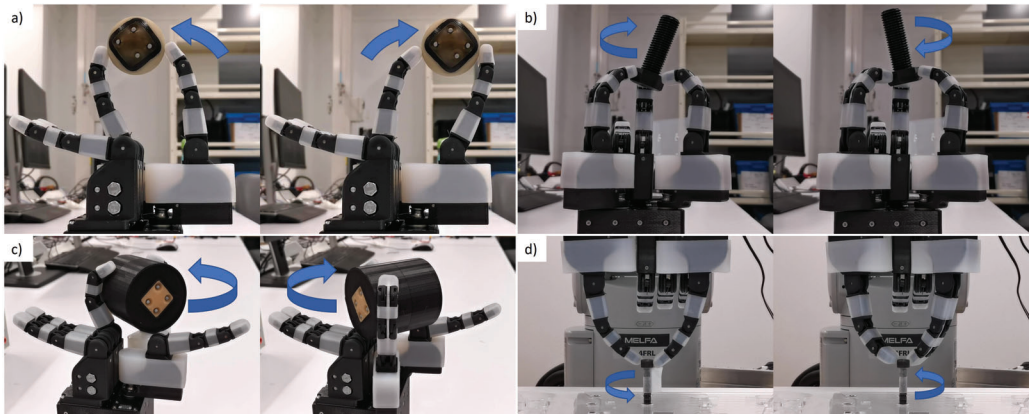

Figure 5.7: The demonstration shows the hand manipulating a bolt, and small sized soft sphere and a medium size rigid cylinder contained in the modular, sensorized object set. Subfigure a) and b) show the hand performing equilibrium point manipulation tasks, while subfigure c) presents the hand executing a finger gaiting motion. Subfigures d) displays the hand utilizing its reconfigurable base to perform finger gaiting to unscrew a bolt.

and a dexterity test board [107]. The multi-grasp hand was used to perform a bolt unscrewing task of the dexterity test board, utilizing its reconfigurable finger base frames to execute finger gaiting, as seen in Fig. 5.7d. The finger gaiting capabilities of the hand can also be extended to allow repositioning of an object from the left side of a finger to the right side. In Fig. 5.7c, a medium sized, rigid surface cylinder is being repositioned to different sides of the ring finger on the hand. In the right image of Fig. 5.7c, the ring finger is hidden behind the object. Other than finger gaiting, the reconfigurable base also allows the hand to perform equilibrium point manipulation (see Fig. 5.7a-b). A series of equilibrium point manipulation tasks are executed with: i) a small 3D printed sphere with a soft surface, as shown in Fig. 5.7a, and ii) a plastic bolt that is used to perform a twirling trajectory, as depicted in Fig. 5.7b. A demonstration video of the hand grasping and manipulating a wide range of everyday life objects can be found below at the following URL:

www.newdexterity.org/hybridhand

5.3.3 Force Exertion Capabilities

This experiment evaluated the force exertion capabilities of the proposed robot hand. Four different grasp configurations (as shown in Fig. 5.2) were assessed: in-

Table 5.1: The maximum grasp forces exerted on the dynamometer.

Configuration	**Grasp Forces (N)**
Interdigitated power grasp	150.6
Anthropomorphic power grasp	126.2
Anthropomorphic pinch grasp	14.3
Tripod grasp	19.2

terdigitated power grasp, anthropomorphic power grasp, anthropomorphic pinch grasp, and tripod grasp. The force measurements of each configuration were collected using a Biopac MP36 data acquisition unit (Biopac Systems, Inc., Goleta, California) equipped with the SS25LA dynamometer. The dynamometer was placed flat on the palm pad of the hand to measure the forces of power grasps. Recordings for the precision grasp forces involved placing the dynamometer on a table surface and grasping the two sides so as to capture the applied forces by the fingertips. The grasps were executed 5 times to acquire the mean of the maximum grasp forces that the hand can achieve, as seen in Table 5.1.

5.3.4 Gripper Comparison

The following table (Table 5.2) analyzes and compares the developed hand to other existing robotic grippers. A comparison of weight, number of actuators and fingers, anthropomorphism, reconfigurability, and in-hand manipulation capabilities of the different end-effectors are evaluated. When assessing the dexterity of the different robot hand, the high degrees of freedom and actuation of the Shadow hand allows it to execute complex manipulation tasks. The opposable thumb and separable fingers from the active MCP joints emulating a real human hand facilitate a variety of grasping strategies that can be chosen. However, the high degree of actuation makes the hand difficult to control and imparts a high weight and large form factor to the design. Alternatively, systems like the Robtiq (2-fingered) gripper, which utilizes core grasping strategies are capable of grasping an array of everyday life objects but are unable to perform in-hand manipulation due to the limited actuation.

Table 5.2: Robot gripper and hand comparison

Hand	**Fingers**	**Actuators**	**Anthropomorphism**	**In-hand Manipulation**	**Reconfigurable**	**Weight (g)**	**Grip Force (N)**
Robotiq (2-Fingered) [108]	2	1	Non-anthropomorphic	No	None	890	30-100
Yale Model T42 [109]	2	2	Non-anthropomorphic	2D manipulation	None	400	9.6
Barrett Hand [110]	3	4	Non-anthropomorphic	Yes[1]	Yes[2]	1200	15
BLT Gripper [99]	3	5	Non-anthropomorphic	Yes[1]	Yes[2]	1200	30-120
Robotiq (3-Fingered) [111]	3	3	Non-anthropomorphic	No	Yes[2]	2300	15-60
iHY Robot Hand [100]	3	4	Non-anthropomorphic	Yes[1]	Yes[2]	1350	15
DLR HIT Hand II [112]	4	5	Anthropomorphic	Yes[1]	None	1500	50
Shadow Hand [68]	5	20	Anthropomorphic	Yes[3]	Yes[4]	4200	Unreported
Proposed Design	5	8	Hybrid[5]	Yes[6]	Yes[7]	1280	14.3-150.6

[2]Some in-hand manipulation capabilities are assumed but not specifically demonstrated. [3]Two finger bases rotate in-sync. [4]Highly dexterous in-hand manipulation capabilities. [5]Opposable thumb and abduction capable MCP joints. [6]Anthropomorphic and non-anthropomorphic. [7]Planar and spatial manipulation. [8]Opposable thumb and pinky with extendable index, middle, and ring finger spacing.

The use of reconfigurable finger base frames like in the Barrett hand, BLT gripper, and iHY hand allow them to optimally utilize the limited number of actuators to perform a range of precision and power grasping strategies (e.g. pinch to interlacing fingers). While reconfiguring the hands can place themselves in configurations to perform different in-hand manipulation tasks. We utilize this reconfiguration concept, but apply this with an anthropomorphic starting configuration to facilitate optimal grasping and operation of human tools, which have finger grooves and holes that are designed to maximize the contact area and grip with the human hand. The reconfigurability allows the proposed robot hand to perform a wide range of grasping and in-hand manipulation tasks while avoiding the high weight and control complexity cost commonly seen with highly functional anthropomorphic robot hands.

5.4 Conclusions

In this chapter, we proposed a multi-grasp, anthropomorphic robot hand that is capable of switching between non-anthropomorphic and human-like grasp configurations. This feature allows the underactuated hand to achieve a wide range of grasps and manipulation modes, while also taking advantage of the shape ergonomics of many objects. This design feature enables the hand to successfully grasp many objects used in everyday-life. By implementing reconfigurable finger base frames, we were able to increase the workspace of the hand by 150% when compared to the workspace of the anthropomorphic configuration base frames alone. The performance of the robot hand was assessed through: i) force exertion capacity tests, ii) grasping experiments that involved everyday-life objects, and iii) demonstrations that included four different manipulation tasks (2D and 3D equilibrium point manipulation and two different finger gating tasks). In the interdigitated configuration, a maximum grasp force of 150.6 N was obtained from the developed hand, while a 19.2 N tripod grasp was generated. In the anthropomorphic configuration, the hand was able to exert 126.2 N of force with a power grasp, and 14.3 N with a pinch grasp.

5.5 Future Directions

Regarding future directions, the addition of sensing elements to the distal phalanges of the fingers will aid in improving the manipulation performance and can indicate when disturbances during manipulation are occurring. Exploration of different control methods that will facilitate optimal grasp mode selection when executing various everyday life tasks with the hand.

Part III

Adaptive Fingers and Hands for Prosthetic Systems

Chapter 6

Adaptive, Tendon-Driven, Affordable Prostheses for Partial Hand Amputations: On Body-Powered and Motor Driven Implementations

6.1 Background

The dexterity of the hand allows humans to execute a wide range of dexterous tasks that no other being is capable of. Loss of one or more fingers compromises some of the capabilities of the human hand and this has a tremendous impact on the lives of amputees. According to [113], more than 60 % of the upper limb amputations are transcarpal. In many cases of partial finger amputation (e.g., thumb amputation, multi-finger amputation), the amputation impedes the execution of important grasps needed to perform activities of daily living (ADLs). Most of these grasps are executed using the thumb, index and middle fingers, while the ring and pinky fingers have a subsidiary role [114].

In this chapter, we propose two compact, lightweight, and affordable prostheses for partial hand amputations (see Fig. 6.1). The first device uses a body-powered mechanism while the second device is an underactuated, externally powered solution. The devices are experimentally tested, and their efficiency is validated using two different types of tests: i) grasping tests that involve different everyday ob-

Figure 6.1: The proposed prosthesis has been designed to support both a body-powered actuation scheme (subfigure a)) and an externally powered, motor driven actuation scheme (subfigure b)).

jects, ii) force exertion capability tests that focus on the finger forces that can be exerted while using the prosthetic devices [1].

The rest of the chapter is organized as follows: Section 6.2 presents the related work, Section 6.3 focuses on the designs of the devices, Section 6.4 details the experimental setup used for the tests and presents the experimental results, Section 6.5 concludes the chapter, and Section 6.6 discusses some future directions.

[1]Majority of the chapter is based on [19], © 2019, IEEE. Reprinted, with permission, from Geng Gao, Lucas Gerez, and Minas Liarokapis, Adaptive, tendon-driven, affordable prostheses for partial hand amputations: On body-powered and motor driven implementations, 41st Annual International Conference of the IEEE Engineering in Medicine and Biology Society (EMBC), 2019.

6.2 Related Work

Despite the significant percentage of finger amputations compared to other upper limb amputations, active prosthetic fingers have not received the required attention from researchers due to the high level of customization needed to fit the design to the patient's hand [115], as well as due to difficulties to embed sensors and actuators to the device as compared to active, full hand prosthetic devices. On the other hand, numerous passive prosthetic fingers have been proposed to replace lost fingers. In [116] and [117], the authors propose prosthetic fingers made out of silicone rubber that mimic the human fingers. These solutions are aesthetically pleasing, however, the finger is rigid and not capable of bending. In [118], the authors present an osseointegrated implant for finger prosthesis, a direct attachment to the bony stump. In [119], the authors describe a method to optimize the fitting of prosthetic fingers for distal amputations. Although the aforementioned solutions certainly provide user satisfaction, the improvement on the grasping capabilities is limited.

Active prosthetic fingers are more functional, enabling the user to execute most of their daily activities [115], and they can be either body-powered or externally powered. In [120], the authors present an overview of the existing surgical and technological solutions for treating partial hand amputations. Regarding body-powered prosthetic fingers, in [121] and [122], the authors propose a linkage-based, wrist-driven prosthesis for amputees with disarticulation of the thumb and index finger. In [123], the authors demonstrate a wrist-powered partial hand prosthesis using a continuum whiffletree mechanism. Other body-powered solutions are the X-Finger (Didrick Medical, Naples, FL) [124], which is a custom fit prosthetic finger that allows flexion and extension of the finger in order to restore dexterous manipulation and the M-finger (Partial Hand Solutions LLC), which is a tendon-driven prosthetic finger. Body-powered devices are usually simple, affordable, and easy to operate, however, the rejection rate of these devices is higher and the harnesses might be uncomfortable if compared to externally powered devices [125]. Regarding externally powered prosthetic fingers, in [126], the authors propose an electromyography (EMG) controlled prosthetic robot finger that can be attached to the end of the finger root bone. The force is transmitted through a linkage system and is controlled using a linear actuator. In [127], the authors present an EMG prosthetic hand for amputees with remaining fingers. In [128], the authors describe a partial hand prosthesis that is actuated by a DC motor combined with a gearhead. A commercially available, externally powered prosthesis for partial

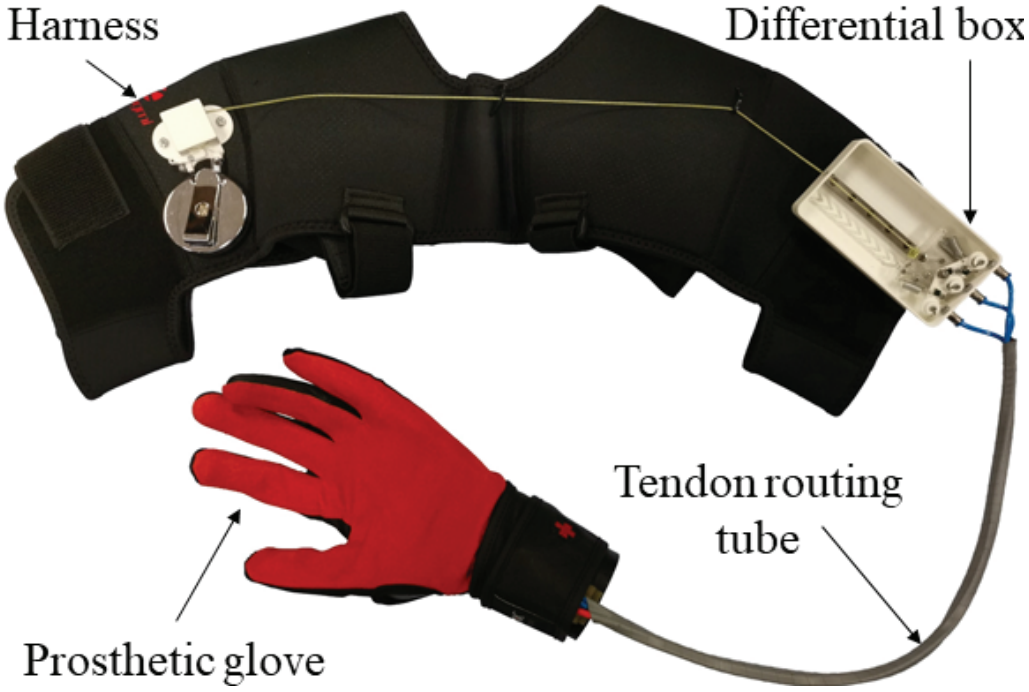

Figure 6.2: The body-powered prosthesis consists of a harness, a differential box, and a prosthetic glove. The harness houses a tensioner located on the left shoulder and a differential box on the right shoulder. The differential contains a linear ratchet for locking the tendon, a whiffle tree for distributing the forces across the prosthetic fingers, and an individual tendon tensioners for each prosthetic finger. The prosthetic glove houses a fake amputee hand and three prosthetic fingers (index, middle, and ring). The fingers are connected to the differential box through tendons guided through tendon routing tubes. The device can be customized to different types of amputations (housing less or more fingers).

hand amputations are the I-digits Quantum (Touch Bionics, Hilliard, OH) [129], a multi-articulating device that can be controlled with simple gestures. Although powerful and attractive, externally powered prosthetic devices are still expensive, heavy, bulky, and have limited autonomy.

6.3 Designs

In this section, the designs of the body-powered and the externally powered, motor driven prostheses are presented and their functionalities are discussed.

6.3.1 Body-powered Partial Hand Prosthesis

The body-powered device was designed to improve the grasping capabilities of the amputee by providing an intuitive, robust, and lightweight solution. The design is based on the well-known, body-powered mechanism that transmits the forces of the upper body (e.g., shoulders) to the prosthetic fingers [130, 125]. The proposed body-powered device is composed of three main parts: the harness, the differential box [131], and the prosthetic glove (which includes the prosthetic fingers), as shown in Fig. 6.2. The final body-powered prototype weighs only 553 g.

In order to operate the device, the amputee must execute simple movements that increase the tension of the cable connecting the harness to the differential. When the cable is tensioned, the differential box distributes the tendon force to the prosthetic fingers through artificial tendons made out of a low friction braided fiber of high-performance Ultra-High Molecular Weight Polyethylene (UHMWPE). Polyurethane tubes that connect the differential mechanism to the glove are used for tendon routing. The routing tubes are attached to the glove through aluminum connections. The glove is used to keep the fingers in place (the prosthetic fingers are stitched to the glove to avoid undesired motions). The device can be adjusted to different body types and sizes. The device personalization occurs only for the prosthetic fingers and the harness, as these components depend on the user's body dimensions. Appropriate anthropometry studies can be employed to derive the finger link lengths from the overall hand length [132, 133]. Alternatively, the dimensions can be measured on the intact hand (if available).

The differential box allows tendon tensioning, force distribution, and position locking of the fingers. The input force for actuating the fingers originates from the shoulders. When the main cable is tensioned the finger tendons are pulled and the whiffletree differential distributes the force among the three fingers. Differential mechanisms are widely used in prosthetic devices to evenly distribute the forces [97, 123]. The linear ratchet on the differential box guarantees that the fingers can be locked at any desired position due to a lever that locks the motion of the system when moved into one of the channels of the linear ratchet. The circular ratchet clutch mechanisms on the whiffletree provide tendon tensioning and length adjustment [134]. When the main tendon is pulled for a second time the lever is disengaged, the system goes to its starting point, and the fingers return to their initial positions. The harness is not only used to connect the main tendon and the differential, but also to maintain the shoulders are aligned in a comfortable and anatomically correct manner.

6.3.2 Externally Powered Partial Hand Prosthesis

The externally powered, motor driven prosthesis was designed to provide the amputee with a solution that offers precise object grasping, requiring minimal user effort. The prosthesis was designed to operate up to two fingers independently and is composed of a motor box with two motors, a control module and a prosthetic glove (which includes the two prosthetic fingers). The electronics and actuators are attached to the wrist strap of the glove. The final prototype weighs only 260 g.

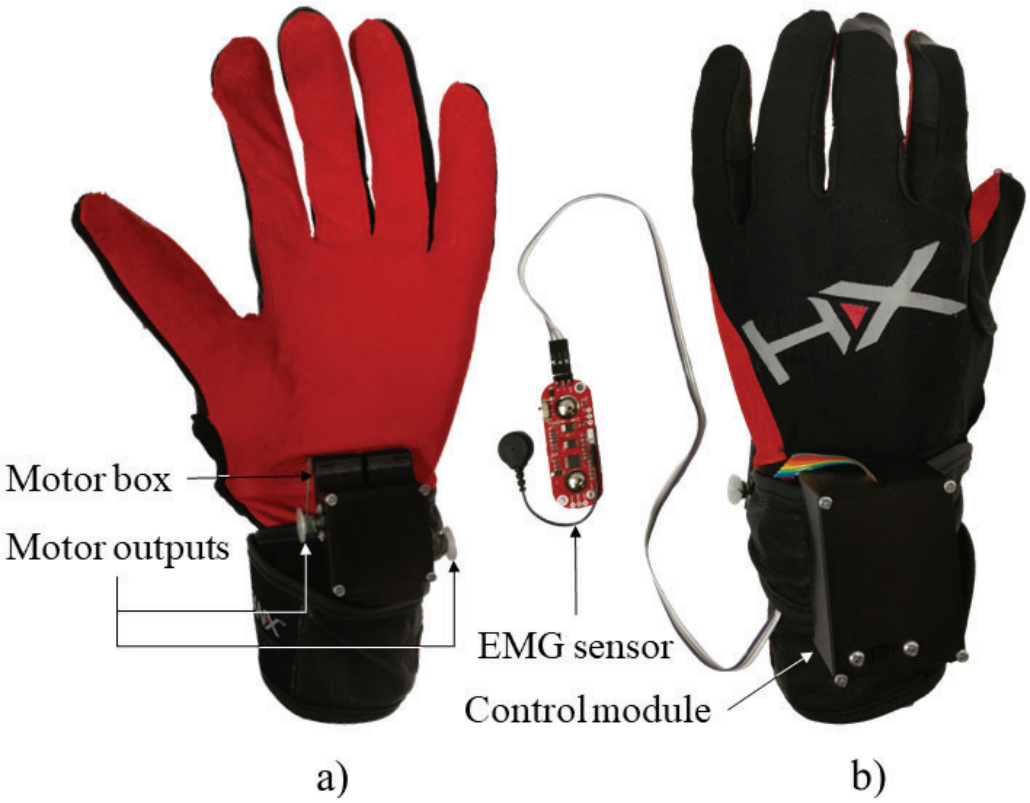

Figure 6.3: The externally powered, motor driven prosthesis contains a motor box with 2 motors as seen in the front view of the hand (subfigure a). The back view of the hand (subfigure b) shows the location of the control module and the EMG sensor of the device. The flex sensor of the externally powered partial prosthesis is located inside the glove at the pinky finger.

The control module accommodates a motor controller, a microcontroller (Arduino Nano) and two 500 mAh Li-Po batteries, while the motor box accommodates two DC motors with encoders and two gearboxes. Two different sensors were connected to the microcontroller in order to control the prosthetic device: a flex sensor

and an EMG sensor. Only one of these sensors is needed to operate the prostheses, however, two sensors were added in order to improve the user experience and robustify the operation of the device. The flex sensor is positioned in the inner side of the glove on one of the remaining fingers (for the experiments performed, the flex sensor was mounted on the pinky finger). When the intact finger bends, the flex sensor detects the angle variations of the finger joints, and the prosthetic fingers are controlled to follow a similar trajectory (using a synergistic approach) employing a PID controller. If the amputee does not have any remaining fingers that can be used to control the prosthetic fingers, the EMG sensor is used. The EMG sensor is located on the skin of the amputee's forearm in order to capture the myoelectric activations of the muscles (*Flexor Digitorum Superficialis* area). The muscle activities that are related to grasping are detected by the EMG sensor board (MyoWare muscle sensor) and the signals are sent to the microcontroller where they are processed, and the motor is controlled through simple thresholding. The whole device is depicted in Fig. 6.3.

6.3.3 Prosthetic Fingers

The prosthetic fingers were designed to replace the amputee's missing phalanges and to assist the remaining phalanges in the grasping process. The fingers were designed to be slim and compact while maintaining an anthropomorphic appearance in order to be accommodated by a glove. Alongside this, the fingers were designed to be modular to allow amputees to easily replace key components of the prosthetic fingers being the phalanges, the interfacing base, and the passive extension elastic bands. Two joints are used per finger instead of the three joints of human index, middle, ring and pinky fingers, with one joint being the metacarpophalangeal (MCP) joint and the other one being the proximal interphalangeal (PIP) joint. The absence of the distal interphalangeal (DIP) joint allows the fingers to have an increased finger pad area for grasping, while also maintaining a compact and slim form factor. The actuation of the fingers is based on a tendon driven system as seen in [135], allowing the fingers to be underactuated and to exhibit an adaptive grasping behavior. The finger structure is manufactured from 3D printed PLA plastic and polyurethane elastomers (Smooth On Vytaflex 30 and Smooth on PMC-780). The softer polyurethane elastomer (Smooth On Vytflex 30) was incorporated into the finger pads to improve conformability of the fingers on the grasped objects while the stiffer polyurethane elastomer (Smooth on PMC-780) was implemented into the passive extension elastic bands and the interfacing

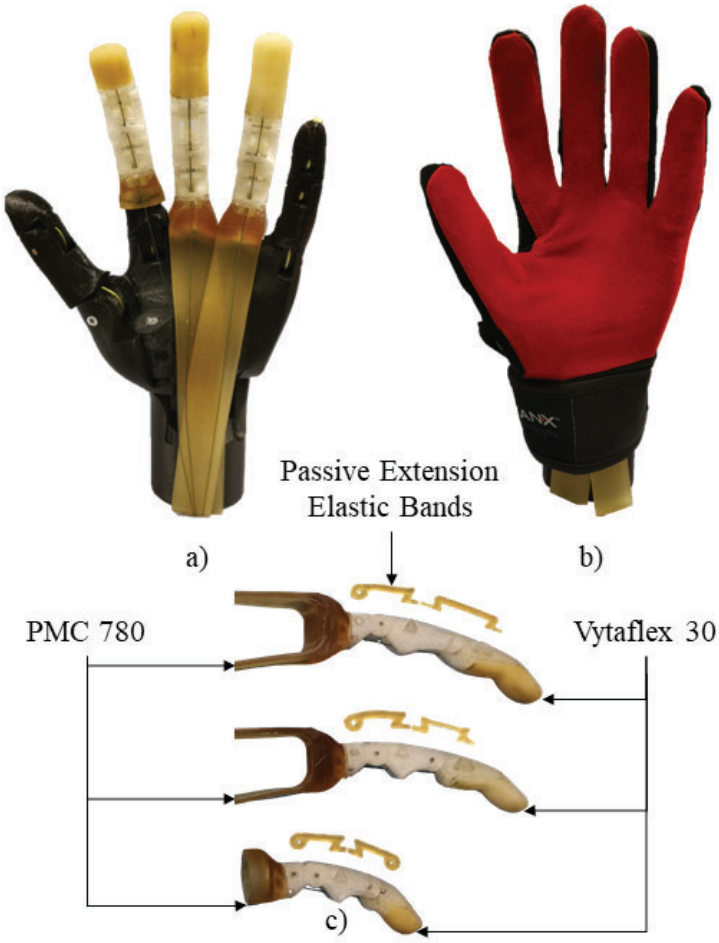

Figure 6.4: The tendon driven prosthetic fingers are attached to a paradigmatic, 3D printed amputee hand, which is missing the index finger's distal and middle phalanges with the middle, and ring fingers being fully amputated (subfigure a)). Subfigure b), shows the compatibility and fit of the prosthetic fingers with the paradigmatic hand inside the glove. Subfigure c), presents the structure of each prosthetic finger and the passive extension elastic bands. The fingers are built using the concept of Hybrid Deposition Manufacturing [46] and they combine 3D printed parts with elastomer materials (SmoothOn Vytaflex 30 and PMC 780 polyurethane rubbers).

bases of the prosthetic fingers. Two types of prosthetic fingers were designed and developed as shown in Fig. 6.4 (subfigure c).

In Fig. 6.4, the first example is a full prosthetic finger, while the second one is a partial prosthetic finger for amputees that are missing the first two phalanges of their finger (middle, and distal). The prosthetic finger link lengths were modelled

after the human hand employing hand anthropometry studies [132] with a hand length of 190 mm, as reported in Table 6.1.

Table 6.1: The prosthetic finger characteristics of the index, middle, and ring fingers for hand length of 190 mm. The proximal link length of the prosthetic fingers is measured from the base of the interfacing part to the PIP joint.

Fingers	Weight (g)	Length of Phalanges (mm)		
		Proximal	Middle	Distal
Index	23.90	-	27.10	18.43
Middle	39.46	50.54	32.30	20.52
Ring	37.24	46.36	31.35	20.33

6.4 Experiments and Results

The experiments that were conducted to assess the performance of the body-powered and the externally powered, motor driven prosthetic device, were divided into two parts. The first part focused on evaluating the grasping forces and the hand configurations, while grasping different objects. The second experiment focused on measuring the grasping forces (in different configurations) that the devices can exert. To execute the experiments, an adapted 3D printed paradigmatic amputee hand was positioned inside the glove to act as a simulated amputee's hand. This anthropomorphic model hand has a fully articulated thumb and pinky finger, a partially amputated index finger that has only a metacarpophalangeal (MCP) joint, and two fully amputated fingers (middle and ring fingers). This hand configuration was chosen in order to be able to test both types of prosthetic fingers designed. Three prosthetic fingers are enough to test both devices, since the body-powered device can actuate up to three fingers and the externally powered, motor driven device up to two. A fully articulated finger on the model hand was chosen to simulate the remaining finger of the amputee's hand, so as for the flex sensor to operate appropriately (in this case, the sensor was connected to the pinky finger).

6.4.1 Object Grasping Performance

The first experiment was executed to evaluate the grasping performance of the proposed prosthetic devices. All eight everyday objects used in this experiment were selected from the YCB object set [104], an object set designed for facilitating benchmarking in robotic grasping and manipulation. The experiments conducted can be seen in Fig. 6.5.

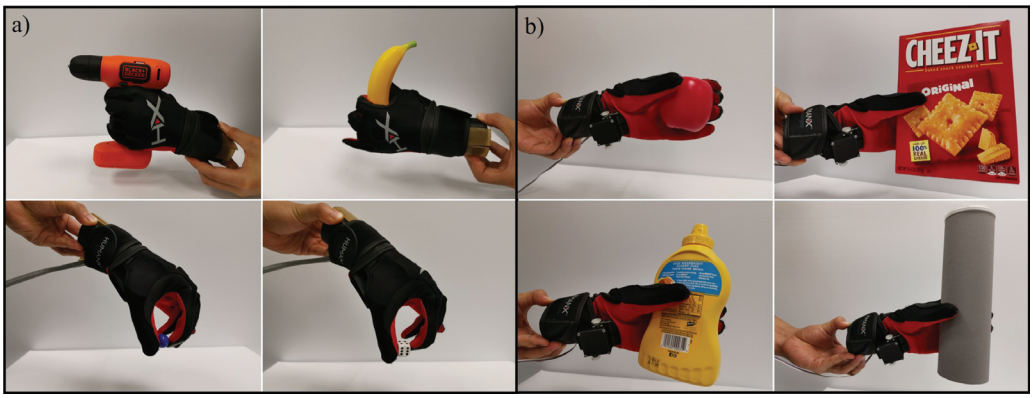

Figure 6.5: The grasping experiments involved eight objects of the YCB object set [104] and they were used to evaluate the grasping capabilities of both the body-powered device (subfigure a)) and the externally powered, motor driven device (subfigure b)). The objects used are a drill, a banana, a marble, a die, an apple, a box, a mustard bottle, and a chip can.

Table 6.2: The maximum grasp forces exerted on the dynamometer. Forces were measured for both pinch and power grasps.

Device	Grasp Forces (N)	
	Pinch Grasp	Power Grasp
Body-Powered Prosthesis	3.8	10.4
Externally Powered Prosthesis	8.2	18

6.4.2 Finger Force Exertion Experiment

The second experiment focused on measuring the amount of grasping force that can be exerted by the devices. The grasp force results can be seen in Table 6.2. Two different grasping types were tested: pinch grasp and power grasp (see Fig. 6.6). The force measurements in each scenario were collected using a Biopac MP36 data acquisition unit (Biopac Systems, Inc., Goleta, California) equipped with the SS25LA dynamometer. For the body-powered device, the power grasp involved the three prosthetic fingers (index, middle, and ring). For the motor driven device, since the motor box is connected to the middle and ring fingers, the pinch grasp was executed using the thumb and middle fingers, while the power grasp was executed using the middle, ring, and thumb.

Figure 6.6: The force experiments were conducted with the partial prosthesis executing a pinch grasp (subfigure a)) and a power grasp (subfigure b)) on a SS25LA dynamometer (by Biopac Systems, Inc., Goleta, California).

6.4.3 Devices Demonstration Video

A video containing the description of the devices and some experiments can be found at the following URL:

http://www.newdexterity.org/prosthetichands

6.5 Discussion and Conclusions

In this chapter, we presented two adaptive, tendon-driven, glove-based, affordable prostheses for partial hand amputations, a body-powered and an externally powered, motor driven version. Two different experiments were executed to assess the efficiency and the grasping performance of the devices and the results demonstrate that the proposed solutions can be used to aid amputees in a range of activities of daily living. Although the body-powered device is heavier and larger than the externally powered device (due to the harness), it is still lightweight, simpler than the motorized device, more affordable and it does not rely on a battery or other electronics, having unlimited operation time. The underactuated, lightweight, externally powered, motor driven prosthesis relies on various sensors and electronic

components, and it offers precise grasping requiring minimal user effort. Both partial hand prostheses are designed in an amputee specific manner offering increased personalization.

6.6 Future Directions

Regarding future directions, we plan to test both devices in clinical trials involving amputees and to redesign them according to the trials feedback. For the motor driven device, we plan to increase the number of motors, to develop multiple versions for different types of partial hand amputations, and to increase the battery life of the prosthetic device by performing an optimal motor selection and energy consumption optimization.

Chapter 7

On Differential Mechanisms for Underactuated, Lightweight, Adaptive Prosthetic Hands

7.1 Background

The human hand is a powerful tool enabling humans to perform a wide range of tasks from interacting with objects used in daily living to executing gestures in social activities. According to [136], approximately 540,000 amputees suffered from upper limb loss in the US with the expected projections to be doubled by 2050. In Italy and the UK, approximately 3,500 and 5,200 upper limb amputations occur every year [113]. Loss of such a limb can have a detrimental effect on an amputee's quality of life, preventing them from executing critical grasps needed in activities of daily living (ADL).

The latest technological advancements have helped to improve the development of prosthetic hands towards becoming increasingly dexterous devices for amputees. Despite this, design tradeoffs between the dexterity of the prosthesis, weight, form factor, and cost of the device still exist [137]. Although there are highly dexterous robot hands [68, 138, 139] capable of emulating the dexterity of the human hand, the number of independent degrees of freedom (DOF) and the actuators utilized make it difficult to control such devices, without compromising the weight, form factor, and affordability needed by amputees to adopt these hands for ADL. Over the past decade, a shift towards adaptive, underactuated, and tendon driven systems have made it possible for robot hands to be lightweight,

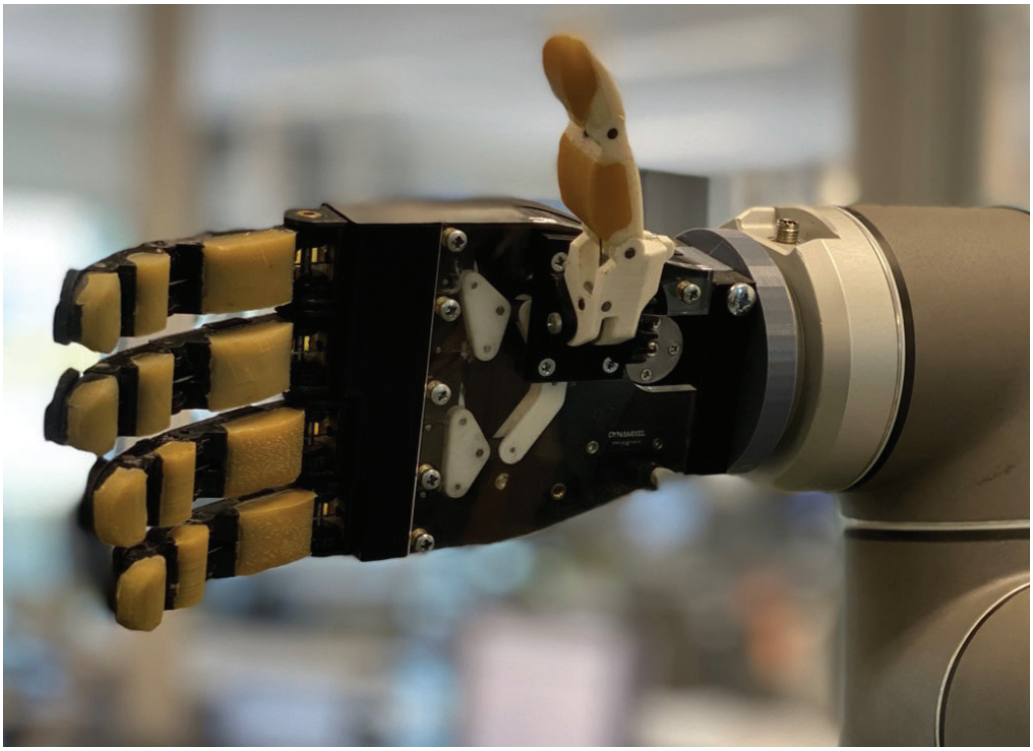

Figure 7.1: The proposed highly underactuated prosthesis capable of performing a variety of controllable grasp poses with only two actuators.

compact, and affordable while remaining highly functional. These systems can perform robust grasping under high object pose uncertainties, by utilizing differential mechanisms and structural compliance to compensate for the reduced independent DOFs. This underactuated property also allows the hand to be intuitively controlled with simple control laws in comparison to previous design approaches. Adaptive hands have been commonly applied to applications related to robotic grasping and manipulation for full robotic arm-hand systems. However, they can also be applied to a variety of alternative applications that range from the development of prosthetic devices for improving the quality of living for amputees [19, 140] to enabling robots and Unmanned Aerial Vehicles (UAVs) / drones to better interact with their environment [141, 142].

In this chapter, we focus on the design, development, and evaluation of a lightweight, affordable, highly underactuated, anthropomorphic prosthetic hands, which use both manual and active selectively lockable differential mechanisms. The locking mechanisms allow for the selection of different fingers to be actuated in underactuated hands, which utilize differentials to perform adaptive grasping.

The mechanism has been implemented so as to block the outputs of three different differentials allowing for increased control of individual fingers [1] [2].

The rest of the chapter is organized as follows: Section 7.2 presents the related work, Section 7.3 presents the design of the locking mechanisms used in the prosthetic hand, Section 7.4 focuses on the experimental setup used to assess the functionality of the prosthetic hand and presents the experimental results, and Section 7.6 concludes the chapter, and Section 7.7 discusses the future directions.

7.2 Related Work

Several prosthetic hands are commercially available ranging from cosmetic devices [143], which are highly anthropomorphic but are non-functional to body powered [144] and externally powered [145] prosthetic hands that provide amputees with a means to interact and grasp objects in ADL. However, most prosthetic devices are expensive costing anywhere between $4,000 to $75,000 depending on the required level of functionality needed [146]. In [147], the authors present the difficulties amputees face in the large costs required for purchasing and maintaining a prosthesis, leading to amputees avoiding the use of the prosthesis in fear of damaging the device. In [148], the authors conduct a study analyzing multiple commercially available prosthetic hands. The results of the comparison showed that the ideal prosthetic hand should weigh <500 g, while remaining highly functional with a low number of actuators.

Similarly, in [137], the authors make the observation that minimalistic approaches (e.g. reducing the number of sensors and actuators used) towards the design of robot hands are a more favorable way of achieving dexterity. Adaptive underactuated devices have adopted a variety of different and intuitive methods to implement dexterity in a minimalistic way. In [149], a compact geared differential capable of actuating four fingers via a single motor was developed. The usage of this differential mechanism enabled the fingers of the device to conform to the shape of various objects maximizing grasp contact to create stable and robust

[1] Majority of the chapter is based on [20], © 2021, IEEE. Reprinted, with permission, from Geng Gao, Anany Dwivedi, and Minas Liarokapis, An Anthropomorphic Prosthetic Hand with an Active, Selectively Lockable Differential Mechanism: Towards Affordable Dexterity, IEEE/RSJ International Conference on Intelligent Robots and Systems (IROS), 2021.

[2] Majority of the chapter is based on [21], © 2021, Frontiers. Reprinted, with permission, from Geng Gao, Mojtaba Shahmohammadi, Lucas Gerez, George Kontoudis, and Minas Liarokapis, On Differential Mechanisms for Underactuated, Lightweight, Adaptive Prosthetic Hands, Frontiers in Neurorobotics, 2021.

grasps. In [150], the authors demonstrate the use of structural compliance in the form of tendon driven flexure joint fingers to perform adaptive power grasps. In [151], the authors present an anthropomorphic prosthetic hand using a whiffletree differential enabling a singular actuator input to power the entire hand to grasp and conform to a variety of object shapes. However, the hand is only able to follow a single grasping trajectory, relying on the object or the environment to obstruct the finger motion and alternate between three grasp types. In [152], the authors propose the use of a bistable ratchet locking mechanism to enable control over the opposition of the thumb allowing for four independent grasping postures to be achieved with a single actuator. In [153], the authors design mechanical selectors, which are capable of obstructing the motion of a whiffletree differential allowing for three grasping modes to be executed with a single actuator by adjusting a slider-selector with the opposite hand. However, this design is limited to a maximum of three grasping postures requiring the user to switch between different slider-selectors to achieve alternative grasping postures. Similarly in [97], the authors utilize manual lockable buttons and latches, which interact with a whiffletree differential to create a highly underactuated prosthetic hand capable of executing 144 different grasping postures. Although the device significantly increased the number of selectable grasping postures for amputees at an affordable cost, the need for another hand to operate the buttons can make it difficult to perform bimanual tasks, or to be used by bilateral amputees. However, by integrating locking mechanisms into prosthetic hands, improved control of individual fingers can be achieved with a minimal set of actuators, reducing their weight, cost, and size.

7.3 Designs

7.3.1 Selectively Lockable Differentials

The design of the selectively lockable differentials is motivated by the multiple grasping strategies that the human hand can choose from for a given task. For that reason, we have proposed a mechanism based on the well-known whiffletree differential, and two other differentials (a four-output geared differential [149], and a series elastic differential [154]). The use of a locking mechanism allows the user to select a grasp strategy from a wide range of possible combinations [97].

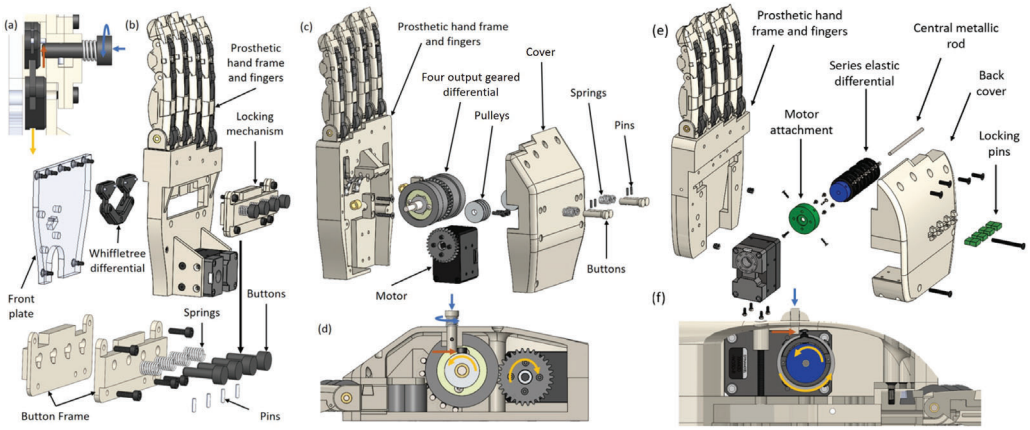

Figure 7.2: The manual selectively lockable mechanism has been integrated into three differentials: the whiffletree differential (subfigure (a) and (b)), the four output geared differential (subfigure (c) and (d)), and the series elastic differential (subfigure (e) and (f)). Subfigure (a) illustrates how the locking mechanism blocks a selected output on the whiffletree differential. Button locking is executed through a pushing and twisting action, which engages the button for locking (this is shown with the blue arrows). When the whiffletree is actuated (represented by the yellow arrow), the button provides a blocking force (orange arrow) holding the selected output in place. Subfigure (b) presents how the manual locking mechanism, and the whiffletree differential are integrated into the prosthetic hand. Similarly, subfigure (c) presents the structure of the prosthetic hand when the lockable four output geared differential is used. The locking mechanism utilizes a similar button mechanism to block the motion of a pulley in the four output geared differential, as depicted in subfigure (d). The exploded view of the series elastic differential is presented in subfigure (e), showcasing the assembly of the locking system when integrated in the series elastic differential. Locking the series elastic differential involves pushing the locking pins down to block the output attachments from rotating. This is illustrated in subfigure (f).

7.3.1.1 Manual Selectively Lockable Differentials

The manual selectively lockable differential mechanisms can block the motion of each finger, using a simple locking mechanism that works like a button, allowing the user to select in an intuitive manner the desired finger combinations and implement different grasping postures or gestures. When the buttons are pressed, they elongate and obstruct the motion of the differentials.

The whiffletree used with the locking mechanism consists of three bars: one bar connects the index and middle fingers (bar 1), one bar connects the ring and pinky fingers (bar 2), and the main bar (bar 3) connects bar 1 and bar 2, as

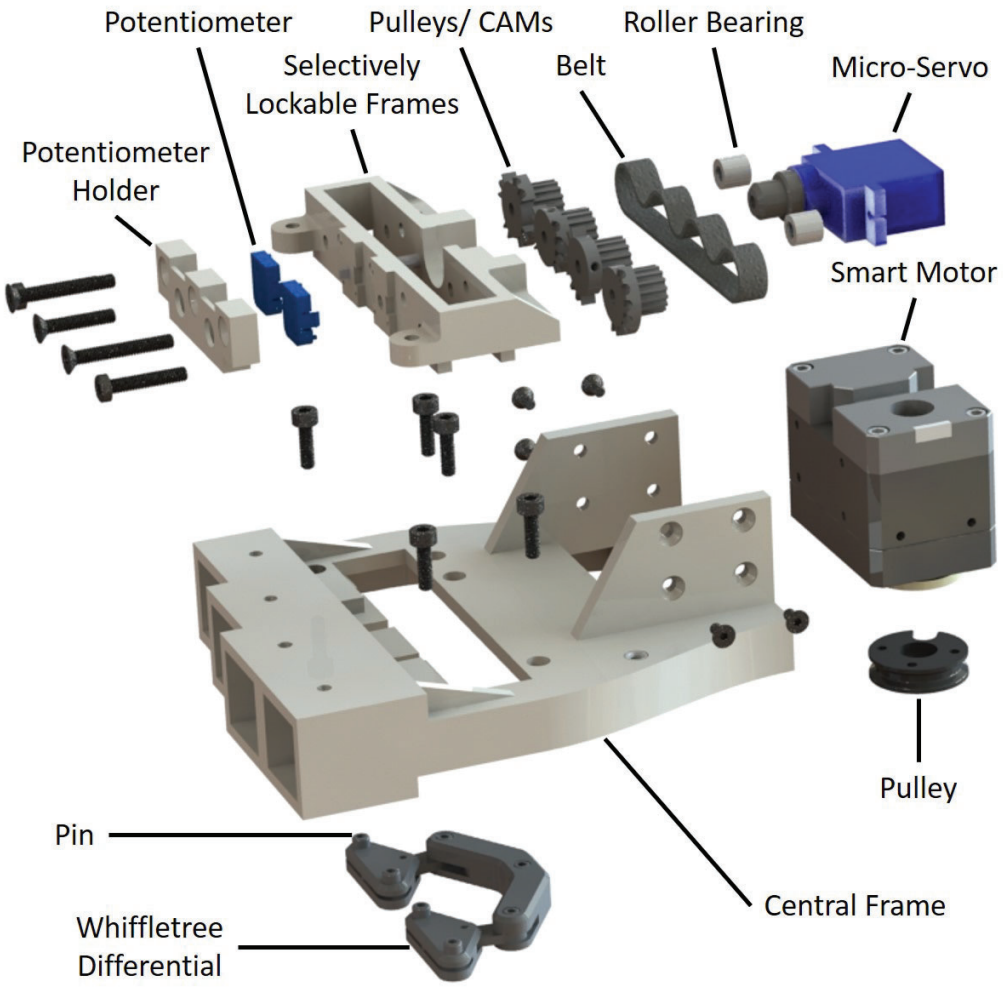

Figure 7.3: The selectively lockable whiffletree differential consists of two main mechanisms: a selector mechanism that rotates to select the differential output behavior, and a whiffletree differential for distributing the input load equally across four outputs. The selector is composed of four pulley/cams, two roller bearings, two potentiometers, a belt, an input pulley, a micro-servo, and a selector frame.

depicted in Figure 7.2a. In this mechanism, the adapted whiffletree upon contact of one finger with the environment or the object surface, the whiffletree facilitates the motion of the rest unconstrained fingers. The whiffletree allows one motor to control multiple fingers in a coordinated fashion, so a small linear displacement of the tendon causes appropriate proportional angular displacements at all robot joints. The whiffletree has been appropriately designed with protruding pins on the top two bars of the whiffletree that interact with the elongated buttons. When

pressed, the button restricts the motion of the whiffletree by blocking the pins from moving. Similar to the whiffletree locking mechanism, buttons and locking pins were employed to block the rotational motion at the outputs of the four-output gear differential and the series elastic differential. Utilizing a similar principle to the whiffletree, the four-output gear differential and the series elastic differential can both be fitted with protruding pins. The pins can be seen in Figure 7.2 and they allow the button locking mechanism to obstruct the differential outputs, facilitating the execution of multiple grasping postures and gestures. This locking mechanism was expanded and integrated into the four output gear differential and the series elastic differential, providing an improved means of controlling the differentials outputs.

7.3.1.2 Automated Selectively Lockable Differential

Similarly to the manually selectively lockable differential, the automated selectively lockable differential utilizes an alternative mechanism capable of facilitating the execution of multiple selectable grasping strategies. Unlike the manually selectively lockable differential, the automated lockable differential uses a small, low torque micro-servo (DFRobot DF 9 g micro-servo) to select the desired differential outputs, rather than manually locking and unlocking buttons/ locking pins in place. The active locking allows the implementation of controllable whiffletrees to be fully automatic in prosthetic hands. This enables amputees to perform bimanual tasks with increased efficiency, as the opposite hand is not required to adjust the grasp pose of the prosthetic hand before the task, since the pose can be selected autonomously during the task. Additionally, the increased autonomy facilitates the used of the device even by bilateral amputees unlike the manually lockable prosthesis. To showcase automated locking, the selectively lockable whiffletree differential was used to select various finger combinations that can facilitate the execution of efficient grasps with underactuated prosthetic hands.

The locking mechanism is composed of four pulleys, a belt, a single actuator, two potentiometers, and a whiffletree differential as seen in Figure 7.3. The whiffletree differential output is connected to four fingers (index, middle, ring, and pinky), while the input of the differential is connected to a single Dynamixel XM430-W350-R smart motor. Each pulley contains a different cam profile, which rotates in sync while interacting with the whiffletree differential's protrusions, providing obstructed and unobstructed tendon motion at the whiffletree outputs. This can be seen in Figure 7.4.

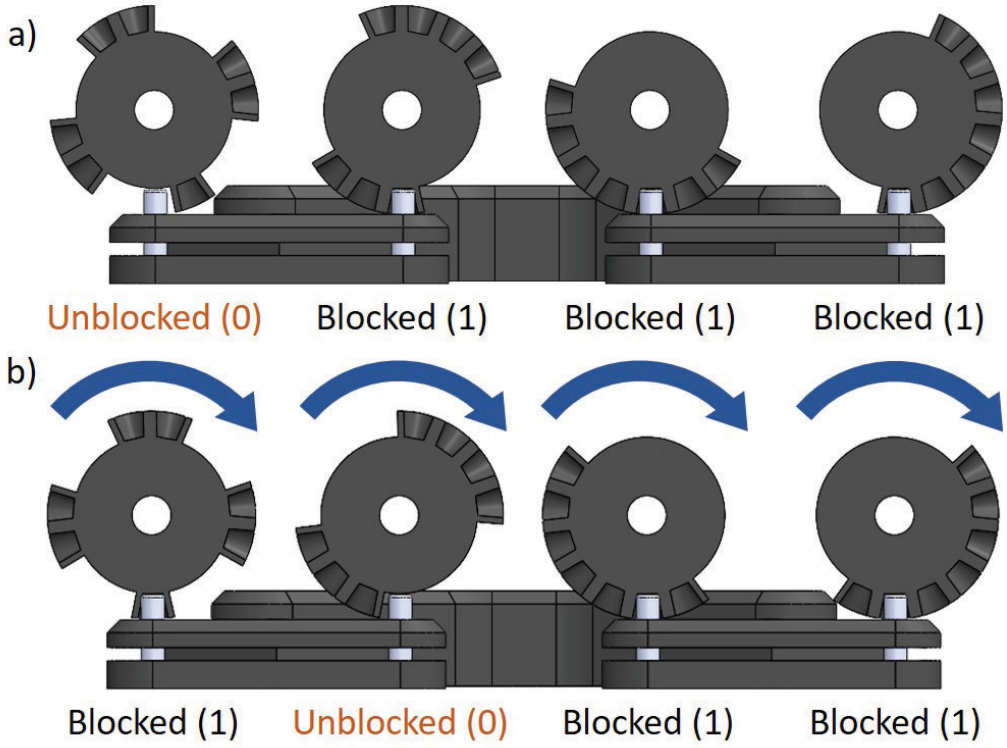

Figure 7.4: The selectively lockable whiffletree differential performs controllable locking by blocking and unblocking the motion of the whiffletree. Subfigure a) shows only the first output being unblocked allowing only this output of the whiffletree to actuate a finger. In subfigure b) the cams are rotated in sync with the micro-servo to facilitate the execution of another differential output, where only the second output is unblocked.

The cam pattern was generated by listing out all the possible finger flexion combinations that can be achieved by blocking the whiffletree outputs ($2^4 = 16$), producing 16 possible combinations. From the 16 combinations the fully blocked combination (where all outputs of the whiffletree are blocked) can be omitted as this pattern can be executed by not actuating the motor to flex the fingers. In order to organize these combinations effectively, during output selections a grey code format was used, over a binary code format. The grey code format organized the blocking (1) and non-blocking (0) states of the cam together to reduce the number of transition zones between blocking and non-blocking, to increase the strength of the cam, and to reduce pattern selection errors during pattern transitions. Attached to two of the cams two potentiometers are connected out of phase from each other in order to detect what the current combination the lock-

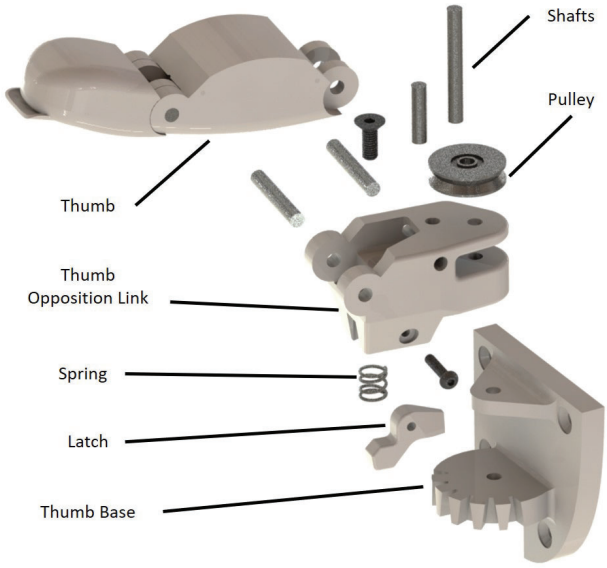

Figure 7.5: The selectively lockable thumb provides an amputee with 6 lockable thumb positions. The mechanism is composed of: a thumb finger, a thumb opposition link, a spring, a latch, a pulley, four shafts, and a thumb base.

able mechanism is in over a full revolution. A total of 16 finger combinations can be achieved with the four fingers (index, middle, ring, and pinky). Although this system is implemented for a whiffletree, the locking mechanism can be adapted to accommodate other differentials.

A video demonstrating the automated locking mechanism implemented in a prosthetic hand performing grasping tasks can be found at the following URL:

www.newdexterity.org/lockableprosthesis

7.3.2 Selectively Lockable Thumb

The selectively lockable thumb is composed of a gear module with a tapered tooth profile and a spring loaded latch which locks the thumb to the gear module, allowing the user to select between six thumb opposition poses. This can be seen in Fig. 7.5. The manual lockable thumb enables amputees to lock the thumb in a range of 0° to 120° (with 0° being the thumb fully abducted to the side of the hand). This increases the combinations of achievable grasp poses/gestures to 96 (16x6) different grasping postures/ gestures that an amputee can select from when using the prosthesis.

Although the thumb locking mechanism created reduces the maximum achievable grasp poses/gestures combinations in comparison to [97] due to the use of a tapered gear tooth profile, this profile ensures better contact between the thumb base and the latch removing backlash.

7.3.3 Finger Design

The prosthetic fingers were designed to be easily fabricated using the hybrid deposition manufacturing technique [46], a process where multi-material components can be created by 3D printing and molding elastomer materials. The fingers are composed of three phalanges each with soft polyurethane elastomer (Smooth On Vytaflex 30) pads for increased conformability during grasping tasks.

The finger structure utilises a passive antagonistic extension element made out of polyurethane rubber (Smooth On PMC-780), while an active flexion is achieved through a tendon-driven actuation system [155]. This allows the finger to exhibit adaptive properties while remaining underactuated.

7.4 Experiments and Results

Different experiments were conducted to assess the performance of the proposed differential mechanisms. The first experiment evaluated how much the fingertip force exertion capabilities were affected when the fingers where selectively locked. The second experiment focused on assessing the selectively lockable differential mechanisms capability in providing various hand gesture combinations with the different differentials. The third experiment assessed the grasping capabilities of the differentials and their corresponding locking mechanisms when they are integrated into prosthetic hands. The fourth and fifth experiments focused on evaluating the maximum tendon tension and maximum tendon displacement that can be achieved at the outputs of the differentials.

7.4.1 Fingertip Force Exertion Experiments

The force exertion experiments were conducted on the selectively lockable differential to investigate the effect on force exertion when the differential mechanism experiences locking/blocking. The relationship between displacement at the input and force exertion at the outputs, is presented in Figure 7.6 with different finger combinations being compared. When blocking the fingers, we are able to maximize

the force applied by the free fingers at their fingertips (e.g., precision grasps). If needed the user can utilize this behavior to maximize the force transmitted from the servo motor to the fewer active fingertips.

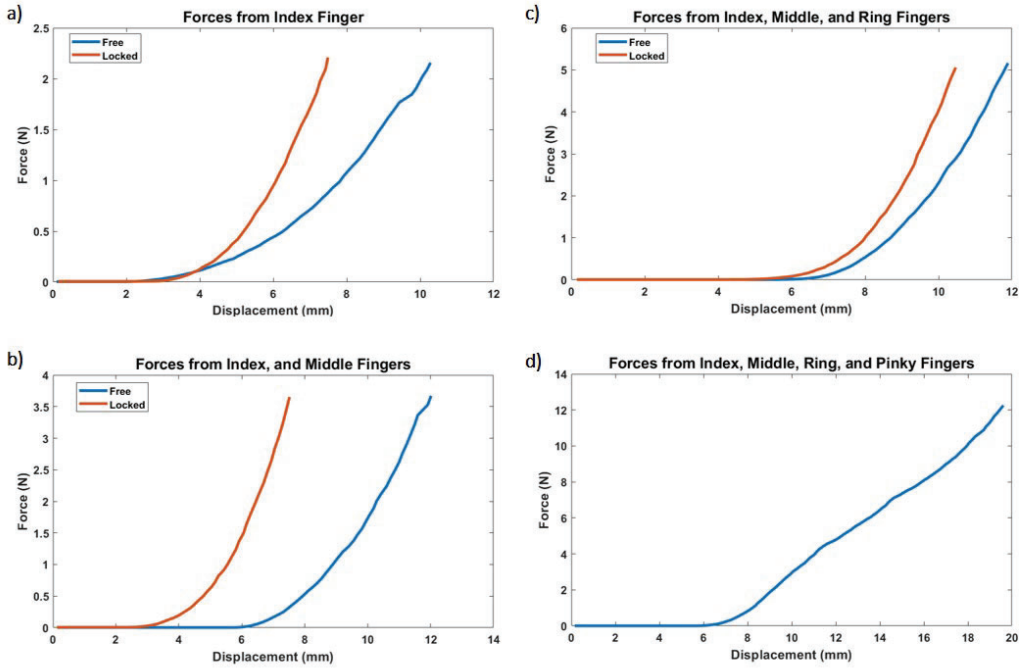

Figure 7.6: These plots present the relationship between the input displacement and the output force exerted by the fingertips when all other fingers of the hand are locked and compares them to the equivalent relationships when not using the locking mechanism. Subfigure a) presents the fingertip force at the index finger. Subfigure b) shows the fingertip forces at the index and middle fingers when locking and no locking is used. Similarly, subfigure c) presents the fingertip forces for the index, middle, and ring fingers. Finally, subfigure d) shows the forces when none of the fingers are locked.

7.4.2 Gesture Execution Experiments

The second experiment assessed the proposed selectively lockable differentials capabilities in executing various grasp poses and hand gestures. To evaluate the abilities of the selectively lockable mechanisms to enhance the performance of all the proposed differentials, the mechanisms were incorporated into a prosthetic hand with a single actuator so as to demonstrate the different achievable hand poses. To showcase the different grasp postures, the buttons of the selectively

lockable differentials were locked into different combinations. The three differentials were capable of achieving the full 16 different combinations. This is depicted in Figure 7.7. The importance of controlling the differential's outputs is critical for selecting grasping strategies and allows: i) different hand gestures to be signed, ii) reaching an object in a narrow space, or iii) executing non-prehensile manipulation tasks (e.g., pressing buttons or moving sliders).

7.4.3 Grasping Performance Experiments

The third experiment was conducted to evaluate the ability of the differentials to improve the grasping performance of prosthetic hands in executing activities of daily living. To do so, the YCB object set designed by [104], was used to evaluate the grasping efficiency of the prosthetic hands with the proposed differentials integrated. Twelve objects from the object set were selected: a credit card, a washer, a die, a marble, a tuna fish can, a golf ball, a pear, a Lego Dublo block, a mustard bottle, a box of sugar, a drill, and a baseball. All hands were capable of grasping all twelve objects. This can be seen in Fig. 7.8, where the selectively lockable differential mechanism allows the hand to execute different grasping postures, achieving optimal grasping performance for the encountered objects.

7.4.4 Tendon Tension Experiments

The fourth experiment focused on testing the mechanical limits of the designed differentials. The experiment consisted of measuring the tendon's tension until either the tendon, the differential, or the motor failed. Hanging weights of increasing masses were attached to the output ends of the differentials until it was unable to lift the weight. To perform the experiment, equal weights of 100 g were incrementally added at the end of the tendon in all four outputs while the differential was running until the system could not withstand the load. The whiffletree differential used in the developed prosthetic hand, was capable of holding up to 42.8 N of tendon tension per output before failure. The four-output geared differential obtained a maximum tendon tension of 39 N per output during the experiments. Although the maximum theoretical tendon tension calculated [149] can be more than 100 N per output, the calculation does not consider efficiency loss due to friction between components, the operating conditions of the motor, or the mechanical resistance of the components used in the differential. When using the series elastic differential, it is capable of switching between a rigid and a compliant mode allowing

the differential to select when the elastic elements should be used. The maximum tendon tension force of 53.8 N per output was achieved when in the rigid mode, while a maximum force of 45.8 N per output was obtained for the compliant mode.

7.4.5 Tendon Displacement Experiment

The last experiment focused on measuring the amount of achievable displacement in each output of the three differential mechanisms. This displacement is important as it offers the required adaptability needed for grasping a wide range of objects, conforming to the object shape, and maximizing the contact patches between the fingers and the object surface, increasing also grasping quality. The three differentials were actuated in an unblocked state to achieve the maximum obtainable displacement at the differential's outputs. Additionally, the three differentials were also tested with three of the four outputs being blocked, allowing for the minimum achievable tendon displacement to be measured. When unblocked the whiffletree was capable of 21 mm of tendon displacement, but was only limited by the available translation length, which is limited by the length of the palm of the prosthetic hand. In the second test scenario where three of the four outputs are blocked, the whiffletree differential was able to obtain a displacement of 10 mm, which was limited by the length of the upper whiffletree bars. The four-output geared differential was able to perform continuous rotations at the outputs in both locked and unlocked scenarios providing continuous displacement. The maximum tendon displacement of this design is only limited by the amount of tendon the pulleys at the output shafts can hold. The series elastic differential when unblocked is capable of continuous rotation similarly to the four-output geared differential, but this continuous rotation only applies to cases when all four outputs are allowed to move continuously. When one or more outputs is blocked, the series elastic differential can only provide displacements up to 43 mm.

7.5 Discussion

Four differentials with locking mechanisms have been proposed, each capable of improving the grasping capabilities of prosthetic hands in different circumstances. The selectively lockable differentials offer increased controllability of the differential outputs facilitating the execution of all 16 finger flexion/extension combinations (e.g., controlled flexion across the index, middle, ring, and pinky fingers on a prosthetic hand). For grasps, which do not need the involvement of all four

fingers (index, middle, ring, and pinky) to oppose the thumb to complete the grasp, the subsidiary fingers can be blocked to maximize the force transmitted to the active fingers by the motor. The developed selectively lockable differentials have been designed to accommodate different user requirements. The selectively lockable whiffletree differential utilizes manually lockable buttons meaning the design does not require additional electronics and actuators to use the mechanism. Hence, utilizing a body-powered approach enables the mechanism to significantly reduce the cost of implementation in a prosthetic device where the price is an essential requirement. Although the automated selectively lockable whiffletree differential requires an additional actuator to operate, unlike the manually lockable whiffletree differential, this actuator does not need a high torque rating as the high loads exerted by the differential are parallel to the axis of the actuator. This allows the chosen actuator to be small and compact, reducing the size, and cost of the total system significantly. The increased autonomy offered by the system's active approach allows the use of selectively lockable differential mechanisms to increase efficiency in bi-manual tasks for amputees and reduce intervention and effort needed to switch the gesture or grasp pose of the hand. The automated selectively lockable differential can also be adopted in robotic systems, where full autonomy is required.

Other than the whiffletree differentials, which have a limited range of motion, rotary mechanisms like the four-output gear differential grant continuous rotation at the outputs. The benefit of using a rotary mechanism is its ability to operate within a fixed volume size. In contrast, traditional pulley and whiffletree differential mechanisms require additional space to accommodate the mechanism's translational motion. This is generally not an issue in anthropomorphic prosthetic hand designs [15, 156], where a large plane usually is available to accommodate the movements of the pulley and whiffletree differentials. However, for prosthetic devices that require large displacements at the differential outputs to reach their maximum range of motion, pulley and whiffletree differentials are not sufficiently compact.

Finally, the series elastic differential offers a simpler and smaller solution than the four-output differential via the implementation and utilization of passive elastic elements. This results in a mechanism with fewer components and reduced weight. However, passive elastic elements in series with the actuator output can produce a parasitic force reducing the maximum achievable force output. This is because the actuator must use some energy to compress the elastic element before

achieving the desired differential displacement. To overcome this, the series elastic differential has been developed such that the differential is capable of switching between a compliant and adaptive mode and a rigid mode based on the rotating direction of the connected actuator. The ability to switch between compliant and rigid modes led to a force output difference of up to 17.4%. Similar to the whiffletree differential, where the maximum displacement between outputs is limited by the bar length, for the series elastic differential, this is constrained by the circumference of the main body and the maximum compressible length of the elastic elements. Thus, this design choice limits the differential's maximum adaptability. However, the total displacement of the series elastic differential is continuous if all outputs wind together. In contrast the whiffletree differential also has a limited total displacement, which is constrained by the operating volume allocated for the differential to translate in. The four-output gear differential, is capable of independently rotating each output continuously until all four outputs experience an equal load, where it will then wind the outputs together providing a continuous total displacement. A comparison of the proposed differential systems is presented in Table 7.1.

Table 7.1: Comparison of the proposed differentials

Differentials	Whiffletree Differential	Four-Output Differential	Series Elastic Differential
Inputs	1	1	1
Outputs	4	4	4
Total Displacement	Limited[1]	Continuous[2]	Continuous[2]
Displacement Between Outputs	Limited[3]	Continuous[2]	Limited[4]
Size[5] (mm)	23 x (54 + T) x 81	41 x 100 x 41	57 x 23 x 23
Weight (g)	46	169.8	22.5
Max Force Output[6] (N)	171	156	215 (rigid mode)

[3] The displacement of the whiffletree is limited by the translation length available
[4] The rotary motion of the mechanism allows continuous winding at the outputs
[5] The adaptability is limited by the length of the whiffletree bars
[6] The adaptability is limited by the max compression of the elastic elements
[7] T is the travel distance needed for the mechanism to adapt
[8] The max force output is the total force of all outputs

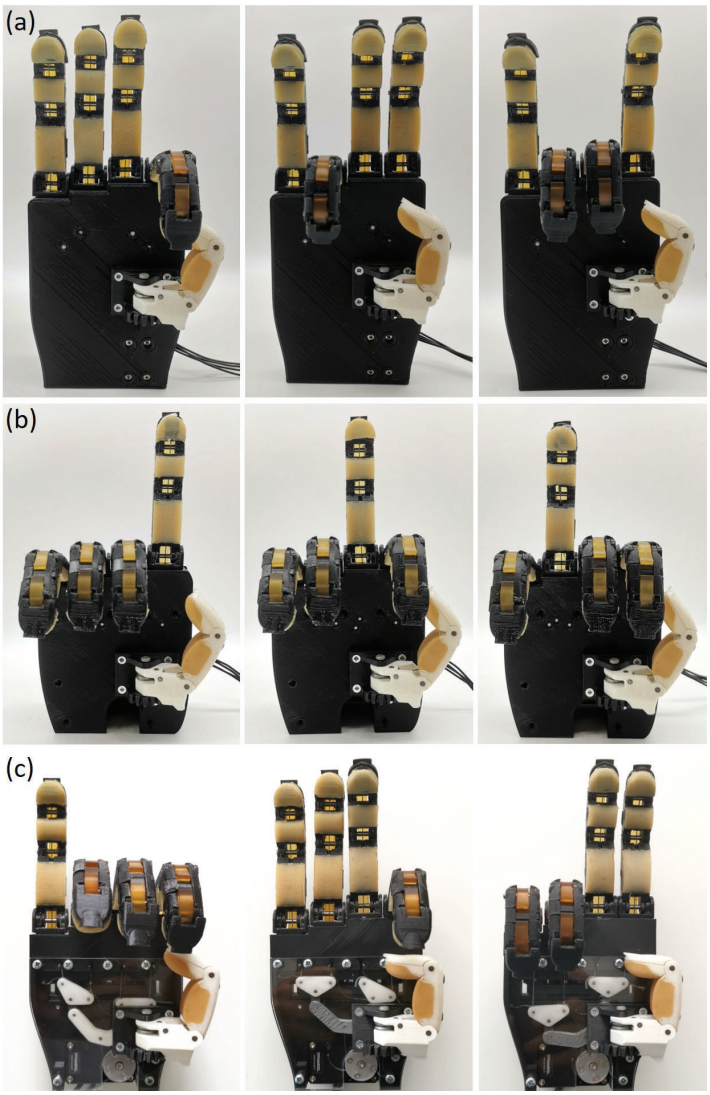

Figure 7.7: Hand gesture combinations executed by a prosthetic hand equipped with a selectively lockable differential mechanism. The Locking mechanism was implemented on the four output geared differential (subfigure (a)), the series elastic differential (subfigure (b)), and the whiffletree (subfigure (c)) on similar prosthetic hands, altering the index, middle, ring, and pinky fingers flexion combination patterns.

Figure 7.8: Grasping experiments conducted with the three prosthetic hands equipped with the proposed differential mechanisms (whiffletree (subfigure (a)), four output gear differential (subfigure (b)), and series elastic (subfigure (c))). The three differentials can be seen allowing a prosthetic hand to execute a variety of grasping strategies (pinch, tripod, and power grasps).

Table 7.2: Prosthetic hand comparison

Prosthesis	DOF	DOA	Locking Mechanism Actuators	Locking Mechanism # Combinations	Individual Finger Control	Size (mm)	Weight (g)	Grasp Force (N)
ILimb pulse [157]	11	5	0	N/A	Y	182 x 80 x 45	465	11.5[5]
Bebionic [158]	11	5	0	N/A	Y	200 x 92 x 50	539	16.1[5]
UT hand I [159]	15	3	4	16	Y	185 x 82 x 26	N/A	N/A
Softhand Pro-D [160]	19	1	0	N/A	N	200 x 91 x 40	285	20
KIT Hand [156]	10	2	0	0	N	232 x 87 x 35	768	8.2-24.2
Open Bionics Hand [97]	15	1	0[1]	16*9	Y	190 x 90 x 62.5	300	9[5]
Belter et al [152]	11	1	1[2]	4[4]	N	N/A	350	5.1
Proposed Design	15	1	1 - 0[3]	16*6	Y	211 x 96 x 48	445	4.5-27.37

[1] The hand contain a locking mechanism actuated by body powered means
[2] The main actuator is shared between actuating the locking mechanism and the fingers
[3] The proposed design can be altered to be both body powered or motorized
[4] The locking mechanism is used to control the thumb position only
[5] Force per finger

The developed prosthetic hands utilized the proposed locking mechanisms were also analyzed and compared with existing prosthetic hand designs (as shown in Table 7.2). A comparison of DOF's, DOA's, locking mechanisms, finger control, size, weight, and grasping force are evaluated. Commercial prosthetic hands like the ILimb pulse [157] and the Bebionic [158] use the lowest number of DOF's and the highest number of actuators to achieve individual control of each finger. Although both hands can exert high grasping forces, the design approach taken results in prosthetic hands that are highly expensive. Underactuated designs like the Softhand Pro-D make prosthetic hands affordable through reducing the number of actuators needed to execute grasping with the hand. However, making the hand highly underactuated limits the control the user has over grasp and gesture selection of the prosthesis. Locking mechanisms can be employed to improve the controllability of highly underactuated hands allowing them to access a wider range of grasping modes and gestures without compromising the cost, weight, and size of the hand. This can be seen with the Open Bionics hand [97], UT hand I [159], the hand developed by Belter et al [152], and the proposed prostheses designs in this chapter. When comparing the different locking based prosthetic hands the proposed designs can be made to be body powered or actuated depending on the users preferences. The automated locking design accomplishes a significantly larger range of grasping combinations with an additional actuator, when compared the other actuated locking systems.

7.6 Conclusions

In this chapter, we proposed locking mechanisms for improving the controllability of the three examined differentials (a four-output geared differential, a series elastic differential, and a whiffletree differential) developed. Two different locking approaches were implemented with one being manual and the other using a small low torque actuator to allow for active control. The locking mechanisms facilitated all 16 different finger flexion and extension combinations (across the index, middle, ring, and pinky fingers). The mechanism allows amputees to perform ADL with increased efficiency. The proposed manual and active mechanism enables the full 16 finger flexion combinations to be selected for the index, middle, ring, and pinky fingers by employing body power or the addition of a small and low-cost actuator. The addition of a manual lockable thumb facilitates the execution of 6 unique thumb configurations, allowing the execution of a total of 96 different

grasping poses to be achieved. By implementing locking mechanisms in prosthetic devices to replace individual actuators for controlling each finger the weight and the cost of the device can be significantly reduced while maintaining its dexterity.

7.7 Future Directions

Regarding future directions, we plan to extend the automated selectively lockable differential mechanism to include the control of the thumb further increasing the dexterity of adaptive prosthetic hands. Additionally, we plan to create derivative versions of the automated selectively lockable mechanism in order to be incorporated into other commonly used differentials like pulley and geared differentials.

Part IV

Soft and Variable Stiffness Systems

Chapter 8

Mechanically Programmable Jamming Based on Articulated Mesh Structures for Variable Stiffness Robots

8.1 Background

As robotics and automation begin to shift towards the execution of complex tasks in unstructured and dynamic environments, the use of soft robotic mechanisms and structural compliance in rigid robots becomes highly necessary. But for rigid robots to efficiently operate in such environments, complex control algorithms and sophisticated proprioception systems are needed to position the robot accurately to perform the given task [13]. Sophisticated sensing is also needed for enabling such robots to operate safely around humans and/or to handle fragile or delicate objects. As a result, there has been a paradigm shift in the materials and methods used to develop robots. Soft robots are the product of this shift, where the integration of flexible materials imparts compliance to the structure of the system facilitating high environmental adaptability with minimal control and sensing complexity. The intrinsic compliance of soft robots allows it to easily adapt to environmental conditions and task specifications, providing safe interactions with humans, their surroundings, and/or fragile artifacts [161]. Elastomeric materials enable soft robots to withstand crushing loads, providing increased durability and robustness [162]. Hence, the selection of materials is an important part of determin-

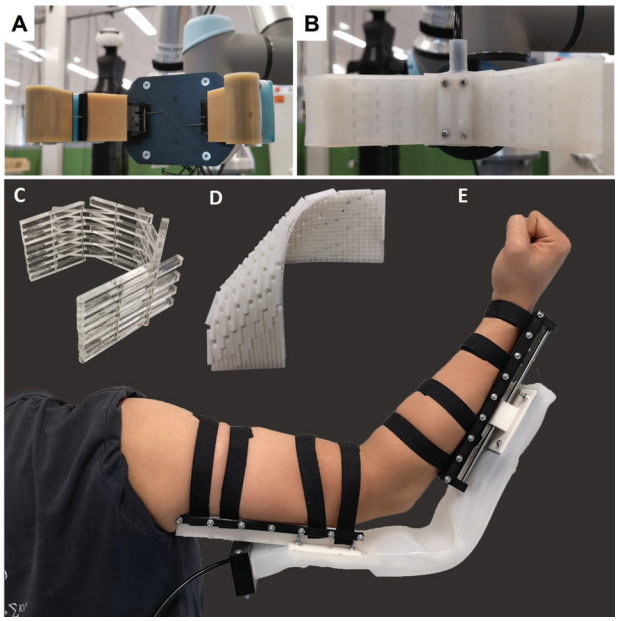

Figure 8.1: The mechanically programmable articulated mesh structure can be used in a diverse set of application. We present the variable stiffness articulated mesh structure being incorporated into the joints of an adaptive underactuated tendon driven robot hand (subfigure (A)) and used to develop a soft robot gripper (subfigure (B)). The articulated mesh structures consist of links connected together through the use of either a pin (subfigure (C)) or a flexure (subfigure (D)) joint allowing for the execution of bending and twisting motions. Additionally, the variable stiffness mesh structure has been integrated into a wearable elbow exo-skeleton (subfigure (E)) to assist in lifting heavy loads.

ing the desired behavior and capabilities of soft robotic mechanisms. Although the utilization of soft materials provides high adaptability and conformation to complex and irregular geometries with simple controls, the use of soft materials also imposes several drawbacks to soft robotic designs, such as low control accuracy, low force exertion capability, and low resistance to deformations [163].

To take advantage of the benefits of soft robots without compromising the force exertion capabilities and control accuracy, several designs of variable stiffness actuators have been proposed to provide an on-demand rigidity to soft systems. Variable stiffness actuators can alter their stiffness in a number of different ways from applying an electrical current to applying pressure depending on the selected materials. Shape memory alloys (SMA) [164, 165, 166] and shape memory polymers (SMP) [167, 168, 169] facilitate stiffness variation through changes in the materials temperature and are capable of providing up to an 18 fold stiffness in-

crease in robotics fingers [170]. However, time required to change the temperature of the material results in a slow response time achieved by such actuators [171, 172, 173]. Another approach is via voltage actuated dielectric elastomer actuators (DEA) where electrostatic chunking [174], active cross section changing [175], or integrating low melting point alloys [176] can be used to vary the stiffness of the system. The deformation and stiffness change accomplished by DEA's are, however, insufficient to bear more than a few grams of weight. Magnetorheological (MR) fluids are composed of magnetizable particles within the carrier fluid and when in the presence of a magnetic field the viscosity and shear modulus of the fluid can be changed allowing for the modulation of stiffness [177, 178, 179]. However, the presence of a strong magnetic field can result in limited interactions with magnetically sensitive materials / objects, potentially damaging them. Finally, jamming based methods utilize soft structures encapsulated in a closed system (e.g., a silicone pouch) where the air within the closed system can be evacuated. By regulating the vacuum pressure within the closed system, the compression force on the enclosed soft structure can be stiffened and softened on command. The soft structures that use jamming based actuators are diverse [180, 181, 182, 183, 184] ranging from granular materials that are highly deformable when unjammed to conform around objects [181], chain mail meshes that can be stiffened to provide additional bracing support [182], fiber materials arranged to provide variable stiffness in an endoscope [185], and laminar sheets which can be organized to act as flexural beams for bending [183, 186].

In this chapter, we propose a variable stiffness actuator based on an articulated mesh structure that serves as the backbone of a multi-layer jamming architecture, which is housed in a vacuum controlled silicone pouch. When jammed the variable stiffness actuator is able to undergo elastic bending without permanent deformation in the jammed state. Alterations to the mesh link geometries within the articulated mesh allows the variable stiffness actuator to be mechanically programmed to take on different shapes when jammed. The controllable variable stiffness structure can be used to develop grippers with improved dexterity and can be integrated into soft exosuits that provide assistance to humans carrying loads. This chapter investigates the behavior of this novel variable stiffness actuator paradigm, the mechanics that allow the compression forces to resist the free motion of the articulated mesh structure, and the various devices and applications in which such an actuator can be employed.

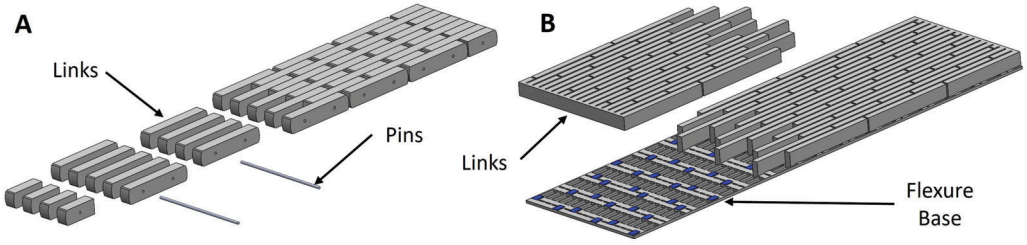

Figure 8.2: The construction of the mesh structure is composed of a pattern of pins and links for the pin jointed mesh (A) while the flexure joint mesh (B) is fabricated as a singular 3D printed body of links printed on a flexure base (the blue patches highlight the attachment points between the links and the flexure base).

8.2 Designs

8.2.1 Mesh Structure

The mesh structures that were composed of pin joints (Fig. 8.2A) to connect the different links together were fabricated using laser cut acrylic sheets. Mesh structures that followed a flexural joint design (Fig. 8.2B) were fabricated with 3D printed polylactic acid (PLA) plastic in order to create a continuum body mesh that was capable of both bending and twisting motions. The envelopes that contained the mesh structures were manufactured using 3D printed molds made from silicone (Smooth-on, Dragon Skin 20). This material not only allowed the confining pressure to be freely applied onto the mesh structure, but the elasticity of the envelop facilitated elastic bending of the variable stiffness actuator when under pressure. PET sheets were added to sandwich the mesh structure to provided additional support to the envelope preventing it from conforming to the mesh structure in a non-optimal manner where the pressure forces applied on the mesh would result in a net zero force for resisting bending. Additionally, the PET sheets allow for reduced friction between the mesh and the envelope facilitating the mechanism to return back to its preprogrammed state.

The yield point (F^{yield}) of the mesh structures for determining the transition between preprogrammed and bent geometries can be altered by controlling the applied pressure that can be calculated as follows,

$$F^{yield} = \sum_{i=1}^{n} 2\frac{f_i^B l_i^B + m f_i^T l_i^T}{L} \tag{8.1}$$

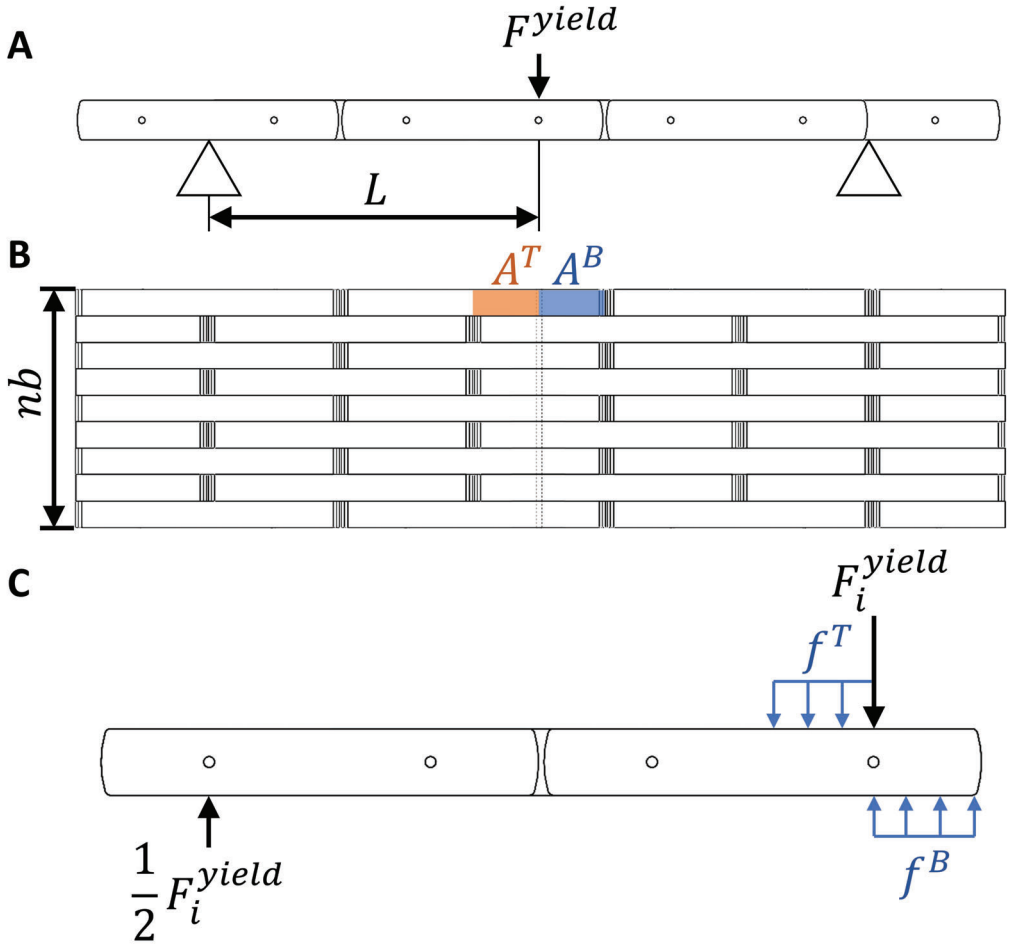

Figure 8.3: The free body diagram of the 3-point bending test (subfigure (A)) for determining the yielding force (F^yeild) of the mesh structure. The load was applied to the center of the structure, which is a distance L from the side of the support span. A top view of the mesh structure shown in subfigure (B), presents the contact area (A^T and A^B) for the top and bottom of the links under a bending load. The number of links (n) per column and the width (b) of the assembled mesh structure is also presented. Subfigure (C) illustrates the forces on one side of the mesh structure. f^T and f^B are the top and bottom forces applied on the mesh by the pouch to resist bending.

$$such\ that \begin{cases} m = 1 & \text{, When symmetric} \\ m = 0 & \text{, When asymmetric} \\ f = PA \end{cases}$$

where n is the total number of links in a row in the mesh structure, and f^B, and f^T, are the distributed pressure forces acting on the bottom and top of the mesh links with l^B, and l^T being the distance from the pivot point at which the distributed pressure forces act. The force on the bottom and top of the mesh links f^B and f^T are calculated from the applied pressure (P) on the envelope and the contact area (A) on the links, which press against the interior of the pouch when trying to bend. The distance L is taken from the distance from the support span to the applied load F^{yield}. The free body diagram of the mesh structure in a three-point bending test can be seen in Fig. 8.3. Depending on the mesh patterns, m will be either 1 for symmetric patterns or 0 for asymmetric patterns because f^T is absent for asymmetric patterns due to the mesh links only pressing against the bottom of the envelope from one side of each pivot point.

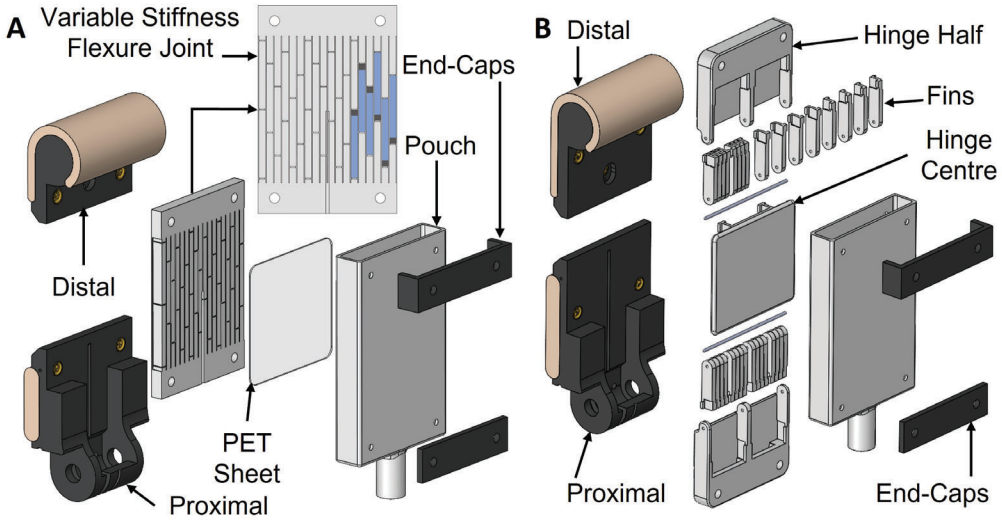

Figure 8.4: The exploded view deconstruction of the variable stiffness flexure joint (A) and pin joint (B) fingers used for improving the grasping capabilities of underactuated adaptive grippers.

8.2.2 Adaptive Gripper with Variable Stiffness

The variable stiffness actuators presented here are capable of rapidly stiffening and elastically returning to their mechanically programmed state when bent. This combination of properties enables such systems to be used as variable stiffness joints capable of adjusting the grasping force and the feasible trajectories of underactuated, adaptive and soft robotic grippers and hands. Depending on the mesh

link shape and attachment point method selected, variable stiffness pin and flexure joints can be developed to be used in improving existing adaptive robotic grippers [109], or allow for the creation of self-actuating soft fingers (Fig. 8.5D).

The adaptive, underactuated robot hand was developed using the model T42 gripper [109] as a base to demonstrate how the variable stiffness actuator can be integrated into existing systems and presents the benefits it provides to adaptive, underactuated grippers and hands. To encompass the most common joint systems used in designing robot grippers and hands [187, 109] two types finger designs were developed comprising of variable stiffness actuators with mesh structures that were either of a flexural joint design (Fig. 8.4A) or a pin joint design (Fig. 8.4B) for the robot gripper. The phalanges of the fingers were fabricated using hybrid deposition manufacturing (HDM) [46] techniques allowing 3D printed polylactic acid (PLA) parts to be combined with soft urethane/ silicone materials. Smooth-On Vytaflex 40 was used to construct the finger pads of the gripper. The silicone pouches enclosing the mesh structures were made from Smooth-On Dragon Skin 20. The actuation scheme of the gripper employs 2 Dynamixel XM430-W350-R smart motors each actuating one finger using a low friction of UHMWPE (Ultra-High Molecular Weight Polyethylene) fiber tendon.

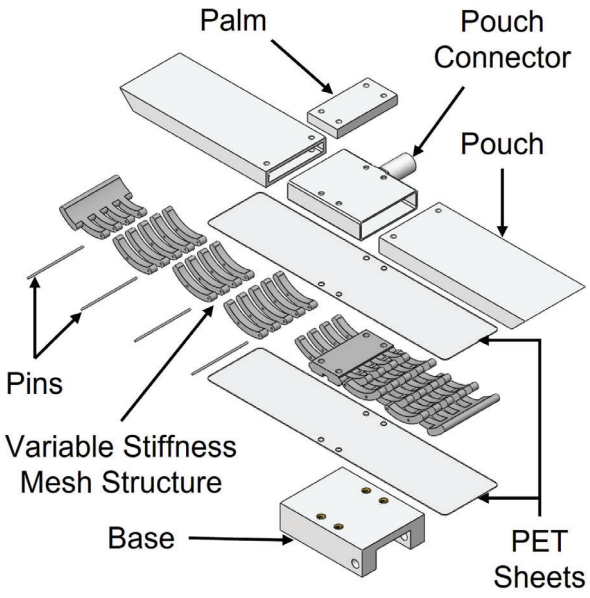

Figure 8.5: The soft gripper is composed of a curved mesh link structure sandwiched between PET sheets and encased in pouches and a pouch connector facilitating active flexion under pressure and passive extension when not pressurized.

8.2.3 Soft Gripper

The flexion action of the soft robot gripper fingers is achieved through a mechanically programmed mesh structure that is comprised of a set of curved links (Fig. 8.5D). When exposed to a vacuum pressure the silicone pouch will compress the mesh structure to its lowest volume state where it will remain in a curved pose until the pressure is released. Two PET sheets of 0.5 mm are used to sandwich the mesh structure facilitating low friction sliding when transitioning between open and closed states. The PET sheets also assist in providing passive extension to the fingers allowing them to fully extend when no pressure in applied within the pouches. The soft components of the gripper (the pouch, pouch connector, and palm) were molded from Smooth-On Dragon Skin 20 while the mesh structure was fabricated with 3D printed PLA and laser cut acrylic. The use of variable stiffness mesh link structures enables the construction of the grippers to be light weight and affordable weighing 128 g and costing 4.84 USD in materials.

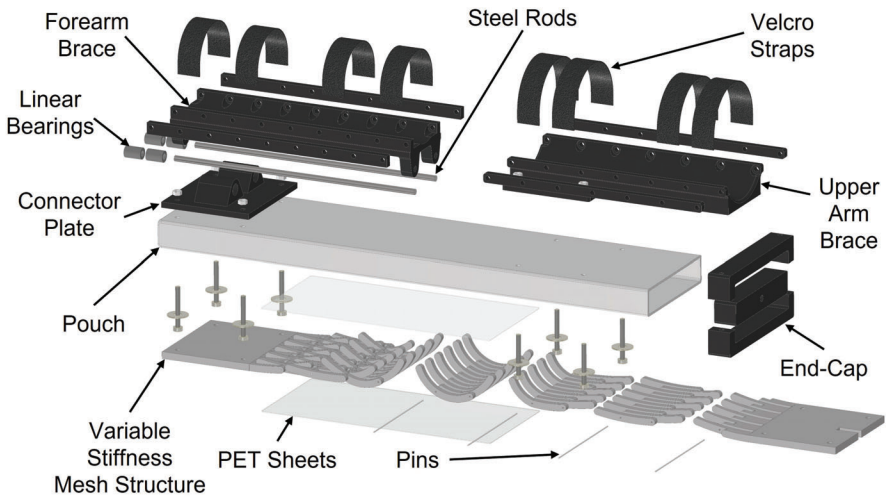

Figure 8.6: The component composition and construction of the wearable exoskeleton uses curved mesh link structures as to provide active bending when pressurized.

8.2.4 Wearable Elbow Exo-Skeleton

Similar to the structure of the soft gripper, by combining straight PET sheets with a curved mesh link structure inside a silicone (Smooth-On Dragon skin 20) pouch a wearable elbow exoskeleton (Fig. 8.6) device can be developed which can be

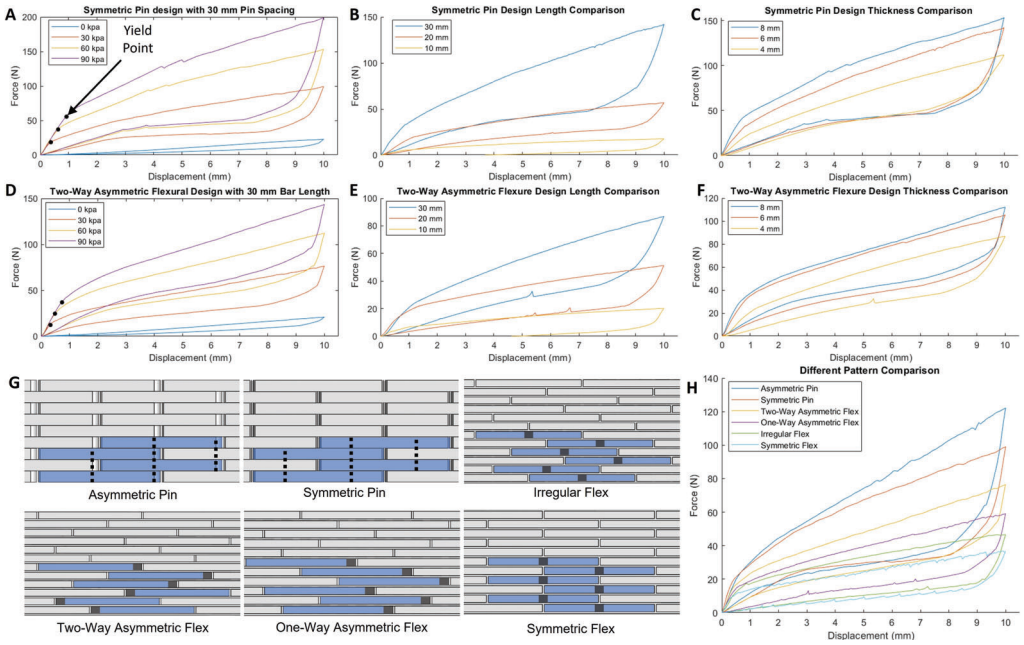

Figure 8.7: A comparison of measured force-displacement curves for a mesh structure composed of a symmetric pin design with 30 mm pin spacing evaluating the effect of different confining pressures, varying pin spacing's at a fixed pressure (60 kPa), and differing thicknesses at a fixed pin spacing (30 mm) and pressure (60 kPa). This is shown in subfigure ((A, B, and C)). Subfigure (D, E, and F) present the force-displacement plot of a two-way asymmetric flexural design with 30 mm bar lengths at various confining pressures, bar lengths (at a fixed confining pressure of 60 kPa), and thicknesses (at a fixed 30 mm bar length and confining pressure of 60 kPa). The fabricated pin joint and flexural joint mesh structures that were evaluated are shown in subfigure (G). Highlighted in blue is the repeating mesh link pattern with the black dotted line indicating the pin joint axis and grey rectangles representing the flexure attachment points. Subfigure (I) shows A force versus displacement comparison of all the patterns when a confining pressure of 30 kPa is applied on designs utilizing either a 30 mm pin spacing or bar lengths at a thickness of 8 mm.

mechanically programmed to do active flexion and passive extension when pressurizing and depressurizing the silicone pouch. Velcro straps attached along the forearm brace and upper arm brace allow the wearable exoskeleton to provide flexion assistance to the elbow joint of the user and facilitate intuitive attachment and removal of the device. Additionally, a linear slide mechanism composed of 2 linear bearings and 2 steel rods attached between the forearm brace and the variable stiffness actuator enables the shortening and lengthening of the variable stiffness actuator when transitioning between extended and flexed poses. The wearable

exo-skeleton demonstrates the scalability of the actuator between smaller sizes required for the development of grippers and end-effectors to larger form factors for the incorporation into assistive devices, such as wearable exoskeletons. When implemented into the wearable exoskeleton: the unjammed state (low stiffness state when no pressure is applied) is highly compliant and allows the user to move freely with the elbow exoskeleton, and the jammed state (high stiffness state when pressure is applied) provides the user with the required assistance to aid them in lifting heavy loads. The assistance can be adjusted by altering the applied pressure on the articulated mesh structure. The weight of the wearable exoskeleton is 1.33 kg.

8.3 Experiments and Results

8.3.1 Bending Test

The three-point flexural bend tests were conducted using an Instron 5567, Instron Limited, UK to characterize the materials mechanical properties. The testing procedures used a 100 mm support span. The load from the instron machine was applied in the center of the sample with a displacement motion of 10 mm at a speed of 0.5 mm/s. The experiment was repeated five separate times at each confining pressure. The mesh structures were sandwiched between two PET sheets of 0.5 mm thickness before being placed inside a silicone envelope connected through a soft tube to a manual vacuum pump with a pressure gauge.

The mesh structures were exposed to different confining pressures (0 kPa, 30 kPa, 60 kPa, and 90 kPa). Different mesh thicknesses, patterns, attachment points, and mesh link lengths were evaluated to determine the effects of the different properties on the actuator performance (Fig. 8.7A to Fig. 8.7F). The articulated mesh structure is composed of links connected together via pins or a flexural base supporting bending. Each specimen was subjected to a displacement of 10 mm and then returned to the initial position. The variable stiffness actuator is shown to be at a low stiffness when no pressure is applied, but once, a confining pressure is applied on the mesh structure the actuator will stiffen allowing it to resist against the displacing loads applied on the structure. The variable stiffness actuator is capable of increasing its stiffness from 2.25 N/mm to 62.9 N/mm for the symmetric pin joint design with 30 mm pin spacing, and from 2.36 N/mm to 52.5 N/mm for the two-way asymmetric flexural design with 30 mm link lengths, giving a 27.96 times and a 22.25 times stiffness increase respectively. When the applied load causes the links of the mesh to be unaligned in the axial direction, a decrease in

stiffness of the actuator occurs causing the confining pressure to apply its load both tangentially and normally on the unaligned mesh links resulting in a reduction in the resisting load. As the links are increasingly rotated out of alignment the normal force will be increased such that the mesh links do not apply sufficient tangential force to allow the mesh structure to overcome the frictional force generated by the normal force preventing the system from returning to its initial state, resulting in conventional jamming behavior. Figure 8.7B and E illustrates this with the designs using the smaller link sizes (10 mm) experiencing permanent deformation that prevents them from fully returning to their initial pose unlike the larger mesh links (20 mm and 30 mm).

Although the yield point estimation works for thicker mesh structures (as shown in Fig. 8.7A and D with 8 mm thick meshes), it was observed that lower thickness mesh structures (Fig. 8.7C and F) would exhibit bending of the mesh links first before misalignment of the mesh links occurring, resulting in a lower stiffness and yield point. A comparison of the different mesh patterns (Fig. 8.7G) with 30 mm pin spacing for pin joint designs and 30 mm long mesh links for flexure patterns was performed and it was found that the asymmetric pin joint design exhibited the best performance. Although the estimated yield point was lower than the symmetric pin design, the asymmetric unfolding of the links allowed the envelope to better conform to the mesh structure during bending, facilitating a higher stiffness and the exertion of higher force post yield.

8.3.2 Object Grasping

The grasping and manipulation performance evaluation used the Yale-CMU-Berkeley (YCB) Object set [104] which is composed of a plethora of everyday life objects selected to facilitate the benchmarking of robotic grasping and manipulation capabilities. The following eleven objects from this object set were selected: a mini soccer ball, golf ball, marble, power drill, hammer, plastic apple, plastic pear, mustard container, chips can, box of sugar, and a small block. Additionally, four objects (1.5 litre bottle, wood block, sponge, and socks) not included in the YCB object set were also used to evaluate the grippers performance when handling heavy or soft objects. These objects were a 1.5 litre bottle (dimensions - 305 mm x 88 mm x 88 mm, and weight - 1523 g), wood block (dimensions - 89 mm x 89 mm x 123 mm, and weight - 2332 g), sponge (dimensions - 212 mm x 58 mm x 102 mm, and weight - 103 g), and socks (dimensions - 50 mm x 80 mm x 270 mm, and weight - 143 g).

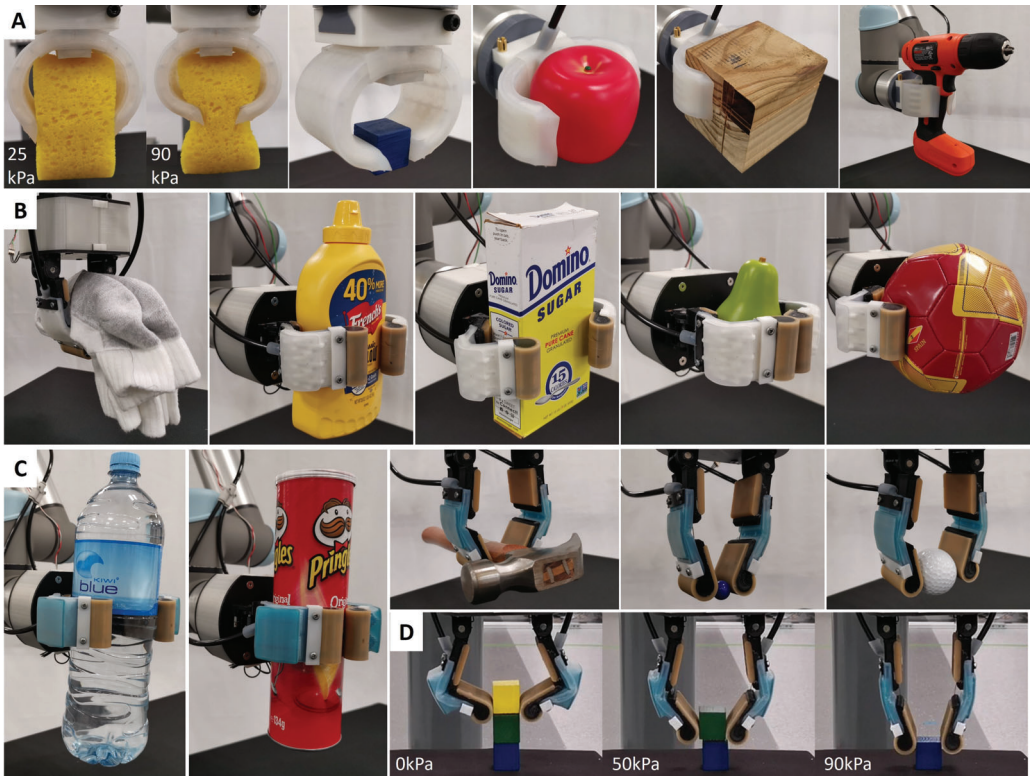

Figure 8.8: Grasping experiments of the developed grippers integrated with the variable stiffness actuators grasping different objects of varying size shape and weights. Subfigure (A) shows the soft gripper grasping a sponge at two different pressures (25 kPa and 90 kPa) demonstrating the capability to vary the grasp force for delicate and forceful grasping. The soft gripper is also presented grasping a small cube, wood block, and drill. Subfigure (B and C) presents the flexure and pin joint variations of the variable stiffness actuators used in the underactuated adaptive, tendon-driven gripper in order to grasp a variety of everyday life objects. Controlling the confining pressures of the variable stiffness joints the gripper is capable of accessing different regions of its workspace allowing the gripper to unstack the small cubes without toppling them (subfigure (D)).

Grasping experiments (Fig. 8.8) were conducted with the grippers, grasping the everyday life objects and moving the UR5e robot arm side to side to introduce perturbation forces on the objects to assess grasping stability and robustness. Figure 8.8A shows the soft gripper grasping a subset of the objects used in the experiments. Upon grasping the sponge, the gripper's actuating pressure was changed from 25 kPa to 90 kPa to demonstrate that the soft gripper can delicately grasp an object without damaging or deforming the object's surface or apply higher grip forces in order to pick up heavier objects. By regulating the input pressure,

the gripper can be intuitively controlled to exert a set amount of force without the need for sophisticated sensing elements or complex control algorithms. When performing a hook grasp with the soft gripper the fingers were able to lift a kettle bell weighing 5 kg, which was more than 39 times the weight of the gripper which weighs 128 g. For the adaptive underactuated gripper, Fig. 8.8B and C present the flexure and pin joint variations of the variable stiffness joints grasping. The video demonstrating the grippers can be seen in Section 8.3.7.

8.3.3 Joint Tracking

The magnetic motion capture system (Polhemus Liberty) was used to track the motions of the phalanges of the robotic gripper when its variable stiffness actuators are exposed to varying pressures. The micro sensors were placed on the proximal and distal phalanges of the adaptive underactuated robot hand in order to measure the joint angles of the MCP and proximal PIP joints.

The control over finger trajectories plays an important role in executing complex grasping and dexterous manipulation tasks with robot grippers and hands. Adaptive, tendon driven grippers typically have fingers that are designed with two or more passive degrees of freedom and are actuated by a single motor [109, 188]. Thus, controlling the fingers is quite simplistic due to the mechanical coupling that constrains the finger motion to follow specific submanifolds in free space (unconstrained bending). The finger trajectories can only be changed post-contact when the gripper starts interacting with the grasped object, preventing optimal selection of finger contact points or the execution of complex in-hand manipulation motions. To improve the controllability of individual joints while maintaining the simplicity and robustness of using passive elastic joints, the variable stiffness actuators were used as variable stiffness PIP pin and flexural joints within the adaptive gripper. Fig. 8.9 illustrates the change in joint trajectories between the MCP joint (θ_1) and PIP joint (θ_2) when actuated through a fixed actuator displacement with varying pressures from 0 kPa to 40 kPa. When no pressure is applied the stiffness of the PIP joint remains lower than the MCP joint allowing θ_2 to increase first enabling the distal phalanx to orient itself before the proximal phalanx. However, as the stiffness of the PIP joint increases with pressure the sequence in which the joint closes shifts from θ_2 closing first to θ_1 closing first, facilitating the selection of a variety of finger trajectories. Although the variable stiffness flexure joint does not achieve full flexion of the PIP joint before the MCP joint at 0kpa (Fig. 8.9B) like the variable stiffness pin joint (Fig. 8.9A), the flexure joint design is capable of

achieving a 61 % larger range of motion in comparison to the pin joint design. The execution of varying joint trajectories is demonstrated in Fig. 8.8D, presenting the hand accessing different regions of its workspace from a fixed end-effector frame.

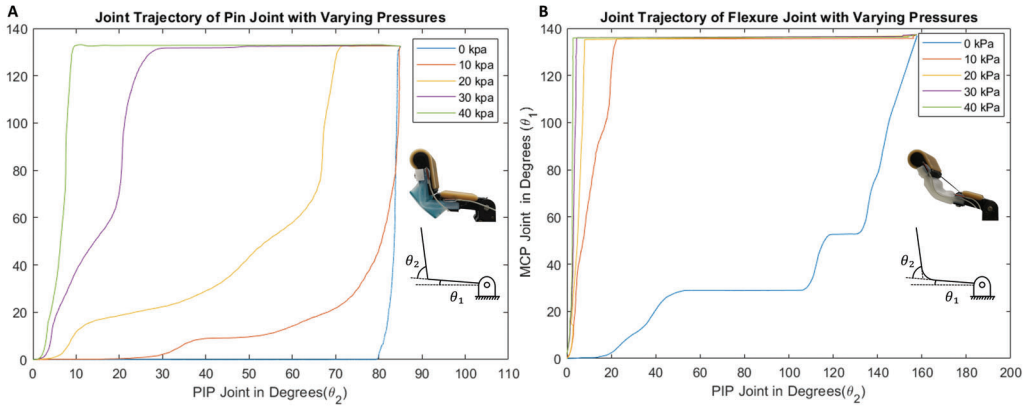

Figure 8.9: The joint trajectory experiments were conducted at varying pressures from 0 kPa to 40 kPa with adaptive underactuated robot fingers composed of two links. θ_1 and θ_2 are the MCP and PIP joint angles. Subfigure (A) presents the motion behavior of a finger using the variable stiffness actuator as a pin joint, and Subfigure (B) shows the results when the variable stiffness actuator is implemented as a flexural joint.

8.3.4 Force Exertion

The force exertion capabilities of a robotic gripper determine its success in grasping a variety of everyday life objects, hence, the maximum pinch and power grasp forces were collected during experiments executed with the developed soft and adaptive, tendon-driven robotic grippers. The maximum force the soft gripper was capable of exerting at 90 kPa was 10.4 N in pinch grasps and 17.9 N of force when performing power grasps. Post contact reconfiguration is a feature that enables underactuated adaptive robot hands to comply and envelope objects during grasping, facilitating robust extractions of grasps under object pose uncertainties in unstructured environments [189]. However, reconfiguration can inhibit the maximum achievable pinch force in such systems [190] and can result in object ejection [15] failing to grasp an object firmly. Although solutions have been proposed in improving the grasp stability in pinch precision grasps with underactuated grippers [191], they reduce the maximum power grasp force of the gripper [192]. By integrating the variable stiffness actuators into the joints of the adaptive, tendon-driven gripper the joint stiffness can be changed to favor a particular grasp type.

For example, applying low pressures to the PIP joint improves power grasp forces, while applying high pressures increases the stiffness of the PIP joint enabling higher pinch forces. When collecting the power grasp forces no pressure was applied to the variable stiffness pin and flexure joints allowing the motors actuating the tendons of the gripper to execute the grasp with minimal resistance. The power grasp force when using the variable stiffness pin joint fingers was 89.3 N, while the variable stiffness flexure joints achieved a grasping force of 72.8 N. The pinch grasp forces were collected under two different pressures 30 kPa and 90 kPa to ensure that the forces were comparable, and the motors of each finger were displaced by the same amount. The variable stiffness pin joint exerted 2.88 N at 30 kPa and 5.26 N at 90 kPa giving a 1.82 times improvement in pinch force exertion, while the variable stiffness flexure joint exerted 1.56 N at 30 kPa and 5.17 N at 90 kPa, providing a 3.31 times improvement in pinch force exertion. The variable stiffness joints can be used to provide adaptive, tendon-driven robot grippers with improved precision and power grasping efficiency during operation.

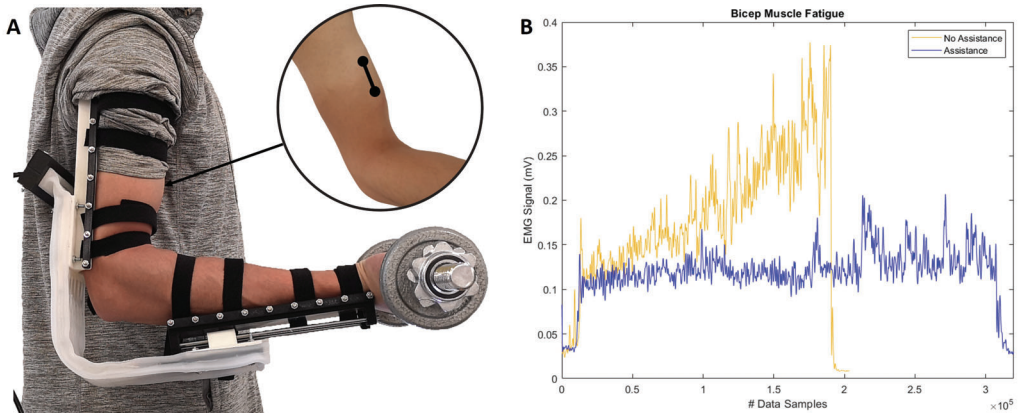

Figure 8.10: The wearable exoskeleton being worn to assist in holding a 5 kg weight. Subfigure (A) presents the bipolar electrode placement for measuring the EMG signals of the bicep muscle when executing an isometric hold of the 5 kg weight at 90 degree elbow flexion with and without the wearable exoskeleton. Subfigure (B) presents the recorded EMG signals of the bicep when holding the 5 kg weight in a fixed pose while using and not using the exoskeleton.

8.3.5 Wearable Elbow Exoskeletons Fatigue Test

An evaluation of the performance enhancement when using the wearable exoskeleton was tested on one participant measuring their surface Electromyography signals from the biceps brachii area when holding a 5 kg weight at a fixed height

for several minutes. This can be seen in Fig. 8.10A. It is evident from Fig. 8.10B the myoelectric activity of the biceps brachii muscle is significantly lower when the wearable elbow exoskeleton system is used, and the user of the device is able to hold the weight for a longer period of time. The EMG data were collected on a Myon 320 wireless sEMG bioamplifier at a frequency of 1000 Hz using surface bipolar active EMG electrodes and they were band-pass filtered (20-450 Hz), full-wave rectified, and low-pass filtered with a fourth-order 8 Hz Butterworth filter.

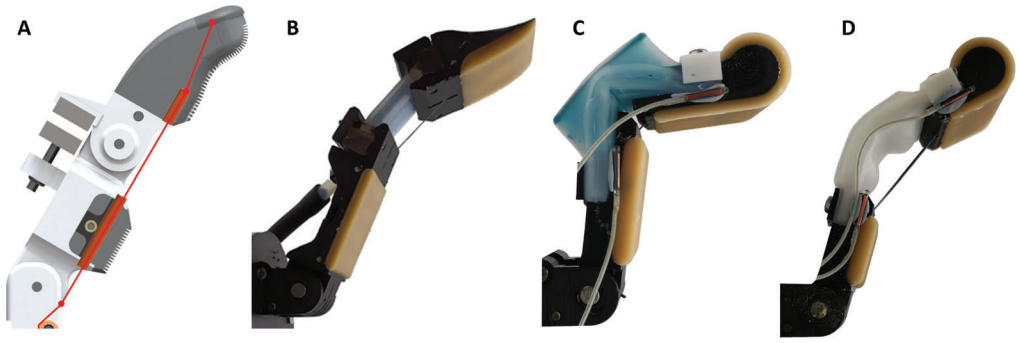

Figure 8.11: Different joint stiffness mechanisms were investigated for improving the grasp force efficiency between precision and power grasps. Subfigure (A) presents the use of magnets to control the bending behavior of the PIP joint. Subfigure (B) shows the integration of a laminar jamming actuator being used to control the stiffness of the PIP joint. Subfigure (C and D) depict the pin and flexure joint articulated mesh structures for use in a robotic finger.

8.3.6 Variable Stiffness comparison

Alternative variable stiffness mechanisms were also investigated alongside the jamming based articulated mesh structures to evaluate the feasibility and improvement provide by magnetic joints (Fig. 8.11A) and laminar jamming joints (Fig. 8.11B) in comparison to the use of articulated mesh structures (Fig. 8.11C and D). The magnetic joint design [190] utilized two magnets attached to the back of the PIP joints of a robot finger composed of two phalanges to aid in improving grasping forces in underactuated hands. When the fingers are fully extended the magnets are engaged with one another facilitating high pinch grasping forces at the fingertips, when the magnets disengage from post contact reconfiguration the holding force at the PIP joint decreases exponentially as the PIP joint bends allowing for minimal resistance during power grasps enabling high power grasp forces. The Laminar jamming joint [186] is composed of paper sheets stacked on

top of each other and placed in a silicone pouch, where a pressure can be applied to vary the stiffness of the actuator. Similar to the magnetic joint and the articulated mesh structure variable stiffness joint, the laminar jamming joint was incorporated into the PIP joint of a finger composed of two phalanges. When no pressure is applied the joint is relaxed and free to flex favoring high power grasp forces. However, when pressure is applied the laminar jamming joint will stiffen facilitating improved fingertip forces for pinch grasp configurations.

The use of magnets can provide high pinch grasp forces increasing the exerted force by up to 6 times without compromising the power grasping capabilities. However, rapid decrease in the PIP joints resistance force when transitioning between straight and bent configurations occurs very fast causing the hand to potentially lose the object it has grasped. The use of magnets also limits such a design from interacting with magnetically sensitive objects and equipment. Laminar jamming addressed this problem, however, to achieve higher joint stiffness rigid materials like paper should be used to gain a higher rigidity. The laminar jamming joint composed of paper layers was capable of facilitating a pinch force increase of 3 time when comparing jammed and unjammed states. To achieve higher joint stiffness to provide a further increase in achievable fingertip forces stiffer laminar materials with high surface friction coefficients should be used. Alternatively stiffer laminar layer can be used, but by using stiffer materials, the bending curvature is limited and bending past theses limits can permanently deform the material and damage / weaken the joint. Hence, such a variable stiffness joint has limited range of motion and low robustness, which is not suitable for real world tasks, which requires a numerous number of grasps to be executed daily [193]. The use of articulated mesh structures addresses this problem of robustness and the mesh is able to freely bend past it yield point without being damaged. Articulated mesh structures are capable of providing a 3.31 times force improvement. Unlike the previous 2 solutions the articulated mesh can be incorporated into both pin and flexure joint designs making it more versatile.

8.3.7 Video Demonstrations

A video demonstrating the developed adaptive underactuated tendon driven hand, soft gripper, and wearable elbow exo-skeleton can be found in the following URL:

www.newdexterity.org/meshjamming

8.4 Discussion and Conclusions

This chapter introduces the use of articulated pin and flexure joint mesh structures in a jamming style configuration that can be controlled to implement variable stiffness actuators. When the envelope (silicone pouch) is pressurized, it will compress the mesh into its lowest volume state facilitating a stiffness change. Unlike conventional jamming structures where the actuators can experience irreversible deformations in their stiffened state, jamming structures based on articulated mesh structures can elastically deform in both jammed and unjammed states. This enables the structure to be used in place of passive elastic elements in robotic mechanisms [194] as the variable stiffness actuator will return to a defined shape.

Although the use of articulated mesh structures prevents the jamming structure from holding different shapes when jammed, the structure can be mechanically programmed by modifying the mesh links such that when the system is pressurized it will actuate itself into the preprogrammed shape of the links. Hence, jamming structures based on articulated mesh structures are not restricted to only straight beam shapes, but can be made to hold curved geometries (Fig. 8.5). Additionally, by combining non-straight links with straight PET sheets an active flexion and passive extension behavior - which switches between straight and curved geometries - can be achieved when pressurizing and depressurizing the pouch encasing them, facilitating not only varied stiffness, but also a self-actuating behavior. This self-actuating and adaptive property can be utilized to develop robotic (Fig. 8.8A) and assistive (Fig. 8.10A) devices that require the synergistic implementation of both compliant and rigid actuation modes.

The yield force required to bend the articulated mesh structure can be controlled by the variation in applied pressure on the mesh enabling the structure to hold increasingly higher loads. The stiffness and yield force can be further tuned by selecting the required mesh link lengths and patterns. Although increasing mesh link lengths provides higher stiffness and load bearing capabilities, a trade-off is made for the conformability of the mesh as the joints are spaced further apart. This is particularly the case for the articulated pin meshes. However, for the flexural mesh designs which consist of a flexure base to hold the links. The spacing of the joints can be condensed regardless of bar length, allowing for higher conformability in flexural meshes. The control of yield force by regulating the applied pressure provides an intuitive way to control the force the mesh structures can exert. For the case of robot grippers and hands, this allows for the selection of grasp strategies that use low forces for the execution of delicate and fragile tasks,

and strategies that use high forces for the execution of heavy-duty tasks. When integrated into exoskeletons this can be used to choose the amount of assistance that is provided to the wearer.

A consideration when developing jamming actuators based on articulated mesh structures needs to be how the envelope encasing the mesh will conform to the mesh structure when bending is occurring. This is important as the pouch can over conform to the mesh structure generating net zero moments on the mesh preventing the structure from elastically returning to its original shape. The addition of laminar materials (e.g., PET sheets) sandwiching the mesh structure can help support and prevent the envelope from over conforming, maintaining the elastic behavior and bending efficacy of the actuator. An alternative approach is to use fanning structures that can collapse into a compact form when folded and fan out to block the pouch from conforming into locations that would compromise the elasticity of the actuator when unfolded. Both implementation examples can be seen in Fig. 8.2 with Fig. 8.4A and Fig. 8.6 utilizing PET sheets for support and Fig. 8.4B using fins that can be collapsed and expanded to provide bracing.

The materials presented here facilitate the variable stiffening, elastic deformation, self-actuating, and incorporation of the developed variable stiffness actuators into different devices and application classes to demonstrate the possible use cases and performance enhancements.

8.5 Future Directions

Regarding future directions, we plan to extend the jamming structures by explore more complex beam geometries to facilitate the design and construction of robots that require specific joint shapes or motion trajectories when self-actuated through jamming. Investigate and implement a more compact vacuum pump solution to enable the system to be more portable, extending its use to a wider range of applications. Integration of flexible sensors into the PET layer of the jamming structure can provide force and pose data of the jamming structure for feedback.

Chapter 9

A Pneumatically Driven, Disposable, Soft Robotic Gripper Equipped with Multi-Stage, Retractable, Telescopic Fingers

9.1 Background

During the last decade, the robotics field has seen an increased interest in creating soft and compliant structures. Robotic hardware is changing, moving from traditional rigid, fully actuated robots to soft robotic devices that take advantage of structural compliance. Such soft robots allow for safer interactions with humans, fragile objects, and have the ability to better operate in unstructured and dynamic environments. Although traditional, rigid robot grippers and hands are capable of performing highly dexterous tasks, simple parallel jaw grippers are still being extensively used. This is due to the fact that they do not require complicated control laws or sophisticated sensing to perform versatile object manipulation and grasping [194, 100]. However, soft robots can further reduce control complexity, providing affordable solutions for the execution of complex grasping tasks.

Robotic grippers employing compliant structures and underactuation have been used to achieve efficient and stable grasping with simple and intuitive control. By adding compliant elements into traditional rigid robot hands, grippers can successfully grasp various objects [195] and execute various tasks under object pose uncertainties [196]. This design strategy enables the system to conform

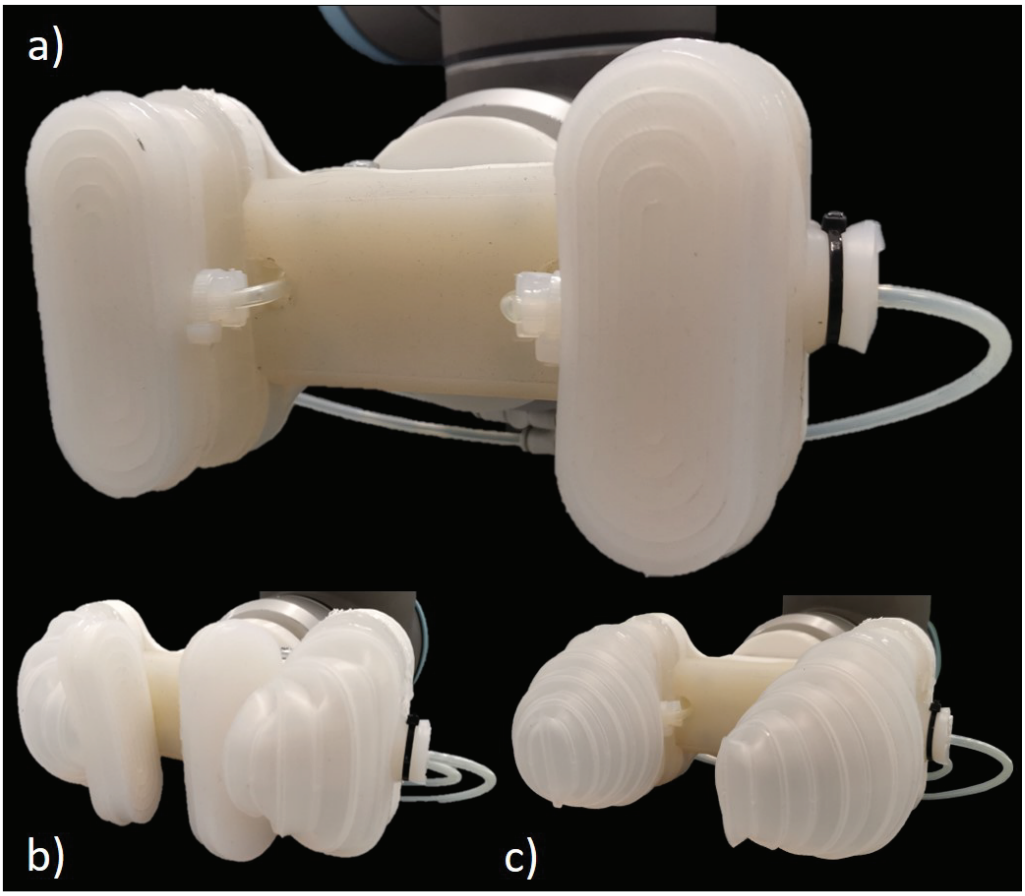

Figure 9.1: The disposable soft multi-stage gripper maintains a compact form factor when deflated (subfigure a)), and is equipped with a set of soft pneumatic actuators capable of abduction motion (subfigure b)) and telescopic extension (subfigure c)).

and adapt around grasped objects and their environment with minimal sensing and control, thus allowing for safer interaction with various soft, compliant objects [197][187]. With soft robotics, elasticity and structural compliance is achieved by manufacturing the entire robot from soft materials, increasing the inherent safety and adaptability of interactions with delicate or fragile objects.

In addition to structural compliance, soft robotic grippers can also be manufactured in a disposable manner [198]. For pneumatic continuum body designs, the pumps and actuator units are commonly separated from the elastic chambers (the body of the robot). Hence, it is possible to quickly replace the used elastic chambers. Such a concept can be applied in the medical field where a simple,

disposable soft robotic gripper can provide an excellent solution for handling contaminated items or for interaction with hazardous objects, such as used syringes or potentially infectious articles. This is especially important when interacting with high volumes of potentially contaminated objects where disinfection or sterilization procedures maybe infeasible due to time constraints or other factors. A disposable design also allows for quick replacement of the damaged components during the gripper lifetime [1].

In this chapter, we focus on the design, development, and evaluation of an affordable, compact, pneumatically driven, soft robotic gripper that employs telescopic fingers. Such a gripper can be used in environments that require disposable devices (e.g., a gripper for handling medical waste that can be easily stored and replaced). The proposed device is composed of two multi-stage, retractable, telescopic fingers. The two stages of the fingers are: i) an abduction / adduction stage that allows re-orientation of the second stage to better encompass the grasped objects, and ii) a telescopic stage that can act as a finger, inflating and maximizing the area of the contact patches between the gripper and the grasped object.

The remainder of the chapter is organized as follows: Section 9.2 presents the related work, Section 9.3 shows the design of the soft robotic gripper, Section 9.4 focuses on the experimental setup and presents the experimental results, and finally Section 9.5 concludes the chapter.

9.2 Related Work

Traditional, rigid robot end-effectors are typically designed for heavy-duty industrial applications. When interacting with fragile or elastic objects, these grippers can easily damage them and thus they require complex and computationally expensive control schemes [46]. With the increased interest in human-robot interaction and service robotics applications, robots are moving from operating in highly structured environments to human-centered environments, where safety, adaptability, task-worthiness, and affordability are of paramount importance [199]. Designs exploring the addition of structural compliance in anthropomorphic robot hands [200, 50], simple underactuated robot grippers [194], and unconventional, hyper-adaptive grippers [201] have been presented in the literature. Structural

[1] Majority of the chapter is based on [22], © 2020, IEEE. Reprinted, with permission, from Geng Gao, Che-ming Chang, Lucas Gerez, and Minas Liarokapis, A Pneumatically Driven, Disposable, Soft Robotic Gripper Equipped With Multi-Stage, Retractable, Telescopic Fingers, IEEE Transactions on Medical Robotics and Bionics, 2021.

compliance can be used to increase grasping robustness by increasing the contact patches between the gripper and the object surface. It also facilitates grasping under significant object pose uncertainties [195] and decreases the grasping force required to extract stable grasps [202]. All these characteristics are highly desirable properties when interacting with fragile and delicate objects.

Soft manipulators trade precision, repeatability, and high force exertion capabilities for significant adaptability that allows them to conform to different object geometries [203]. Among the broad field of soft robotics, continuum body manipulators are perhaps the most common approach that employs a pneumatic network or bellow structures. Designs such as Festo's tentacle gripper [204] and the mGrip from Soft Robotics Inc. [205] are commercial examples of this class of robotic grippers. Other examples include designs where a series of inflatable pouches are connected on a strip of elastic backbone material [206]. Such types of expandable segment approaches require a large initial or deflated profile and rely upon pouch inflation to cause bending or twisting of the structure [207]. Alternatively, the initial size can be reduced by using inflatable elastomeric origami structures [208].

Other than positive pressure systems, soft grippers can also use negative pressure for actuation [181]. Versaball [209] and vacuum suction grippers [210] are examples that take advantage of this type of actuation. Positive pressure soft grippers can operate between 30 kPa and 120 kPa [211] [206]. Some can operate at pressures that range from 0 kPa to 310 kPa[212], while negative pressure systems can operate at approximately -85 kPa [181, 210]. As soft grippers excel at handling fragile and irregular shaped objects, they have been used to handle food [213] or biological samples [212]. For applications with strict hygienic and sterile requirements, disposable personal protection equipment and single-use end-effectors are often used to prevent contamination. In healthcare and medicine, robots must be free of microbes to prevent the spreading of contagious diseases to other patients [214]. With most surgical end-effectors designed for single use [215], service robots operating in these environments must also be sterilized periodically as they can become infectious carriers [216] or sources of contaminations. Disposable devices are a good alternative to sophisticated gripper designs that require materials that can endure the extreme environmental conditions of the sterilization processes [217].

9.3 Designs

In this section, we describe the design of the soft robotic gripper's structure. The developed soft robotic gripper comprises of four main components: two detachable,

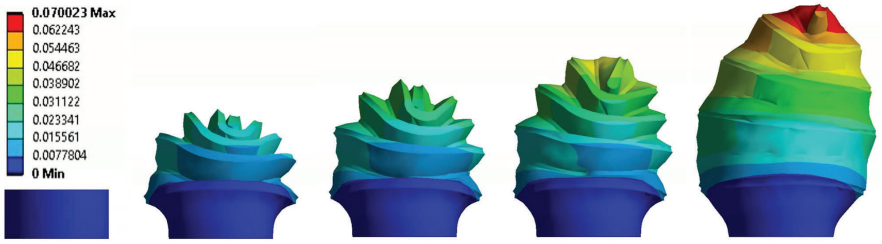

Figure 9.2: The FEA model of the soft telescopic actuator is used to understand the deformation behavior. The analysis shows the total deformation of the actuator in meters when it is inflated from 0 kPa to 10 kPa (left to right).

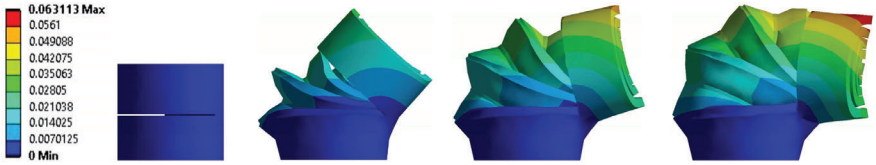

Figure 9.3: The FEA model of the soft abduction actuator is used to understand the inflation behavior. The analysis shows the total deformation of the actuator in meters when it is inflated from 0 kPa to 10 kPa (left to right).

soft, pneumatically driven, multi-stage fingers, a soft palm pad, and a base plate. The soft, pneumatic, multi-stage fingers are designed to be affordable, costing only $2 USD in raw materials to fabricate, while the soft palm pad costs $1.6 USD. The high affordability and modularity of the fingers and palm pad allows the gripper to be used in a disposable manner. This enables the gripper to be used in scenarios where the tools have a single time use or can be easily contaminated and then disposed (e.g. medical environment). The soft pneumatic multi-stage fingers are composed of two stages: a telescoping stage and an abduction / adduction stage that facilitates prepositioning of the telescopic actuator. To execute the movements of the two stages, two types of soft actuators were developed: a soft telescopic actuator that inflates into a soft finger from a low and compact profile, and a soft abduction/adduction actuator, which provides the telescopic actuator with the required mobility to preposition the telescopic mechanisms and encompass objects during grasping. The gripper is powered by two low-pressure mini air pumps, each connected to the two separate modules of the fingers (one pump powering the two soft abduction actuators and one pump for inflating the two telescopic actuators). By connecting the telescopic actuator module pair and the abduction actuator module pair to individual air pumps, a fluidic t-pipe differential [218] is formed. The air in the soft actuators can redistribute between each other

producing differential outputs. This allows the fingers of the soft gripper to better adapt and grasp objects in an unstructured environment. A solenoid valve is used to release the internal pressure of the actuators, allowing them to deflate to their original compact state passively.

9.3.1 Soft Abduction/Adduction Actuator Design

The soft abduction/ adduction actuator is made out of silicone rubber (Smooth-On Dragon skin 30) with 1 mm thick walls. The soft abduction/ adduction actuator uses a pre-folded structure to create a compact actuator [219]. The folded structure has multiple folds, which occupy one side of the actuator. By employing this structure, the pre-folded side can extend when it is inflated causing a bending motion towards the unfolded side, which is unable to extend on the actuator. The range of motion of the soft abduction/ adduction actuator is 0° to 105°.

A Finite Element Analysis (FEA) model of the soft actuator deformation was developed to understand the structure's inflation behavior. A Yeoh second-order hyperelastic model [220] was used to model the material properties of the soft actuator. Assuming incompressibility of the silicone rubber, the Yeoh second-order hyperelastic parameters of the simulation used, are: C_1 = 100 kPa and C_2 = 119 kPa. The FEA model was created using ANSYS Workbench 2020 R1 computer-aided engineering (CAE) software. The simulation utilized a fixed base for the actuator and a normal pressure force applied to the internal walls of the actuator. The simulated behavior during inflation can be seen in Fig. 9.3. The angular displacement of the structure was evaluated with different actuator heights (h), ranging from 5 mm to 10 mm. The actuator inflation trajectory with different heights (h) can be seen in Fig. 9.4. The actuator height utilized in the proposed gripper was 10 mm because of the 105° range of motion provided, giving the soft telescopic actuators full range of motion to perform encompassing grasps while inflated and deflated.

A validation experiment was conducted to evaluate the similarity of the results of the simulated model with the actual actuator results. The angular displacement was captured using an optical motion capture system composed of eight cameras (Vicon Motion System Ltd., UK) with retroreflective markers attached to the top surface of the actuator. The internal actuator pressure was measured using the Honeywell 40PC150G2A pressure sensor attached to the pressure supply line. The results are depicted in Fig. 9.5, which shows the simulated model and five different experimental trials.

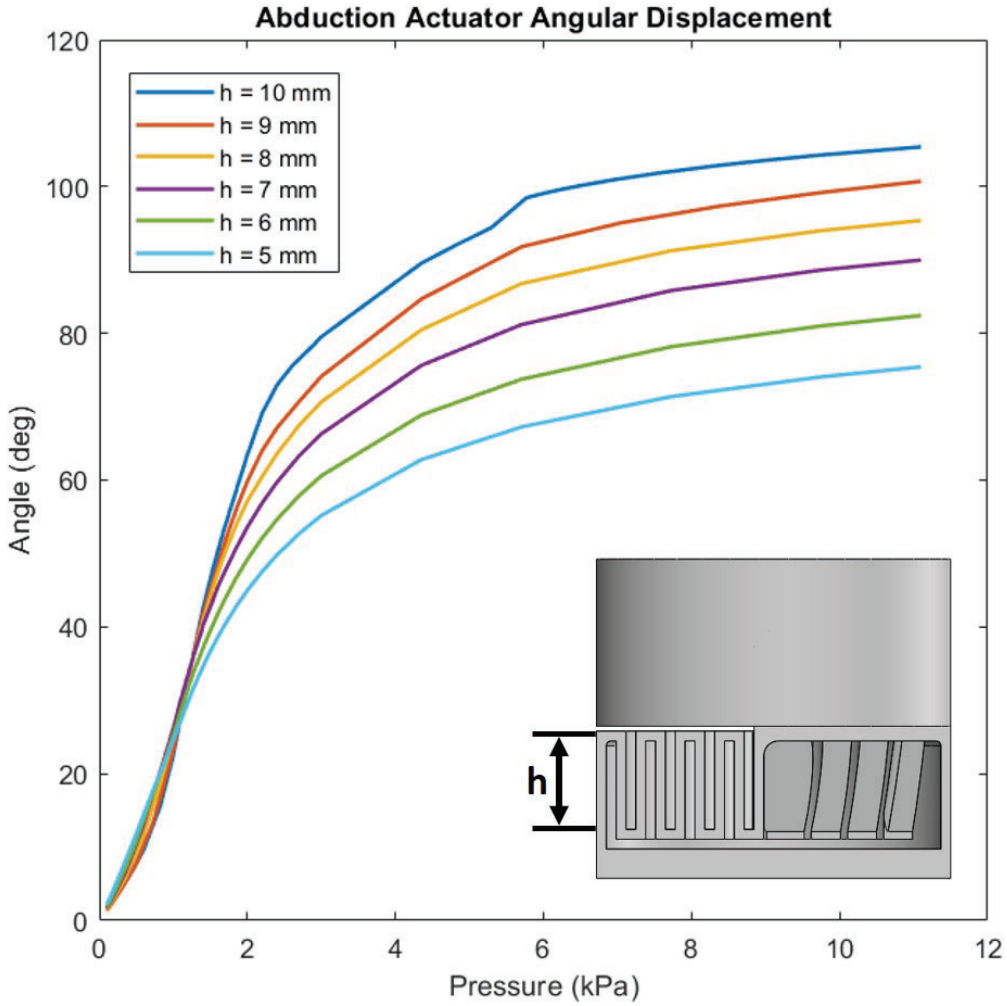

Figure 9.4: FEA simulations of different pre-fold heights were conducted to analyze the maximum achievable angular displacement and trajectory of the soft abduction actuator when pressurized from 0 kPa to 10 kPa.

However, the experimental results show some differences between the actual actuator behavior and the FEA model results. This discrepancy could have been due to errors in the manufacturing process, which can change the mechanical properties of the material (e.g variations in mix ratio, or sub-optimal curing can alter the stiffness of the material). This is probable due to the fact that the variation of displacement around 10 kPa for rings further outside deviates more than rings near the center of the mechanism. The spikes and vibration in measured displacements also come from the unfolding and elastic deformation of the rings as they expand. Although there is a variation in the results, the FEA model and the experimental

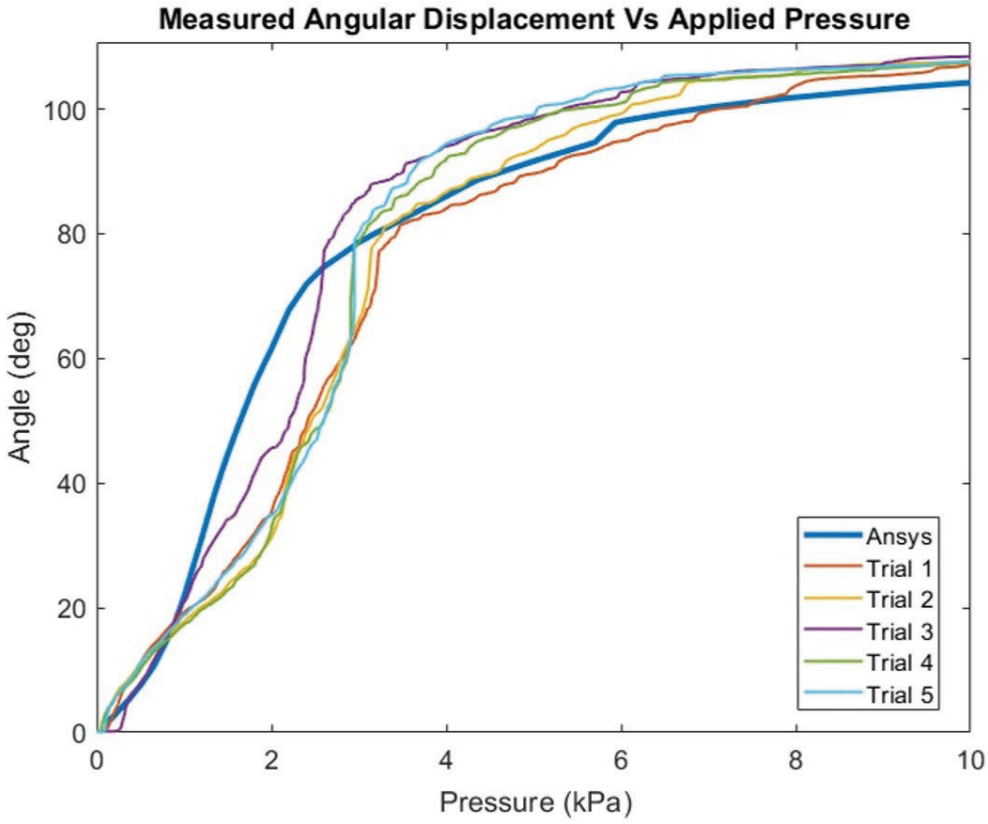

Figure 9.5: A comparison of the simulated FEA based angular displacements of the actuator and five experimentally measured angular displacements.

trials still follow similar trajectories. Hence, the model can be used to optimize the design allowing for various materials and configurations to be easily compared and tested in simulations.

9.3.2 Soft Telescopic Actuator Design

Similar to the soft abduction/adduction actuator, the soft telescopic actuator also adopts a silicone rubber (Smooth-On Dragon Skin 30) pre-folded structure with 1 mm thick walls. Unlike the abduction/adduction actuator, the pre-folded structure of the telescopic actuator forms concentric rings that provide a low form factor actuator with an ability to be significantly elongated. When inflated the actuator is capable of expanding up to 4.71 times its initial height (expanding from 17 mm when deflated to 80 mm when fully inflated), the pre-folded structure and the intrinsic elasticity of the actuator provides a passive retraction behavior

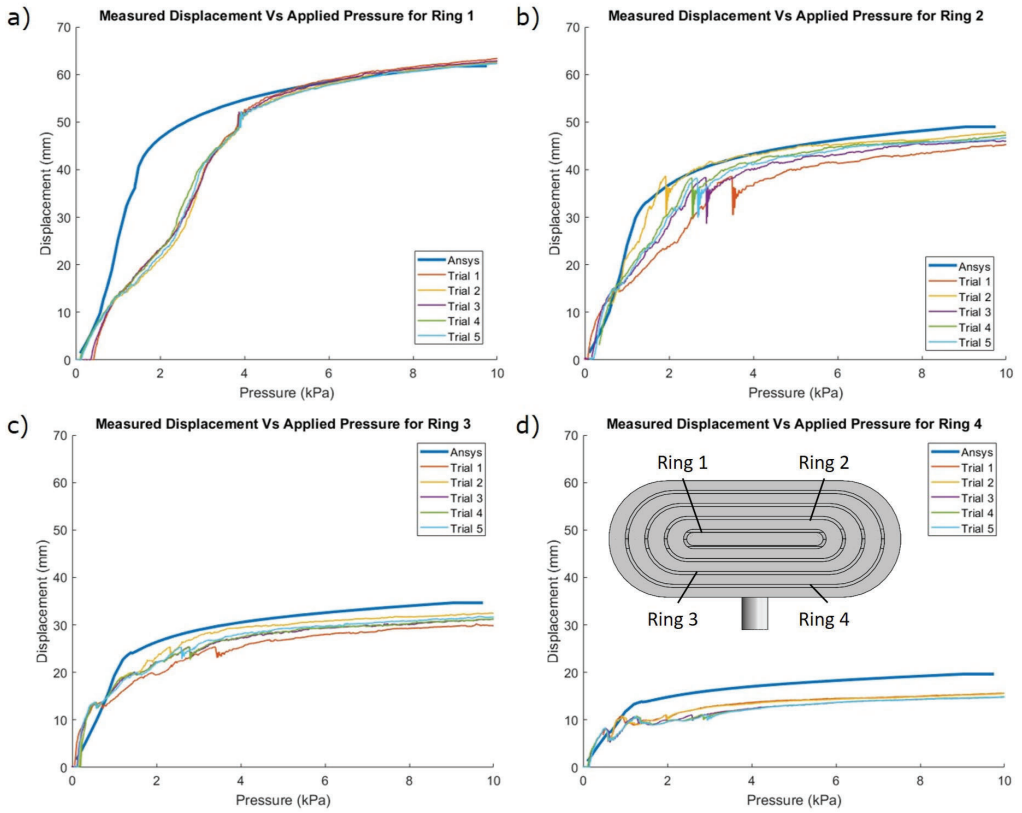

Figure 9.6: The vertical Z-axis displacement of the FEA simulated telescopic actuator during inflation was compared with experimentally measured vertical displacements of five different inflation trials. Four points were selected, one on each ring starting from the center of the actuator.

for the actuator that allows it to return to its original state when deflated. Each ring has different heights at the front side and back side in the folded structure of the ring causing an asymmetric inflation profile when the actuator is viewed from the side. This is illustrated in Fig. 9.2, where the tip of the actuator bends to the right as it is gradually inflated. The actuator operates at 10 kPa allowing for affordable, compact, and low-pressure air pumps to be used. This enables the soft telescopic actuator to be highly portable in comparison to other soft actuator designs, which require large high-pressure pumps.

To understand the behavior of the telescopic actuator and the maximum achievable expansion height, a series of simulation and motion capture experiments were conducted. An FEA model of the telescopic actuator was developed using the same hyperelastic model, constants, and constraints used in the defor-

mation analysis of the soft abduction/adduction actuator. The simulated behavior during inflation can be seen in Fig. 9.2. A comparison between the simulated and the experimental measurements was performed in Fig. 9.6 for the different layers of the actuator. The comparison evaluated rings one to four with the fifth ring being excluded as it is the outermost edge of the actuator, which experiences negligible vertical displacement. The displacement motion of each ring of the actuator was measured using a similar method to the angular displacement of the abduction/adduction actuator. An optical motion capture system was used with retroreflective markers attached to each ring of the soft telescopic actuator.

Sharp changes that are evident in the experimental trials demonstrate a rapid unfolding of the deflated structures unlike the simulation. This is due to frictionless contact in the model that enables the ring folds in the simulation to slide past each other smoothly. Although the experimental trials do not fully match the trajectories of the simulated model (like the inflation trajectory at the tip of the actuator represented by ring 1, shown by Fig. 9.6a), the maximum displacement at the tip of the actuator when it reaches full inflation matches that of the FEA model. This allows the model to be used in determining the max inflation height of a particular telescopic designs if different elongation heights are considered.

9.3.3 Manufacturing Process

The manufacturing process of a soft, pneumatic, multi-stage finger involves six molding steps. This process is depicted in Fig. 9.7.i to Fig. 9.7.vi. The first steps involve molding the abduction and telescopic structures of the multi-stage actuators. This is illustrated in Fig. 9.7.i and Fig. 9.7.iv where a mold composed of four parts is used to fabricate the upper sections of the corresponding structures. Once these components are cured, the next two steps involve combining these sections with their respective bases and to merge them at the edges with additional silicone (this is indicated with the blue line shown in Fig. 9.7.ii and Fig. 9.7.v). The abduction actuator has an additional step where the Hybrid Deposition Manufacturing (HDM) technique [46] is used to add a rigid base material into the actuator so as to provide a secure and detachable mounting point for the modular base to connect to. Finally, the last step involves bonding the base of the soft telescopic actuator to the top flat section of the soft abduction/adduction actuator, producing a soft, multi-stage, pneumatic finger (see Fig. 9.7.vi). The soft palm pad of the gripper is constructed using an HDM mold, a rigid plastic plate, and silicone rubber for

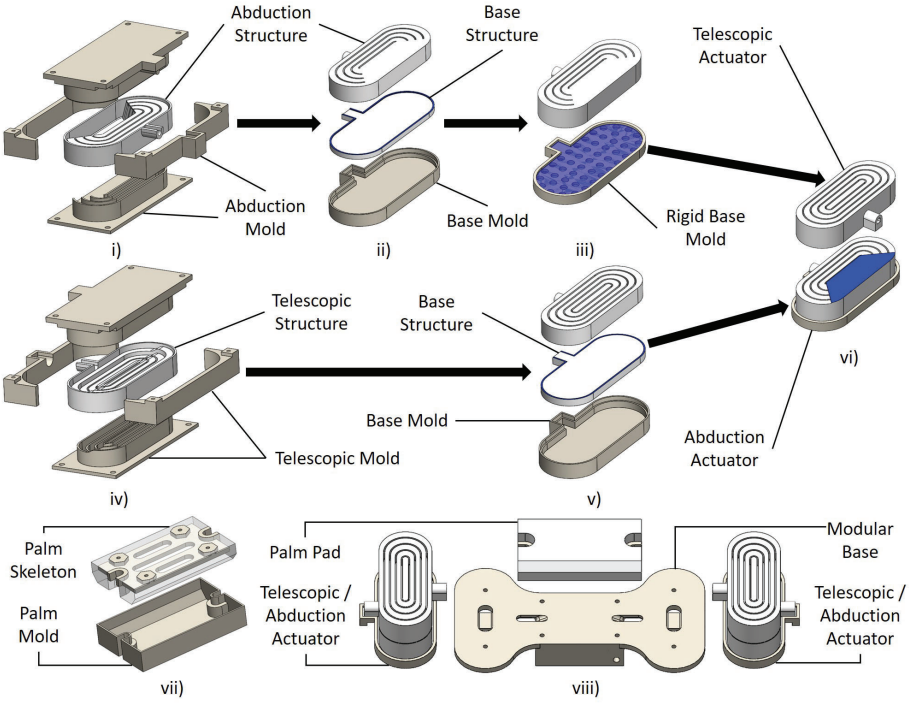

Figure 9.7: The soft telescopic and abduction actuators are made out of silicone rubber (Smooth On Dragon Skin 30) and involve a 6 step molding process: i) the pre-folded structure of the abduction actuator is fabricated using a four-part mold, ii) once the top section of the actuator is molded, a base mold is used to attach the top section of the actuator to the base section of the actuator, iii) a rigid base is molded into the soft abduction actuator by employing the Hybrid Deposition Manufacturing (HDM) technique, iv) Similarly, to step i) the pre-folded structure of the telescopic actuator is created using a similar mold structure, v) following the same approach as in step ii) the base of the telescopic actuator is merged with the actuator, vi) once the two separate actuators are made they are combined through the use of additional silicone as adhesive at the blue contact surface. All blue sections illustrate connection points. Subfigure vii) shows the HDM fabrication process that is used to embed the rigid palm pad skeleton into the soft silicone material and finally, subfigure viii) presents the exploded view of a complete pneumatically driven soft robotic gripper.

the pad. This is presented in Fig. 9.7.vii. The exploded view of the soft robotic gripper can be seen in Fig. 9.7.viii.

Figure 9.8: Grasping experiments were conducted with the soft robot gripper grasping a variety of objects. The objects consisted of everyday life objects from the YCB object set an object set designed to facilitate benchmarking. Additionally, fragile (subfigures n) to o)) and medical (subfigures r) to y)) related objects were selected to further assess the grippers capabilities.

9.4 Experiments and Results

9.4.1 Grasping Experiments

The first experiment focused on the grasping capabilities of the soft robotic gripper, and it involved a wide variety of different everyday life objects. A total of 28 everyday life objects were selected, while 16 of the 28 objects were selected from the YCB object set [34]. The YCB object set is designed to facilitate the assessment of the grasping and manipulation capabilities of robot grippers and hands. The remaining 12 objects are: an egg, a cherry, a syringe, a petri dish, a sponge, a bandage roll, a used glove, used tissues, a used mask, a pair of tweezers, a scalpel, and a chemical jar. This additional assortment of objects that are external to the YCB object range provided insight into the capabilities of the gripper when

Table 9.1: Object grasping and grasp stability results

Objects	**Properties**		**Grasp**	**Stability**
	Weight (g)	**Dimensions (mm)**		
Bleach Bottle	292.5	250 x 54 x 95	Y	Y
Mustard Bottle	230.2	193 x 55 x 95	Y	Y
Jello Box	410.6	109 x 89 x 34	Y	Y
Chips Can	212.2	232 x 67 x 67	Y	Y
Wine Cup	670.0	138 x 84 x 84	Y	Y
Plastic Pear	261.0	105 x 66 x 66	Y	Y
Plastic Lemon	156.7	66 x 53 x 53	Y	Y
Plastic Banana	337.2	192 x 35 x 71	Y	Y
Tennis Ball	297.3	65 x 65 x 65	Y	Y
Marble	24.7	16 x 16 x 16	Y	Y
Dice	25.9	16 x 16 x 16	Y	Y
Hammer	3254	330 x 135 x 25	N	N
Card	24.0	1 x 85 x 54	N	N
Fork	157.7	200 x 25 x 12	Y	Y
Drill	641	185 x 50 x 175	Y	N
Wood Block	2332	89 x 89 x 123	Y	N
Egg	334.5	60 x 45 x 45	Y	Y
Cherry	65.7	30 x 27 x 24	Y	Y
Syringe	41.2	105 x 30 x 21	Y	Y
Petri dish	39.7	84 x 84 x 16	Y	Y
Sponge	103.0	212 x 58 x 102	Y	Y
Bandage	39.3	79 x 28 x 28	Y	Y
Used Glove	27.5	133 x 110 x 25	Y	Y
Used Tissue	22.4	80 x 85 x 67	Y	Y
Used Mask	13.7	175 x 95 x 1	Y	Y
Tweezers	147.0	143 x 12 x 13	Y	Y
Scalpel	122.2	140 x 12 x 5	Y	Y
Chemical Jar	2930	180 x 45 x 45	Y	N

handling fragile objects, medical tools, and medical waste, which are not present in the YCB object set. The full list of objects can be found in Table 9.1. The grasping procedure started with each object being placed on a flat surface before being grasped. Once grasped, the UR5 robot arm was used to move the gripper and the grasped object in 3D space so as to assess the stability of the grasp. The gripper and the grasped objects are depicted in Fig. 9.8.

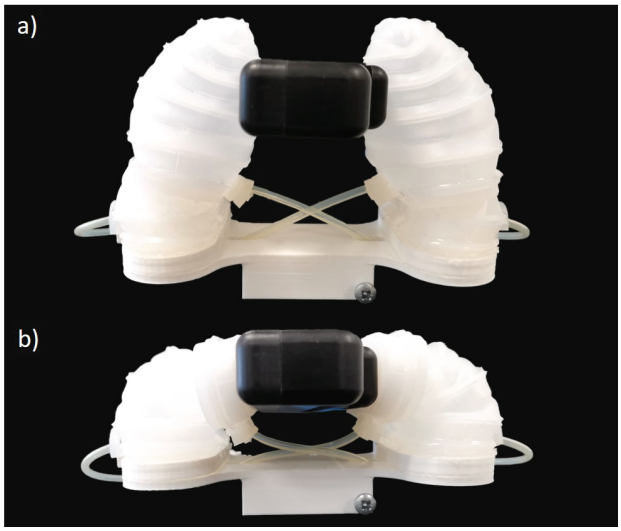

Figure 9.9: The force exertion capability experiments of the gripper were conducted with a dynamometer being placed and grasped in-between the two fingers of the soft robotic gripper. Two configurations were evaluated: i) when the forces are applied on the sensor with the telescopic actuators fully inflated, and ii) when the forces are applied on the sensor with the telescopic actuators deflated.

While conducting the experiments, a total of 24 out of the 28 objects were grasped successfully (85.7%). The soft telescopic gripper failed to grasp the credit card, the hammer, and the wood block. The highly flat geometries like the credit card make it difficult for the gripper to establish contact points on the sides of the object, which are needed in order to grasp it off the table surface. In such cases, many gripper designs employ the use of fingernails to scope underneath the object or utilize a suction cup to pick them up. For heavy objects with irregular geometries and a center of mass far away from the geometric centroid (e.g., like the hammer) a sub-optimal grasp is needed (grasping at the handle). For such cases, the gripper lacks the required grasping force needed to hold onto the object. However, for heavy objects like the regularly shaped wood block the object can be easily grasped. Although some heavy objects can be easily grasped, the grasps lack stability and can only transpose the objects at slow speeds (e.g., drill grasps and chemical jar grasps). In order to mitigate this, the use of either stiffer materials, or higher wall thicknesses is required so as for the soft telescopic actuators to operate at higher pressures. This can enable the gripper to apply higher forces and resist larger disturbance forces, increasing also the energy required to operate the soft robotic gripper.

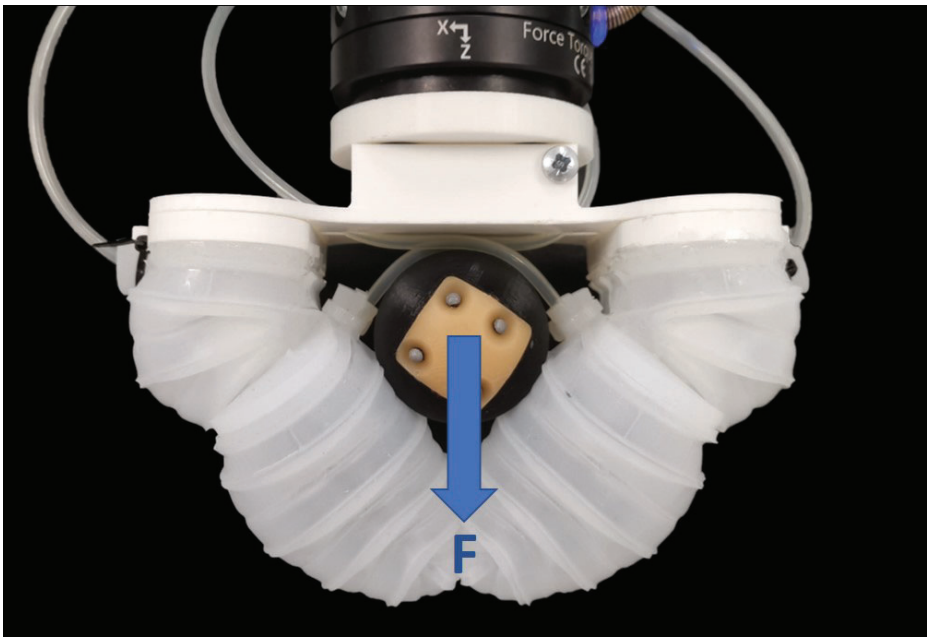

Figure 9.10: The pull-out force experiments were conducted with three different object geometries: a sphere, a cylinder, and a cube. Once the objects were grasped, a force in the z-direction of the force/torque sensor (FT300, Robotiq, Canada) was applied so as to pull them out of the gripper's full grasp.

9.4.2 Grasp Force Experiment

The second experiment conducted assessed the maximum achievable grasp force that the gripper is capable of exerting through the soft actuators during grasping. The grasp forces were collected with a Biopac MP36 data acquisition unit (Biopac Systems, Inc., Goleta, California) through the use of a SS25LA dynamometer placed in the center of the grasp. Two grasp configurations of the soft gripper were assessed. The first configuration required the abduction modules of the soft robotic gripper to be inflated at 0° so as for the force to be transmitted through the inflated retractable, telescopic structures. The second configuration inflated the abduction modules to 90° before inflating the telescopic fingers. The two configurations of the soft gripper can be seen in Fig. 9.9. The maximum force exerted in the 0° configuration was 13.57 N and the maximum grasp force applied in the 90° configuration was 14.53 N.

9.4.3 Pull Out Force Experiment

When grasping objects, a gripper must also handle disturbances post grasp to prevent dropping a grasped object. To assess this, three objects of varying geometries (a sphere, a cube, and a cylinder) were selected from a set of sensorized objects [16]. Once the object was grasped, it was then pulled-out of the soft grippers grasp with a force normal to the base plate of the gripper. This was repeated 10 times. The maximum pull out force was measured with a force/torque sensor (FT300, Robotiq, Canada) mounted at the base of the robot gripper. The maximum achievable pull-out force that was needed to remove the objects examined from the gripper grasp can be seen in Table 9.2.

Table 9.2: Maximum pull out force to eject objects from grasp

Object Type	**Dimension (mm)**	**Pull Foce (N)**
Sphere	⌀50	17.68
Cylinder	⌀50 x 50	17.58
Cube	50 x 50 x 50	20.90

9.4.4 Soft Gripper Comparison

A comparison between the developed pneumatically actuated multistage soft telescopic gripper and the articulated mesh soft gripper presented in Section 8.2.3 was conducted to evaluate the difference in using the developed variable stiffness structure in-comparison to traditional inflatable structures. Soft robots that rely on negative pressure like the developed variable stiffness structure to operate, are safer for use around humans in comparison to inflatable structures because they are not prone to the possibility of exploding if the inflation pressure is higher than the vessels maximum allowable operating pressure. Additionally, this property also allows negatively pressure soft robots to take small punctures [221], although the efficiency of the device decreases, the ability to still operate enables such soft systems to be more robust at executing tasks. Although the use of articulated mesh structures adds some rigidity to the soft structure preventing the articulated mesh soft gripper from being fully soft like the telescopic soft gripper, the articulated mesh provides rigidity to out of plane motions aiding in grasping heavy loads. Depending on the actuation motion required employing an inflatable structure can be more advantageous in developing extending/ expanding type actuating motions, as the use of vacuum pressure compresses the structure preventing it

from enlarging. Both grippers were capable of executing grasp forces adequate for activities of daily living (ADL) where the grasping forces are around 10 N to 15 N with pinching forces being lower than 10.5 N for daily life tasks [105, 222]. The articulated mesh soft gripper was capable of a max pull force of 31.76 N with the sphere, 31.29 N with the cylinder, and 56.28 N with the cube, whereas the telescopic soft gripper was capable of a max pull force of 17.68 N with the sphere, 17.58 N with the cylinder, and 20.90 N with the cube. The hybrid design of rigid articulated links and soft materials in the articulated mesh soft gripper facilitates a higher resistance to deformation forces, which can be beneficial when handling heavier loads. Although the articulated mesh is capable of bending and flexing freely the links are still rigid, meaning the design is not able to take crushing loads to the same degree as a fully soft system that can freely deform like the inflatable multi-stage, telescopic gripper.

9.4.5 Video Demonstration

The demonstration video of the proposed soft robotic gripper and its performance can be found at the following URL:

www.newdexterity.org/softdisposablegripper

9.5 Conclusion

In this chapter, we presented a soft, pneumatic, multi-stage, soft robotic gripper equipped with telescopic, retractable fingers attached to soft abduction/adduction actuators. The combination of the two actuators allows the gripper to expand from a compact form factor to grasp a variety of everyday life objects (from the YCB object set) and medical supplies, in a stable manner using low pressures of approximately 10 kPa. The actuator's pre-folded structures and the intrinsic elasticity of the material that were used to construct the gripper facilitate passive retraction. The fluidic t-pipe differential allowed asymmetric grasps to be performed if a finger is obstructed. The telescopic gripper can perform pinching and caged grasping by actuating the upper and lower actuators separately. The gripper was able to exert 14.53 N of force during grasping, and a max pull out force on the sensorized cube of 20.90 N. The low-cost of the material used ($2 USD) to fabricate the actuators and the highly modular components enable the gripper to be used in a disposable manner, as the full cost of the robotic gripper is $6.6 USD.

9.6 Future Directions

Regarding future improvements, we plan to integrate force sensors into the soft structure and to improve the modularity of the disposable components with better interfacing. The base and air supply modules can be further integrated towards a standalone unit. A series of telescopic pad designs with variant network layouts can be investigated so as to improve the operating modes and the inflation profiles, facilitating the execution of new, complex tasks (e.g., reaching into narrow spaces).

Part V

Conclusion and Discussion

Chapter 10

Conclusions and Major Contributions

10.1 Conclusions

In this PhD thesis, we focus on the design, analysis, and development of different design methodologies and mechanisms for addressing different problems with adaptive and soft underactuated systems, in turn enhancing their grasping and manipulation capabilities. The proposed solutions focus on different levels of structural compliance, reconfigurable base frames, locking mechanisms, and variable stiffness systems.

For robotic systems executing assembly based tasks in manufacturing environments, a multi-modal gripper combining different grasping modes which synergize with each other to enable the execution of tasks in a fast and efficient manner. Accompanying the gripper a compliance control and CAD based localization system form a flexible manufacturing system. The gripper incorporates both a parallel jaw gripper, rotary module, and magnetic element to minimize retooling delays and enable the execution of a variety of tasks. The integration of a local degree of freedom through a rotary module imparts increased dexterity in an efficient manner. Additionally, a localized complaint axis at both the rotary and magnetic modules allows the gripper to passively compensate for localization and calibration errors within the control system facilitating robust execution of assembly tasks. The developed system placed first at the Robotic Grasping and Manipulation Competitions manufacturing track hosted at the IEEE/RSJ International Conference on Intelligent Robots and Systems (IROS) 2019 and place third in the

IROS 2020 version of the competition. Additionally, the work was nominated for best paper award under the robot mechanism and design category in IROS 2020.

In the context of robotic systems in human-centric environments anthropomorphic robot hands were designed to better interact with tools and objects designed with ergonomics for the use of humans. In order to efficiently utilize the limited degrees of actuation within underacted hands, reconfigurable finger base frames were proposed. This allows the hand to not only leverage the human hand form, but to reconfigure into non-anthropomorphic configurations allowing the fingers to re-arrange for increased workspace, different grasp types, and different in-hand manipulation modes. By employing reconfigurable finger base frames to alter the robot hand structure, the in-hand manipulation capabilities of the hand can be improved to accommodate a wider range of object sizes.

Adaptive and soft underactuated hands are capable of providing affordable dexterity to robotic and prosthetic systems. For robots, soft multistage inflatable structures were proposed, which can effortlessly adapt and grasp a diverse range of objects, while being low cost for disposable use scenarios (e.g., handling medical waste). In the case of impaired individuals, we proposed prosthetic systems for a variety of different hand amputation types. Wearable gloves, which can be personalized to house different kinds of adaptive fingers with different actuating modes (body-powered and motorized) were developed to accommodate partial hand amputations. For full hand amputees, lockable mechanisms of both body-powered and motorized implementation for different differential mechanism were developed facilitating increased control over underactuated hands while neither compromising the weight, size, cost, and control of the devices.

To improve the force exertion efficiency and control of different joints in adaptive and soft underactuated systems. We proposed variable stiffness actuators in the form of articulated mesh structures capable of stiffening when exposed to vacuum pressure. The actuator is capable of switching between compliant and rigid states facilitating different fingertip trajectories and grasping modes. The proposed variable stiffness actuator can also be designed to not only stiffen, but also self-actuate facilitating the development of soft self-actuating fingers, and assistive wearable devices (e.g., wearable elbow exo-skeleton).

10.2 Major Contributions

The major contributions of this PhD thesis are summarized as follows:

Adaptive Robotic Grippers and Hands for Robotic Systems

We focus on the design, analysis, and development of a series of adaptive robot grippers and hands for executing robust grasping and dexterous manipulation tasks. In particular, the contribution of this part are on the design, analysis, and development of:

- Multi-modal gripping systems equipped with structural compliance and local manipulation oriented degrees of freedom to execute efficiently complex assembly tasks in manufacturing scenarios.
- Monolithic finger structures that combine flexible and rigid materials to create fingertips with localized compliance at the DIP joint for the development of adaptive robot hands capable of robust caging grasping.
- Reconfigurable finger base frame structures for increasing the workspace, and improving the available grasp/manipulation strategies without sacrificing the anthropomorphic appearance and structure of humanlike adaptive robot hands.

Adaptive Fingers and Hands for Prosthetic Systems

We focus on the design, analysis, and development of a variety of prosthetic hands for enhancing the dexterity of amputees. In particular, the contribution of this section focuses on the design, analysis, and development of:

- Partial hand prostheses based on soft wearable gloves that enclose modular finger structures to accommodate different partial hand amputations.
- Body powered and selectively lockable differential mechanisms for increasing the controllability of underactuated adaptive hands in performing individual finger motions for grasping and gesture execution.

Soft and Variable Stiffness Systems

We focus on the design, analysis, and development of soft and variable stiffness systems to improve the grasping and manipulation capability of grippers and hands.

In particular, the contribution of this section are on the design, analysis, and development of:

- Multi-stage, soft, ultra-affordable actuators that have been designed to create affordable end-effectors for handling dangerous materials (e.g., medical waste).
- Variable stiffness jamming structures, which can elastically bend past their yield point, acting as variable stiffening passive elastic elements.
- Mechanically programmable variable stiffness structures that can be designed to self-actuate, transitioning between straight and mechanically programmable (e.g., curved) profiles to offer increased dexterity in adaptive/soft robotic grippers, and wearable exo-skeletons.

Modular, Accessible, and Sensorized objects

We developed a highly modular, diverse, and accessible object set for evaluating in-hand manipulation of robot gripper and hands:

- The modularity of the object set allows the weight, shape, surface friction and size of the objects to be changed providing a diverse object set with a minimal number of objects.
- The object set has been made open source and can be 3D printed and manufactured with HDM processes allowing it to be highly affordable and accessible to the robotics community.

10.3 Future Directions

This PhD thesis focuses on the design, analysis, and development of different actuation systems, design methodologies, and mechanisms, which can be used to develop adaptive, underactuated, and soft hands for robotic and prosthetic systems to perform robust grasping and dexterous manipulation in unstructured and dynamic environments. Regarding the future work for this thesis:

- Perform clinical trials with the prosthetic and assistive devices to quantify the level of usability and assistance the devices provide to patients.

- Expand the design of the automated locking mechanism to include autonomous control of the thumb and develop alternative versions to include other differential mechanisms.
- The current mechanically programmable jamming based on articulated mesh structures use a manual vacuum pump which is not portable. Investigation and implementation of a compact pumping unit for portability can further extend the applicable scenarios such a structure can be used in.
- Perform fatigue and life cycle analysis of the different mechanisms and devices developed to determine their robustness, failure points, and life span during general long-term operation.
- Integration of force sensors into soft structures to facilitate the incorporation of sensing to be incorporated into the soft finger pads and palm pads of adaptive grippers, or into the body of soft robots.

Part VI

Appendix

Appendix A

Thesis Outcomes

A.1 Journal Publications

7. Nathan Elangovan, Che-Ming Chang, **Geng Gao**, and Minas Liarokapis, "An Accessible, Open-Source Dexterity Test: Evaluating the Grasping and Dexterous Manipulation Capabilities of Humans and Robots," Frontiers on Neurorobotics, 2022.

6. **Geng Gao**, Mojtaba Shahmohammadi, Lucas Gerez, George Kontoudis, and Minas Liarokapis, "On Differential Mechanisms for Underactuated, Lightweight, Adaptive Prosthetic Hands", Frontiers on Neurorobotics, 2021.

5. Gal Gorjup, **Geng Gao**, Anany Dwivedi, and Minas Liarokapis, "A Flexible Robotic Assembly System Combining CAD Based Localization, Compliance Control, and a Multi-Modal Gripper", IEEE Robotics and Automation Letters, 2021.

4. **Geng Gao**, Che-Ming Chang, Lucas Gerez, and Minas Liarokapis, "A Pneumatically Driven, Disposable, Soft Robotic Gripper Equipped With Multi-Stage, Retractable, Telescopic Fingers", IEEE Transactions on Medical Robotics and Bionics, 2021.

3. Nathan Elangovan, Lucas Gerez, **Geng Gao**, and Minas Liarokapis, "Improving Robotic Manipulation without Sacrificing Grasping Efficiency: A Multi-Modal, Adaptive Gripper with Reconfigurable Finger Bases", IEEE Access, 2021.

2. Lucas Gerez, **Geng Gao**, Anany Dwivedi, and Minas Liarokapis, "A Hybrid Exoskeleton Glove Equipped with Variable Stiffness Joints, Abduction Capabilities, and a Telescopic Thumb", IEEE Access, 2020.

1. **Geng Gao**, Gal Gorjup, Ruobing Yu, Patrick Jarvis, and Minas Liarokapis, "Modular, Accessible, Sensorized Objects for Evaluating the Grasping and Manipulation Capabilities of Grippers and Hands", IEEE Robotics and Automation Letters (RA-L), 2020.

A.2 Conference Publications

16. **Geng Gao**, Junbang Liang, and Minas Liarokapis, "Mechanically Programmable Jamming Based on Articulated Mesh Structures for Variable Stiffness Robots," IEEE/RSJ International Conference on Intelligent Robots and Systems (IROS), Kyoto, 2022.

15. Che-Ming Chang, Felipe Sanches, **Geng Gao**, Samantha Johnson, and Minas Liarokapis, "An Adaptive, Affordable, Humanlike Arm Hand System for Deaf and DeafBlind Communication with the American Sign Language," IEEE/RSJ International Conference on Intelligent Robots and Systems (IROS), Kyoto, 2022.

14. Gal Gorjup, Lucas Gerez, **Geng Gao**, and Minas Liarokapis, "On the Efficiency, Usability, and Intuitiveness of a Wearable, Affordable, Open-Source, Generic Robot Teaching Interface," 30th Mediterranean Conference on Control and Automation (MED 2022), Greece, 2022.

13. **Geng Gao**, Anany Dwivedi, and Minas Liarokapis, "An Anthropomorphic Prosthetic Hand with an Active, Selectively Lockable Differential Mechanism: Towards Affordable Dexterity," IEEE/RSJ International Conference on Intelligent Robots and Systems (IROS), Prague, 2021.

12. Gal Gorjup, Che-Ming Chang, **Geng Gao**, Lucas Gerez, Anany Dwivedi, and Minas Liarokapis, "The ARoA Platform: An Autonomous Robotic Assistant with a Reconfigurable Torso System and Dexterous Manipulation Capabilities," IEEE/RSJ International Conference on Intelligent Robots and Systems (IROS), Prague, 2021.

11. Nathan Elangovan, Lucas Gerez, **Geng Gao**, and Minas Liarokapis, "A Multi-Modal Robotic Gripper with a Reconfigurable Base: Improving Dexterous Manipulation without Compromising Grasping Efficiency," IEEE/RSJ International Conference on Intelligent Robots and Systems (IROS), Prague, 2021.

10. **Geng Gao**, Jayden Chapman, Saori Matsunaga, Toshisada Mariyama, Bruce MacDonald, and Minas Liarokapis, "A Dexterous, Reconfigurable, Adaptive Robot Hand Combining Anthropomorphic and Interdigitated Configurations," IEEE/RSJ International Conference on Intelligent Robots and Systems (IROS), Prague, 2021.

9. Samantha Johnson, **Geng Gao**, Todd Johnson, Minas Liarokapis, and Chiara Bellini, "An Adaptive, Affordable, Open-Source Robotic Hand for Deaf and Deaf-Blind Communication Using Tactile American Sign Language," 43rd Annual International Conference of the IEEE Engineering in Medicine and Biology Society (EMBC), 2021.

8. Nathan Elangovan, **Geng Gao**, Che-Ming Chang, and Minas Liarokapis, "A Modular, Accessible, Affordable Dexterity Test for Evaluating the Grasping and Manipulation Capabilities of Robotic Grippers and Hands," IEEE International Symposium on Safety, Security, and Rescue Robotics, 2020.

7. Gal Gorjup, George kontoudis, Anany Dwivedi, **Geng Gao**, Saori Matsunaga, Toshisada Mariyama, Bruce MacDonald, and Minas Liarokapis, "Combining Programming by Demonstration with Path Optimization and Local Replanning to Facilitate the Execution of Assembly Tasks," IEEE International Conference on Systems, Man, and Cybernetics, 2020.

6. Lucas Gerez, **Geng Gao**, and Minas Liarokapis, "Laminar Jamming Flexure Joints for the Development of Variable Stiffness Robot Grippers and Hands," IEEE International Conference on Intelligent Robots and Systems (IROS), 2020.

5. Gal Gorjup, **Geng Gao**, Anany Dwivedi, and Minas Liarokapis,"Combining Compliance Control, CAD Based Localization, and a Multi-Modal Gripper for Rapid and Robust Programming of Assembly Tasks," IEEE International Conference on Intelligent Robots and Systems (IROS), 2020.

4. Andrew John McLaren, Zak Fitzgerald, **Geng Gao**, and Minas Liarokapis,"A Passive Closing, Tendon Driven, Adaptive Robot Hand for Ultra-Fast, Aerial Grasping and Perching," IEEE/RSJ International Conference on Intelligent Robots and Systems (IROS), Macau, China, 2019.

3. Lucas Gerez, **Geng Gao**, and Minas Liarokapis,"Employing Magnets to Improve the Force Exertion Capabilities of Adaptive Robot Hands in Precision Grasps" IEEE/RSJ International Conference on Intelligent Robots and Systems (IROS), Macau, China, 2019.

2. **Geng Gao**, L. Gerez, and M. Liarokapis,"Adaptive, Tendon-Driven, Affordable Prostheses for Partial Hand Amputations: On Body-powered and Motor Driven Implementations," 41st Annual International Conference of the IEEE Engineering in Medicine and Biology Society (EMBC), Berlin, Germany, 2019.

1. **Geng Gao**, Anany Dwivedi, Nathan Elangovan, Yige Cao, Lucy Young, and Minas Liarokapis, "The New Dexterity Adaptive, Humanlike Robot Hand", IEEE International Conference on Robotics and Automation (ICRA), 2019.

A.3 Nominations and Awards

7. 3rd place, IEEE International Conference on Robotics and Automation (ICRA), 2022 - Robotic Grasping and Manipulation Competition, Manufacturing Track, Philadelphia, USA.

6. Silver award, IEEE Region 10 Conference (TENCON), 2021 - Robot Design Competition, Auckland, New Zealand.

5. 1st place, IEEE International Conference on Intelligent Robots and Systems (IROS), 2021 - Best Paper on Robot Mechanism and Design, Prague, Czech Republic.

4. 3rd Prize, IEEE International Conference on Intelligent Robots and Systems (IROS), 2020 - Robotic Grasping and Manipulation Competition, Manufacturing Track, Las Vegas, USA.

3. 1st Prize, Assistive Devices Challenge, 2020 Hackaday Prize, Sponsored by United Cerebral Palsy Los Angeles.

2. Best Paper Nomination, IEEE International Conference on Intelligent Robots and Systems (IROS), 2020, Las Vegas, USA.

1. 1st Prize, IEEE International Conference on Intelligent Robots and Systems (IROS), 2019 - Robotic Grasping and Manipulation Competition, Manufacturing Track, Macau, China.

A.4 Patent

A New Zealand provisional patent application (application number NZ 793415) has been submitted for the work on the mechanically programmable jamming based on articulated mesh structures.

References

[1] Anne M Gilroy et al. *Atlas of anatomy*. Thieme Stuttgart, 2008, pp. 346–352.

[2] Shadow Robot Company. *Shadow Dexterous Hand Technical Specification*. `https://www.shadowrobot.com/wp-content/uploads/shadow_dexterous_hand_technical_specification_E_20190221.pdf`. Accessed: 2019-08-16.

[3] M. Grebenstein et al. "The DLR hand arm system". In: *IEEE International Conference on Robotics and Automation (ICRA)*. May 2011, pp. 3175–3182. DOI: 10.1109/ICRA.2011.5980371.

[4] Uikyum Kim et al. "Integrated linkage-driven dexterous anthropomorphic robotic hand". In: *Nature communications* 12.1 (2021), pp. 1–13.

[5] Sungjae Min and Sooyeong Yi. "Development of cable-driven anthropomorphic robot hand". In: *IEEE Robotics and Automation Letters* 6.2 (2021), pp. 1176–1183.

[6] Raymond R Ma and Aaron M Dollar. "On dexterity and dexterous manipulation". In: *2011 15th International Conference on Advanced Robotics (ICAR)*. IEEE. 2011, pp. 1–7.

[7] Taku Senoo et al. "Skillful manipulation based on high-speed sensory-motor fusion". In: *2009 IEEE International Conference on Robotics and Automation*. IEEE. 2009, pp. 1611–1612.

[8] Thomas H Speeter. "Primitive based control of the Utah/MIT dextrous hand". In: *Proceedings. 1991 IEEE International Conference on Robotics and Automation*. IEEE. 1991, pp. 866–877.

[9] Ilge Akkaya et al. "Solving rubik's cube with a robot hand". In: *arXiv preprint arXiv:1910.07113* (2019).

[10] Jun Shintake et al. “Soft robotic grippers”. In: *Advanced materials* 30.29 (2018), p. 1707035.

[11] Lael U Odhner and Aaron M Dollar. “Stable, open-loop precision manipulation with underactuated hands”. In: *The International Journal of Robotics Research* 34.11 (2015), pp. 1347–1360.

[12] Lael U Odhner, Raymond R Ma, and Aaron M Dollar. “Open-loop precision grasping with underactuated hands inspired by a human manipulation strategy”. In: *IEEE Transactions on Automation Science and Engineering* 10.3 (2013), pp. 625–633.

[13] George M Whitesides. “Soft robotics”. In: *Angewandte Chemie International Edition* 57.16 (2018), pp. 4258–4273.

[14] Bruno Massa et al. “Design and development of an underactuated prosthetic hand”. In: *Proceedings 2002 IEEE international conference on robotics and automation (Cat. No. 02CH37292)*. Vol. 4. IEEE. 2002, pp. 3374–3379.

[15] Thierry Laliberté, Lionel Birglen, and Clement Gosselin. “Underactuation in robotic grasping hands”. In: *Machine Intelligence & Robotic Control* 4.3 (2002), pp. 1–11.

[16] Geng Gao et al. “Modular, Accessible, Sensorized Objects for Evaluating the Grasping and Manipulation Capabilities of Grippers and Hands”. In: *IEEE Robotics and Automation Letters* 5.4 (2020), pp. 6105–6112.

[17] Gal Gorjup et al. “A Flexible Robotic Assembly System Combining CAD Based Localization, Compliance Control, and a Multi-Modal Gripper”. In: *IEEE Robotics and Automation Letters* 6.4 (2021), pp. 8639–8646.

[18] Geng Gao et al. “A Dexterous, Reconfigurable, Adaptive Robot Hand Combining Anthropomorphic and Interdigitated Configurations”. In: *2021 IEEE/RSJ International Conference on Intelligent Robots and Systems (IROS)*. IEEE, pp. 7209–7215.

[19] Geng Gao, Lucas Gerez, and Minas Liarokapis. “Adaptive, Tendon-Driven, Affordable Prostheses for Partial Hand Amputations: On Body-Powered and Motor Driven Implementations”. In: *2019 41st Annual International Conference of the IEEE Engineering in Medicine and Biology Society (EMBC)*. IEEE. 2019, pp. 6656–6660.

[20] Geng Gao, Anany Dwivedi, and Minas Liarokapis. "An Anthropomorphic Prosthetic Hand with an Active, Selectively Lockable Differential Mechanism: Towards Affordable Dexterity". In: *2021 IEEE/RSJ International Conference on Intelligent Robots and Systems (IROS)*. IEEE. 2021, pp. 6147–6152.

[21] Geng Gao et al. "On Differential Mechanisms for Underactuated, Lightweight, Adaptive Prosthetic Hands". In: *Frontiers in Neurorobotics* 15 (2021).

[22] Geng Gao et al. "A Pneumatically Driven, Disposable, Soft Robotic Gripper Equipped With Multi-Stage, Retractable, Telescopic Fingers". In: *IEEE Transactions on Medical Robotics and Bionics* 3.3 (2021), pp. 573–582.

[23] S. Garrido-Jurado et al. "Automatic generation and detection of highly reliable fiducial markers under occlusion". In: *Pattern Recognition* 47.6 (2014), pp. 2280–2292.

[24] G. Bradski. "The OpenCV Library". In: *Dr. Dobb's Journal of Software Tools* (2000).

[25] Polhemus Inc. *Polhemus Liberty User Brochure*. URL: `https://polhemus.com/_assets/img/LIBERTY_Brochure_1.pdf` (visited on 03/19/2022).

[26] National Institute of Standards and Technology. *Grasping Performance Metrics and Test Methods*. https://www.nist.gov/el/intelligent-systems-division-73500/robotic-grasping-and-manipulation-assembly/grasping. Accessed: 2018-11-1.

[27] Amber Turner et al. "Comparing Machine Learning Methods and Feature Extraction Techniques for the EMG Based Decoding of Human Intention". In: *2021 43rd Annual International Conference of the IEEE Engineering in Medicine & Biology Society (EMBC)*. IEEE. 2021, pp. 4738–4743.

[28] Berk Calli et al. "The YCB object and model set: Towards common benchmarks for manipulation research". In: *2015 international conference on advanced robotics (ICAR)*. IEEE. 2015, pp. 510–517.

[29] Ian M. Bullock, Raymond R. Ma, and Aaron M. Dollar. "A hand-centric classification of human and robot dexterous manipulation". In: *IEEE Transactions on Haptics* 6.2 (2013), pp. 129–144.

[30] Steffen W Ruehl et al. “Experimental evaluation of the schunk 5-finger gripping hand for grasping tasks”. In: *2014 IEEE International Conference on Robotics and Biomimetics (ROBIO 2014)*. IEEE. 2014, pp. 2465–2470.

[31] H. Liu et al. “Multisensory Five-Finger Dexterous Hand: The DLR/HIT Hand II”. In: *2008 IEEE/RSJ International Conference on Intelligent Robots and Systems, IROS*. Nice, 2008, pp. 3692–3697.

[32] Schunk. *SDH*. `https://schunk.com/de_en/gripping-systems/series/sdh/`. Accessed: 2019-08-16.

[33] Che-Ming Chang et al. “On Alternative Uses of Structural Compliance for the Development of Adaptive Robot Grippers and Hands”. In: *Frontiers in Neurorobotics* 13 (2019), p. 91.

[34] B. Calli et al. “Benchmarking in Manipulation Research: Using the Yale-CMU-Berkeley Object and Model Set”. In: *IEEE Robotics and Automation Magazine* 22.3 (2015), pp. 36–52.

[35] Balakumar Sundaralingam and Tucker Hermans. “Relaxed-rigidity constraints: kinematic trajectory optimization and collision avoidance for in-grasp manipulation”. In: *Autonomous Robots* 43.2 (2019), pp. 469–483.

[36] N. Correll et al. “Analysis and Observations From the First Amazon Picking Challenge”. In: *IEEE Transactions on Automation Science and Engineering* 15.1 (2018), pp. 172–188.

[37] Jurgen Leitner et al. “The ACRV picking benchmark: A robotic shelf picking benchmark to foster reproducible research”. In: *IEEE International Conference on Robotics and Automation*. Singapore, 2017, pp. 4705–4712.

[38] Alessandro Altobelli. “Sensorized Object Approach”. In: *Haptic Devices for Studies on Human Grasp and Rehabilitation*. Cham: Springer International Publishing, 2016, pp. 21–41. ISBN: 978-3-319-47087-0. DOI: `10.1007/978-3-319-47087-0_3`. URL: `https://doi.org/10.1007/978-3-319-47087-0_3`.

[39] R. Kõiva, R. Haschke, and H. Ritter. “Development of an intelligent object for grasp and manipulation research”. In: *2011 15th International Conference on Advanced Robotics (ICAR)*. June 2011, pp. 204–210. DOI: `10.1109/ICAR.2011.6088549`.

[40] M. A. Roa, R. Kõiva, and C. Castellini. "Experimental evaluation of human grasps using a sensorized object". In: *2012 4th IEEE RAS EMBS International Conference on Biomedical Robotics and Biomechatronics (BioRob)*. June 2012, pp. 1662–1668. DOI: 10.1109/BioRob.2012.6290670.

[41] Joe Falco et al. "Grasping the Performance". In: *IEEE Robotics and Automation Magazine* 22.4 (2015), pp. 125–136.

[42] Arjun Singh et al. "BigBIRD: A Large-Scale 3D Database of Object Instances". In: *IEEE International Conference on Robotics and Automation*. 4. Hong Kong, 2014, pp. 509–516.

[43] Alexander Kasper, Zhixing Xue, and Rüdiger Dillmann. "The KIT object models database: An object model database for object recognition, localization and manipulation in service robotics". In: *International Journal of Robotics Research* 31.8 (2012), pp. 927–934.

[44] Corey Goldfeder et al. "The Columbia Grasp Database". In: *IEEE International Conference on Robotics and Automation*. Kobe, 2009, pp. 1710–1716.

[45] Raymond R Ma and Aaron M Dollar. "An underactuated hand for efficient finger-gaiting-based dexterous manipulation". In: *2014 IEEE International Conference on Robotics and Biomimetics (ROBIO 2014)*. IEEE. 2014, pp. 2214–2219.

[46] Raymond R Ma, Joseph T Belter, and Aaron M Dollar. "Hybrid deposition manufacturing: design strategies for multimaterial mechanisms via three-dimensional printing and material deposition". In: *Journal of Mechanisms and Robotics* 7.2 (2015), p. 021002.

[47] Sebastian Madgwick. "An efficient orientation filter for inertial and inertial/magnetic sensor arrays". In: *Report x-io and University of Bristol (UK)* 25 (2010), pp. 113–118.

[48] Markus Windolf, Nils Götzen, and Michael Morlock. "Systematic accuracy and precision analysis of video motion capturing systems—exemplified on the Vicon-460 system". In: *Journal of Biomechanics* 41.12 (2008), pp. 2776–2780. ISSN: 0021-9290. DOI: https://doi.org/10.1016/j.jbiomech.2008.06.024. URL: http://www.sciencedirect.com/science/article/pii/S0021929008003229.

[49] *Liberty User Manual 240/16*. Rev. H. Polhemus, Aug. 2012.

[50] Geng Gao et al. “The New Dexterity adaptive, humanlike robot hand”. In: *IEEE International Conference on Robotics and Automation*. 2019.

[51] Raymond Ma and Aaron Dollar. “Yale OpenHand Project: Optimizing Open-Source Hand Designs for Ease of Fabrication and Adoption”. In: *IEEE Robotics and Automation Magazine* 24.1 (2017), pp. 32–40.

[52] Wonkyoung Shin and Minyong Park. “Ergonomic interventions for prevention of work-related musculoskeletal disorders in a small manufacturing assembly line”. In: *International Journal of Occupational Safety and Ergonomics* 25.1 (2019), pp. 110–122.

[53] Hossein Rajabalipour Cheshmehgaz et al. “Accumulated risk of body postures in assembly line balancing problem and modeling through a multi-criteria fuzzy-genetic algorithm”. In: *Computers & Industrial Engineering* 63.2 (2012), pp. 503–512. ISSN: 0360-8352. DOI: https://doi.org/10.1016/j.cie.2012.03.017.

[54] L. Dürkop et al. “Analyzing the engineering effort for the commissioning of industrial automation systems”. In: *2015 IEEE 20th Conference on Emerging Technologies Factory Automation (ETFA)*. July 2015, pp. 1–4.

[55] Heiner Lasi et al. “Industry 4.0”. In: *Business & information systems engineering* 6.4 (2014), pp. 239–242.

[56] Gal Gorjup et al. “Combining Compliance Control, CAD Based Localization, and a Multi-Modal Gripper for Rapid and Robust Programming of Assembly Tasks”. In: *2020 IEEE/RSJ International Conference on Intelligent Robots and Systems (IROS)*. 2020, pp. 9064–9071. DOI: 10.1109/IROS45743.2020.9340869.

[57] Jörgen Frohm et al. “Levels of Automation in Manufacturing”. In: *Ergonomia-an International journal of ergonomics and human factors* 30.3 (2008).

[58] Karl Van Wyk, Joe Falco, and Elena Messina. “Robotic Grasping and Manipulation Competition: Future Tasks to Support the Development of Assembly Robotics”. In: *Robotic Grasping and Manipulation*. Ed. by Yu Sun and Joe Falco. Cham: Springer International Publishing, 2018, pp. 190–200. ISBN: 978-3-319-94568-2.

[59] Yasuyoshi Yokokohji et al. “Assembly Challenge: a robot competition of the Industrial Robotics Category, World Robot Summit – summary of the pre-competition in 2018”. In: *Advanced Robotics* 33.17 (2019), pp. 876–899.

[60] Malaka Miyuranga Kaluarachchi and Fawaz Yahya Annaz. "GUI teaching pendant development for a 6 axis articulated robot". In: *International Conference on Intelligent Robotics, Automation, and Manufacturing*. Springer. 2012, pp. 111–118.

[61] Sang Choi et al. "Lead-through robot teaching". In: *2013 IEEE Conference on Technologies for Practical Robot Applications (TePRA)*. IEEE. 2013, pp. 1–4.

[62] Josie Hughes et al. "Flexible, adaptive industrial assembly: driving innovation through competition". In: *Intelligent Service Robotics* (2019), pp. 1–10.

[63] Danica Kragic, Henrik I Christensen, et al. "Survey on visual servoing for manipulation". In: *Computational Vision and Active Perception Laboratory, Fiskartorpsv* 15 (2002), p. 2002.

[64] T. Nammoto et al. "High Speed/Accuracy Visual Servoing Based on Virtual Visual Servoing With Stereo Cameras". In: *2013 IEEE/RSJ International Conference on Intelligent Robots and Systems*. 2013, pp. 44–49.

[65] Joachim Michniewicz, Gunther Reinhart, and Stefan Boschert. "CAD-Based Automated Assembly Planning for Variable Products in Modular Production Systems". In: *Procedia CIRP* 44 (2016). 6th CIRP Conference on Assembly Technologies and Systems (CATS), pp. 44–49.

[66] C. Schlette et al. "Towards robot cell matrices for agile production – SDU Robotics' assembly cell at the WRC 2018". In: *Advanced Robotics* (2019), pp. 1–17.

[67] S. Wade-McCue et al. "Design of a Multi-Modal End-Effector and Grasping System: How Integrated Design helped win the Amazon Robotics Challenge". In: *CoRR* abs/1710.01439 (2017). arXiv: `1710.01439`.

[68] Anna Kochan. "Shadow delivers first hand". In: *Industrial robot: an international journal* (2005).

[69] Markus Grebenstein et al. "The DLR hand arm system". In: *2011 IEEE International Conference on Robotics and Automation*. IEEE. 2011, pp. 3175–3182.

[70] Aude Billard and Danica Kragic. "Trends and challenges in robot manipulation". In: *Science* 364.6446 (2019).

[71] Graham Robinson and J Bruce C Davies. "Continuum robots-a state of the art". In: *Proceedings 1999 IEEE international conference on robotics and automation (Cat. No. 99CH36288C)*. Vol. 4. IEEE. 1999, pp. 2849–2854.

[72] Can Erdogan, Armin Schröder, and Oliver Brock. "Coordination of intrinsic and extrinsic degrees of freedom in soft robotic grasping". In: *2018 IEEE International Conference on Robotics and Automation (ICRA)*. IEEE. 2018, pp. 4251–4256.

[73] Jesús M Gómez-de-Gabriel and Helge A Wurdemann. "Adaptive Underactuated Finger with Active Rolling Surface". In: *IEEE Robotics and Automation Letters* 6.4 (2021), pp. 8253–8260.

[74] Manuel G Catalano et al. "Adaptive synergies for the design and control of the Pisa/IIT SoftHand". In: *The International Journal of Robotics Research* 33.5 (2014), pp. 768–782.

[75] Oussama Khatib et al. "Ocean one: A robotic avatar for oceanic discovery". In: *IEEE Robotics & Automation Magazine* 23.4 (2016), pp. 20–29.

[76] Zhaopeng Chen et al. "Experimental study on impedance control for the five-finger dexterous robot hand dlr-hit ii". In: *2010 IEEE/RSJ International Conference on Intelligent Robots and Systems*. IEEE. 2010, pp. 5867–5874.

[77] Lael U Odhner, Raymond R Ma, and Aaron M Dollar. "Precision grasping and manipulation of small objects from flat surfaces using underactuated fingers". In: *2012 IEEE International Conference on Robotics and Automation*. IEEE. 2012, pp. 2830–2835.

[78] Kazuki Mitsui, Ryuta Ozawa, and Toshiyuki Kou. "An under-actuated robotic hand for multiple grasps". In: *2013 IEEE/RSJ International Conference on Intelligent Robots and Systems*. IEEE. 2013, pp. 5475–5480.

[79] Agisilaos G Zisimatos et al. "Open-source, affordable, modular, lightweight, underactuated robot hands". In: *IEEE/RSJ International Conference on Intelligent Robots and Systems*. 2014, pp. 3207–3212.

[80] Diego Ospina and Alejandro Ramirez-Serrano. "Sensorless in-hand manipulation by an underactuated robot hand". In: *Journal of Mechanisms and Robotics* 12.5 (2020), p. 051009.

[81] Nathan Elangovan et al. "A Multi-Modal Robotic Gripper with a Reconfigurable Base: Improving Dexterous Manipulation without Compromising Grasping Efficiency". In: *2021 IEEE/RSJ International Conference on Intelligent Robots and Systems (IROS)*. IEEE, pp. 6124–6130.

[82] Júlia Borràs and Aaron M Dollar. "Dimensional synthesis of three-fingered robot hands for maximal precision manipulation workspace". In: *The International Journal of Robotics Research* 34.14 (2015), pp. 1731–1746.

[83] Nathan Elangovan et al. "Improving Robotic Manipulation without Sacrificing Grasping Efficiency: A Multi-Modal, Adaptive Gripper with Reconfigurable Finger Bases". In: *IEEE Access* (2021).

[84] Joshua Z Zheng, Sara De La Rosa, and Aaron M Dollar. "An investigation of grasp type and frequency in daily household and machine shop tasks". In: *2011 IEEE International Conference on Robotics and Automation*. IEEE. 2011, pp. 4169–4175.

[85] J Krishnan and L Chipchase. "Passive axial rotation of the metacarpophalangeal joint". In: *The Journal of Hand Surgery: British & European Volume* 22.2 (1997), pp. 270–273.

[86] Skyler A Dalley et al. "Design of a multifunctional anthropomorphic prosthetic hand with extrinsic actuation". In: *IEEE/ASME Transactions on Mechatronics* 14.6 (2009), pp. 699–706.

[87] Ashish D Deshpande et al. "Mechanisms of the anatomically correct testbed hand". In: *IEEE/ASME Transactions on Mechatronics* 18.1 (2013), pp. 238–250.

[88] Cai-Hua Xiong et al. "Design and implementation of an anthropomorphic hand for replicating human grasping functions". In: *IEEE Transactions on Robotics* 32.3 (2016), pp. 652–671.

[89] Zhe Xu and Emanuel Todorov. "Design of a highly biomimetic anthropomorphic robotic hand towards artificial limb regeneration". In: *IEEE Int. Conf. on Robotics and Automation*. 2016, pp. 3485–3492.

[90] CS Lovchik and Myron A Diftler. "The robonaut hand: A dexterous robot hand for space". In: *IEEE International Conference on Robotics and Automation*. Vol. 2. 1999, pp. 907–912.

[91] Jörg Butterfaß et al. “DLR-Hand II: Next generation of a dextrous robot hand”. In: *IEEE International Conference on Robotics and Automation*. Vol. 1. 2001, pp. 109–114.

[92] Haruhisa Kawasaki, Tsuneo Komatsu, and Kazunao Uchiyama. “Dexterous anthropomorphic robot hand with distributed tactile sensor: Gifu hand II”. In: *IEEE/ASME Tr. on Mechatronics* 7.3 (2002), pp. 296–303.

[93] Schunk. *PGN-plus-P*. `https://schunk.com/de_en/gripping-systems/series/pgn-plus-p/`. Accessed: 2021-03-05.

[94] Aaron M Dollar and Robert D Howe. “The highly adaptive SDM hand: Design and performance evaluation”. In: *The International Journal of Robotics Research* 29.5 (2010), pp. 585–597.

[95] Daniel M Aukes et al. “Design and testing of a selectively compliant underactuated hand”. In: *The International Journal of Robotics Research* 33.5 (2014), pp. 721–735.

[96] Matei Ciocarlie et al. “The Velo gripper: A versatile single-actuator design for enveloping, parallel and fingertip grasps”. In: *The Int. Journal of Robotics Research* 33.5 (2014), pp. 753–767.

[97] George P Kontoudis et al. “Open-source, anthropomorphic, underactuated robot hands with a selectively lockable differential mechanism: Towards affordable prostheses”. In: *IEEE/RSJ International Conference on Intelligent Robots and Systems*. 2015, pp. 5857–5862.

[98] Raphael Deimel and Oliver Brock. “A novel type of compliant and underactuated robotic hand for dexterous grasping”. In: *The International Journal of Robotics Research* 35.1-3 (2016), pp. 161–185.

[99] Yong-Jae Kim, Hansol Song, and Chan-Young Maeng. “BLT Gripper: An Adaptive Gripper With Active Transition Capability Between Precise Pinch and Compliant Grasp”. In: *IEEE Robotics and Automation Letters* 5.4 (2020), pp. 5518–5525.

[100] Lael U Odhner et al. “A compliant, underactuated hand for robust manipulation”. In: *The International Journal of Robotics Research* 33.5 (2014), pp. 736–752.

[101] Zhengtao Hu, Weiwei Wan, and Kensuke Harada. “Designing a mechanical tool for robots with two-finger parallel grippers”. In: *IEEE Robotics and Automation Letters* 4.3 (2019), pp. 2981–2988.

[102] Patrick Slade et al. "Tact: Design and performance of an open-source, affordable, myoelectric prosthetic hand". In: *2015 IEEE International Conference on Robotics and Automation (ICRA)*. IEEE. 2015, pp. 6451–6456.

[103] Rafiq Elmansy. "Designing the 3D-Printed prosthetic hand". In: *Design Management Review* 26.1 (2015), pp. 24–31.

[104] Berk Calli et al. "Yale-CMU-Berkeley dataset for robotic manipulation research". In: *The International Journal of Robotics Research* 36.3 (2017), pp. 261–268.

[105] Panagiotis Polygerinos et al. "Soft robotic glove for hand rehabilitation and task specific training". In: *IEEE International Conference on Robotics and Automation (ICRA)*. 2015, pp. 2913–2919.

[106] Geng Gao et al. "Modular, Accessible, Sensorized Objects for Evaluating the Grasping and Manipulation Capabilities of Grippers and Hands". In: *IEEE Robotics and Automation Letters* 5.4 (2020), pp. 6105–6112. DOI: 10.1109/LRA.2020.3010484.

[107] Nathan Elangovan et al. "A modular, accessible, affordable dexterity test for evaluating the grasping and manipulation capabilities of robotic grippers and hands". In: *2020 IEEE International Symposium on Safety, Security, and Rescue Robotics (SSRR)*. IEEE. 2020, pp. 304–310.

[108] Robotiq. *2F-85 and 2F-140 Grippers*. https://robotiq.com/products/2f85-140-adaptive-robot-gripper. Accessed: 2021-03-05.

[109] Raymond Ma and Aaron Dollar. "Yale openhand project: Optimizing open-source hand designs for ease of fabrication and adoption". In: *IEEE Robotics & Automation Magazine* 24.1 (2017), pp. 32–40.

[110] Javier Felip and Antonio Morales. "Robust sensor-based grasp primitive for a three-finger robot hand". In: *2009 IEEE/RSJ International Conference on Intelligent Robots and Systems*. IEEE. 2009, pp. 1811–1816.

[111] Robotiq. *3-Finger Adaptive Robot Gripper*. https://robotiq.com/products/3-finger-adaptive-robot-gripper. Accessed: 2021-03-05.

[112] Hong Liu et al. "Multisensory five-finger dexterous hand: The DLR/HIT Hand II". In: *2008 IEEE/RSJ international conference on intelligent robots and systems*. IEEE. 2008, pp. 3692–3697.

[113] Francesca Cordella et al. "Literature review on needs of upper limb prosthesis users". In: *Frontiers in neuroscience* 10 (2016), p. 209.

[114] Minas V Liarokapis, Panagiotis K Artemiadis, and Kostas J Kyriakopoulos. "Quantifying anthropomorphism of robot hands". In: *IEEE International Conference on Robotics and Automation (ICRA)*. 2013, pp. 2041–2046.

[115] Douglas P Murphy. *Fundamentals of amputation care and prosthetics*. Demos Medical Publishing, 2013.

[116] N Shanmuganathan et al. "Aesthetic finger prosthesis". In: *The Journal of Indian Prosthodontic Society* 11.4 (2011), pp. 232–237.

[117] Mokhtar Arazpour et al. "Design and fabrication of a finger prosthesis based on a new method of suspension". In: *Prosthetics and orthotics international* 37.4 (2013), pp. 332–335.

[118] P Manurangsee et al. "Osseointegrated finger prosthesis: An alternative method for finger reconstruction". In: *The Journal of hand surgery* 25.1 (2000), pp. 86–92.

[119] Michael EL Leow, C Prosthetics, and Robert WH Pho. "Optimal circumference reduction of finger models for good prosthetic fit of a thimble-type prosthesis for distal finger amputations". In: *Journal of rehabilitation research and development* 38.2 (2001), pp. 273–280.

[120] Ilario Imbinto et al. "Treatment of the partial hand amputation: an engineering perspective". In: *IEEE reviews in biomedical engineering* 9 (2016), pp. 32–48.

[121] Jae-Ho Shim et al. "Wrist-driven prehension prosthesis for amputee patients with disarticulation of the thumb and index finger". In: *Archives of physical medicine and rehabilitation* 79.7 (1998), pp. 877–878.

[122] A Wedderburn et al. "A wrist-powered prosthesis for the partial hand". In: *J Assoc Child Prosthetic Clinics* 21 (1986), pp. 42–45.

[123] Kai Xu et al. "Wrist-Powered Partial Hand Prosthesis Using a Continuum Whiffle Tree Mechanism: A Case Study". In: *IEEE Transactions on Neural Systems and Rehabilitation Engineering* 26.3 (2018), pp. 609–618.

[124] Didrick Medical INC. *X-Finger Models*. `https://www.x-finger.com/x-finger-models.html`. Accessed: 2019-04-24.

[125] CM Fryer and JW Michael. "Harnessing and controls for body-powered devices". In: *Atlas of Amputations and Limb Deficiencies–Surgical, Prosthetic and Rehabilitation Principles*. Amer. Acad. Orthopedic Surgeons, 2004, pp. 131–143.

[126] Giho Jang et al. "Robotic index finger prosthesis using stackable double 4-BAR mechanisms". In: *Mechatronics* 23.3 (2013), pp. 318–325.

[127] Yuta Murai et al. "Designs of tailor-made myoelectric prosthetic hand for trans-metacarpal amputations with remaining fingers and joint moving functions". In: *IEEE International Conference on Cyborg and Bionic Systems (CBS)*. 2017, pp. 119–124.

[128] Joseph Lake and Michael Ergo. *Partial hand prosthesis*. a US Patent App. 11/081,402. Sept. 2006.

[129] David James Gow. *Prostheses with mechanically operable digit members*. US Patent 8,808,397. Aug. 2014.

[130] Joseph A Doeringer and N Hogan. "Performance of above elbow body-powered prostheses in visually guided unconstrained motion tasks". In: *IEEE Transactions on Biomedical Engineering* 42.6 (1995), pp. 621–631.

[131] Lucas Gerez, Junan Chen, and Minas Liarokapis. "On the Development of Adaptive, Tendon-Driven, Wearable Exo-Gloves for Grasping Capabilities Enhancement". In: *IEEE Robotics and Automation Letters* 4.2 (2019), pp. 422–429.

[132] Bryan Buchholz, Thomas J Armstrong, and Steven A Goldstein. "Anthropometric data for describing the kinematics of the human hand". In: *Ergonomics* 35.3 (1992), pp. 261–273.

[133] Esteve Peña Pitarch. *Virtual human hand: Grasping strategy and simulation*. Universitat Politècnica de Catalunya, 2008.

[134] Lucas Gerez and Minas Liarokapis. "A compact ratchet clutch mechanism for fine tendon termination and adjustment". In: *2018 IEEE/ASME International Conference on Advanced Intelligent Mechatronics (AIM)*. IEEE. 2018, pp. 1390–1395.

[135] Minas V Liarokapis et al. "Open-source, low-cost, compliant, modular, underactuated fingers: Towards affordable prostheses for partial hand amputations". In: *2014 36th Annual International Conference of the IEEE Engineering in Medicine and Biology Society*. IEEE. 2014, pp. 2541–2544.

[136] Kathryn Ziegler-Graham et al. "Estimating the prevalence of limb loss in the United States: 2005 to 2050". In: *Archives of physical medicine and rehabilitation* 89.3 (2008), pp. 422–429.

[137] Antonio Bicchi. "Hands for dexterous manipulation and robust grasping: A difficult road toward simplicity". In: *IEEE Transactions on robotics and automation* 16.6 (2000), pp. 652–662.

[138] Ilaria Cerulo et al. "Teleoperation of the SCHUNK S5FH under-actuated anthropomorphic hand using human hand motion tracking". In: *Robotics and Autonomous Systems* 89 (2017), pp. 75–84.

[139] Markus Grebenstein et al. "A method for hand kinematics designers 7 billion perfect hands". In: (2010).

[140] Nikola Dechev, WL Cleghorn, and S Naumann. "Multiple finger, passive adaptive grasp prosthetic hand". In: *Mechanism and machine theory* 36.10 (2001), pp. 1157–1173.

[141] Matei Ciocarlie, Fernando Mier Hicks, and Scott Stanford. "Kinetic and dimensional optimization for a tendon-driven gripper". In: *2013 IEEE International Conference on Robotics and Automation*. IEEE. 2013, pp. 2751–2758.

[142] Andrew McLaren et al. "A passive closing, tendon driven, adaptive robot hand for ultra-fast, aerial grasping and perching". In: *2019 IEEE/RSJ International Conference on Intelligent Robots and Systems (IROS)*. IEEE. 2019, pp. 5602–5607.

[143] Ottobock. *Silicone finger and partial hand prosthetics*. `https://www.ottobockus.com/prosthetics/upper-limb-prosthetics/solution-overview/custom-silicone-prosthetics/`. Accessed: 2021-08-01.

[144] Ottobock. *Body-powered prosthetic solutions*. `https://www.ottobockus.com/prosthetics/upper-limb-prosthetics/solution-overview/body-powered-prosthetic-solutions/`. Accessed: 2021-08-01.

[145] Stefan Schulz. "First experiences with the vincent hand". In: *Proceedings of the MyoElectric Controls/Powered Prosthetics Symposium Fredericton (Canada, 2011)*. 2011, pp. 14–19.

[146] Linda Resnik et al. "Advanced upper limb prosthetic devices: implications for upper limb prosthetic rehabilitation". In: *Archives of physical medicine and rehabilitation* 93.4 (2012), pp. 710–717.

[147] D. Edeer, C. W. Martin. *Silicone finger and partial hand prosthetics*. https://www.worksafebc.com/en/resources/health-care-providers/guides/upper-limb-prostheses-a-review-of-the-literature-with-a-focus-on-myoelectric-hands?lang=en. Accessed: 2021-08-01.

[148] Joseph T Belter et al. "Mechanical design and performance specifications of anthropomorphic prosthetic hands: A review." In: *Journal of Rehabilitation Research & Development* 50.5 (2013).

[149] Lucas Gerez and Minas Liarokapis. "An Underactuated, Tendon-Driven, Wearable Exo-Glove With a Four-Output Differential Mechanism". In: *2019 41st Annual International Conference of the IEEE Engineering in Medicine and Biology Society (EMBC)*. IEEE. 2019, pp. 6224–6228.

[150] Maria Chiara Carrozza et al. "A cosmetic prosthetic hand with tendon driven under-actuated mechanism and compliant joints: ongoing research and preliminary results". In: *Proceedings of the 2005 IEEE International Conference on Robotics and Automation*. IEEE. 2005, pp. 2661–2666.

[151] Thierry Laliberté et al. "Towards the design of a prosthetic underactuated hand". In: *Mechanical Sciences* 1.1 (2010), pp. 19–26.

[152] Joseph T Belter and Aaron M Dollar. "Novel differential mechanism enabling two DOF from a single actuator: Application to a prosthetic hand". In: *2013 IEEE 13th International Conference on Rehabilitation Robotics (ICORR)*. IEEE. 2013, pp. 1–6.

[153] Mathieu Baril et al. "On the design of a mechanically programmable underactuated anthropomorphic prosthetic gripper". In: *Journal of Mechanical Design* 135.12 (2013).

[154] Mojtaba Shahmohammadi and Minas Liarokapis. "A series elastic, compact differential mechanism: On the development of adaptive, lightweight robotic grippers and hands". In: *2021 IEEE/RSJ International Conference on Intelligent Robots and Systems (IROS)*. IEEE. 2021, pp. 6110–6116.

[155] Irfan Hussain et al. "Modeling and prototyping of an underactuated gripper exploiting joint compliance and modularity". In: *IEEE Robotics and automation letters* 3.4 (2018), pp. 2854–2861.

[156] Pascal Weiner et al. "The KIT prosthetic hand: design and control". In: *2018 IEEE/RSJ International Conference on Intelligent Robots and Systems (IROS)*. IEEE. 2018, pp. 3328–3334.

[157] Olga Van Der Niet and Corry K van der Sluis. "Functionality of i-LIMB and i-LIMB Pulse hands: Case report". In: *Journal of rehabilitation research and development* 50.8 (2013), p. 1123.

[158] Courtney Medynski and Bruce Rattray. "Bebionic prosthetic design". In: Myoelectric Symposium. 2011.

[159] Bart Peerdeman et al. "UT hand I: A lock-based underactuated hand prosthesis". In: *Mechanism and machine theory* 78 (2014), pp. 307–323.

[160] Cristina Piazza et al. "Softhand pro-d: Matching dynamic content of natural user commands with hand embodiment for enhanced prosthesis control". In: *2016 IEEE International Conference on Robotics and Automation (ICRA)*. IEEE. 2016, pp. 3516–3523.

[161] Daniela Rus and Michael T Tolley. "Design, fabrication and control of soft robots". In: *Nature* 521.7553 (2015), pp. 467–475.

[162] Michael T Tolley et al. "A resilient, untethered soft robot". In: *Soft robotics* (2014), pp. 213–223.

[163] Panagiotis Polygerinos et al. "Soft robotics: Review of fluid-driven intrinsically soft devices; manufacturing, sensing, control, and applications in human-robot interaction". In: *Advanced Engineering Materials* 19.12 (2017), p. 1700016.

[164] Vincent Wall, Raphael Deimel, and Oliver Brock. "Selective stiffening of soft actuators based on jamming". In: *2015 IEEE International Conference on Robotics and Automation (ICRA)*. IEEE. 2015, pp. 252–257.

[165] Michelle C Yuen, R Adam Bilodeau, and Rebecca K Kramer. "Active variable stiffness fibers for multifunctional robotic fabrics". In: *IEEE Robotics and Automation Letters* 1.2 (2016), pp. 708–715.

[166] Thomas P Chenal et al. "Variable stiffness fabrics with embedded shape memory materials for wearable applications". In: *2014 IEEE/RSJ International Conference on Intelligent Robots and Systems*. IEEE. 2014, pp. 2827–2831.

[167] Amir Firouzeh, Marco Salerno, and Jamie Paik. "Stiffness control with shape memory polymer in underactuated robotic origamis". In: *IEEE Transactions on Robotics* 33.4 (2017), pp. 765–777.

[168] Andreas Lendlein. "Fabrication of reprogrammable shape-memory polymer actuators for robotics". In: *Science Robotics* 3.18 (2018), eaat9090.

[169] Binjie Jin et al. "Programming a crystalline shape memory polymer network with thermo-and photo-reversible bonds toward a single-component soft robot". In: *Science advances* 4.1 (2018), eaao3865.

[170] Mingfang Liu et al. "A novel design of shape-memory alloy-based soft robotic gripper with variable stiffness". In: *International journal of advanced robotic systems* 17.1 (2020), p. 1729881420907813.

[171] Liyu Wang, Utku Culha, and Fumiya Iida. "A dragline-forming mobile robot inspired by spiders". In: *Bioinspiration & biomimetics* 9.1 (2014), p. 016006.

[172] Wei Wang et al. "Shape memory alloy-based soft finger with changeable bending length using targeted variable stiffness". In: *Soft robotics* 7.3 (2020), pp. 283–291.

[173] Yong Zhong et al. "Investigation on a New Approach for Designing Articulated Soft Robots with Discrete Variable Stiffness". In: *IEEE/ASME Transactions on Mechatronics* (2021).

[174] Hiroya Imamura, Kevin Kadooka, and Minoru Taya. "A variable stiffness dielectric elastomer actuator based on electrostatic chucking". In: *Soft matter* 13.18 (2017), pp. 3440–3448.

[175] Wen-Bo Li et al. "Bioinspired variable stiffness dielectric elastomer actuators with large and tunable load capacity". In: *Soft robotics* 6.5 (2019), pp. 631–643.

[176] Jun Shintake et al. "Variable stiffness actuator for soft robotics using dielectric elastomer and low-melting-point alloy". In: *2015 IEEE/RSJ International Conference on Intelligent Robots and Systems (IROS)*. IEEE. 2015, pp. 1097–1102.

[177] Juan De Vicente, Daniel J Klingenberg, and Roque Hidalgo-Alvarez. "Magnetorheological fluids: a review". In: *Soft matter* 7.8 (2011), pp. 3701–3710.

[178] Anders Pettersson et al. "Design of a magnetorheological robot gripper for handling of delicate food products with varying shapes". In: *Journal of Food Engineering* 98.3 (2010), pp. 332–338.

[179] Takeshi Nishida, Yuki Okatani, and Kenjiro Tadakuma. "Development of universal robot gripper using MR α fluid". In: *International Journal of Humanoid Robotics* 13.04 (2016), p. 1650017.

[180] Allen Jiang et al. “Robotic granular jamming: Does the membrane matter?” In: *Soft Robotics* 1.3 (2014), pp. 192–201.

[181] John R Amend et al. “A positive pressure universal gripper based on the jamming of granular material”. In: *IEEE transactions on robotics* 28.2 (2012), pp. 341–350.

[182] Yifan Wang et al. “Structured fabrics with tunable mechanical properties”. In: *Nature* 596.7871 (2021), pp. 238–243.

[183] Yashraj S Narang, Joost J Vlassak, and Robert D Howe. “Mechanically versatile soft machines through laminar jamming”. In: *Advanced Functional Materials* 28.17 (2018), p. 1707136.

[184] Margherita Brancadoro et al. “Fiber jamming transition as a stiffening mechanism for soft robotics”. In: *Soft robotics* 7.6 (2020), pp. 663–674.

[185] Buse Aktaş and Robert D Howe. “Tunable anisotropic stiffness with square fiber jamming”. In: *2020 3rd IEEE International Conference on Soft Robotics (RoboSoft)*. IEEE. 2020, pp. 879–884.

[186] Lucas Gerez, Geng Gao, and Minas Liarokapis. “Laminar Jamming Flexure Joints for the Development of Variable Stiffness Robot Grippers and Hands”. In: *2020 IEEE/RSJ International Conference on Intelligent Robots and Systems (IROS)*. IEEE. 2020, pp. 8709–8715.

[187] Hannah Stuart et al. “The Ocean One hands: An adaptive design for robust marine manipulation”. In: *The International Journal of Robotics Research* 36.2 (2017), pp. 150–166.

[188] Paul E Glick et al. “Robust capture of unknown objects with a highly underactuated gripper”. In: *2020 IEEE International Conference on Robotics and Automation (ICRA)*. IEEE. 2020, pp. 3996–4002.

[189] Minas Liarokapis and Aaron M Dollar. “Post-contact, in-hand object motion compensation for compliant and underactuated hands”. In: *2016 25th IEEE International Symposium on Robot and Human Interactive Communication (RO-MAN)*. IEEE. 2016, pp. 986–993.

[190] Lucas Gerez, Geng Gao, and Minas Liarokapis. “Employing magnets to improve the force exertion capabilities of adaptive robot hands in precision grasps”. In: *2019 IEEE/RSJ International Conference on Intelligent Robots and Systems (IROS)*. IEEE. 2019, pp. 7630–7635.

[191] Lionel Birglen and Clement M Gosselin. "On the force capability of underactuated fingers". In: *IEEE International Conference on Robotics and Automation (ICRA)*. Vol. 1. 2003, pp. 1139–1145.

[192] Stefan AJ Spanjer et al. "Underactuated gripper that is able to convert from precision to power grasp by a variable transmission ratio". In: *Advances in Reconfigurable Mechanisms and Robots I*. Springer, 2012, pp. 669–679.

[193] Aaron M Dollar. "Classifying human hand use and the activities of daily living". In: *The Human Hand as an Inspiration for Robot Hand Development*. Springer, 2014, pp. 201–216.

[194] Raymond R Ma, Lael U Odhner, and Aaron M Dollar. "A modular, open-source 3D printed underactuated hand". In: *Robotics and Automation (ICRA), 2013 IEEE International Conference on*. IEEE. 2013, pp. 2737–2743.

[195] Minas Liarokapis and Aaron M Dollar. "Learning the post-contact reconfiguration of the hand object system for adaptive grasping mechanisms". In: *2017 IEEE/RSJ International Conference on Intelligent Robots and Systems (IROS)*. IEEE. 2017, pp. 293–299.

[196] Sangbae Kim, Cecilia Laschi, and Barry Trimmer. "Soft robotics: a bioinspired evolution in robotics". In: *Trends in biotechnology* 31.5 (2013), pp. 287–294.

[197] Kevin Tai et al. "State of the art robotic grippers and applications". In: *Robotics* 5.2 (2016), p. 11.

[198] Jun Shintake et al. "Soft pneumatic gelatin actuator for edible robotics". In: *2017 IEEE/RSJ International Conference on Intelligent Robots and Systems (IROS)*. IEEE. 2017, pp. 6221–6226.

[199] Mohammed Owais Qureshi and Rumaiya Sajjad Syed. "The impact of robotics on employment and motivation of employees in the service sector, with special reference to health care". In: *Safety and health at work* 5.4 (2014), pp. 198–202.

[200] C Piazza et al. "A century of robotic hands". In: *Annual Review of Control, Robotics, and Autonomous Systems* 2 (2019), pp. 1–32.

[201] Che Ming Chang et al. "On Alternative Uses of Structural Compliance for the Development of Adaptive Robot Grippers and Hands". In: *Frontiers in Neurorobotics* 13 (2019), p. 91.

[202] Carmel Majidi. "Soft robotics: a perspective—current trends and prospects for the future". In: *Soft Robotics* 1.1 (2014), pp. 5–11.

[203] Josie Hughes et al. "Soft manipulators and grippers: a review". In: *Frontiers in Robotics and AI* 3 (2016), p. 69.

[204] Festo. *Adaptive gripper DHDG*. 2011. URL: http://www.festo.com.

[205] SoftRoboticsInc. *mGrip - Soft Robotics*. 2021. URL: https://www.softroboticsinc.com/products/mgrip/.

[206] Yufei Hao et al. "Universal soft pneumatic robotic gripper with variable effective length". In: *2016 35th Chinese control conference (CCC)*. IEEE. 2016, pp. 6109–6114.

[207] Tianyu Wang, Lisen Ge, and Guoying Gu. "Programmable design of soft pneu-net actuators with oblique chambers can generate coupled bending and twisting motions". In: *Sensors and Actuators A: Physical* 271 (2018), pp. 131–138.

[208] Ramses V Martinez et al. "Elastomeric origami: programmable paper-elastomer composites as pneumatic actuators". In: *Advanced functional materials* 22.7 (2012), pp. 1376–1384.

[209] Empire Robotics. *Products*. 2021. URL: http://www.empirerobotics.com/products/.

[210] Universal Robots. *UR+ Solutions | VG10 Vacuum gripper*. 2021. URL: https://www.universal-robots.com/plus/urplus-components/handling-grippers/vg10-vacuum-gripper/.

[211] J. Zhou, S. Chen, and Z. Wang. "A Soft-Robotic Gripper With Enhanced Object Adaptation and Grasping Reliability". In: *IEEE Robotics and Automation Letters* 2.4 (2017), pp. 2287–2293. DOI: 10.1109/LRA.2017.2716445.

[212] Kevin C Galloway et al. "Soft robotic grippers for biological sampling on deep reefs". In: *Soft robotics* 3.1 (2016), pp. 23–33.

[213] Zhongkui Wang, Yuuki Torigoe, and Shinichi Hirai. "A prestressed soft gripper: design, modeling, fabrication, and tests for food handling". In: *IEEE Robotics and Automation Letters* 2.4 (2017), pp. 1909–1916.

[214] Jaydev P Desai et al. "Toward patient-specific 3d-printed robotic systems for surgical interventions". In: *IEEE transactions on medical robotics and bionics* 1.2 (2019), pp. 77–87.

[215] Shivaramakrishnan Balasubramanian et al. "The era of robotics: dexterity for surgery and medical care: narrative review". In: *International Surgery Journal* 7.4 (2020), pp. 1317–1323.

[216] Jess H Lonner, Julian Zangrilli, and Sundeep Saini. "Emerging Robotic Technologies and Innovations for Hospital Process Improvement". In: *Robotics in Knee and Hip Arthroplasty* (2019), pp. 233–243.

[217] William Rutala and David Weber. *Sterilization | Disinfection & Sterilization Guidelines | Guidelines Library | Infection Control | CDC*. CDC, 2016. URL: `https://www.cdc.gov/infectioncontrol/guidelines/disinfection/sterilization/index.html`.

[218] Lionel Birglen and Clément M Gosselin. "Force analysis of connected differential mechanisms: Application to grasping". In: *The International Journal of Robotics Research* 25.10 (2006), pp. 1033–1046.

[219] Lucas Gerez and Minas Liarokapis. "A pneumatically driven, disposable, soft robotic gripper equipped with retractable, telescopic fingers". In: *2020 8th IEEE RAS/EMBS International Conference for Biomedical Robotics and Biomechatronics (BioRob)*. IEEE. 2020, pp. 36–41.

[220] Luc Marechal et al. "Toward a Common Framework and Database of Materials for Soft Robotics". In: *Soft Robotics* (2020).

[221] Zhongdong Jiao et al. "Vacuum-powered soft pneumatic twisting actuators to empower new capabilities for soft robots". In: *Advanced Materials Technologies* 4.1 (2019), p. 1800429.

[222] Niels Smaby et al. "Identification of key pinch forces required to complete functional tasks." In: *Journal of Rehabilitation Research & Development* 41.2 (2004).